INTERNATIONAL ATOMIC ENERGY AGENCY
INTERNATIONAL CENTRE FOR THEORETICAL PHYSICS
I.C.T.P., P.O. BOX 586, 34100 TRIESTE, ITALY, CABLE: CENTRATOM TRIESTE

H4.SMR/1058-15

WINTER COLLEGE ON OPTICS

9 - 27 February 1998

Passive and Active Integrated Optics in Glass: Physics and Technology

G. Righini

Optoelectronics and Photonics Department, IROE CNR, Firenze, Italy

International Centre for Theoretical Physics
Winter College on Optics
9-27 February 1998

Passive and Active Integrated Optics in Glass:

Physics and Technology

Giancarlo C. Righini

Optoelectronics and Photonics Department
Istituto di Ricerca sulle Onde Elettromagnetiche *Nello Carrara*
(IROE CNR)
Via Panciatichi 64, 50127 Firenze, Italy
[*e-mail:* righini@iroe.fi.cnr.it]

Outline of lectures:

Tuesday, 17 February 1998

Glasses for integrated optics: an historical perspective.

Fabrication processes of optical waveguides in/on glass:

- Vacuum deposition processes
- Ion-exchange.
-

Waveguide characterization techniques.

Wednesday, 18 February 1998

Sol-gel deposition process.

Design and fabrication of integrated optical components:

- Waveguide lenses and gratings
- Directional couplers.

Thursday, 19 February 1998

Active and nonlinear optical waveguides and components:

- Ion-exchanged waveguides in CdS_xSe_{1-x} -doped glasses
- Sol-gel CdS-doped thin-film waveguides
- Erbium-doped glasses / waveguides / amplifiers / lasers.

Chapter 1

INTRODUCTION TO INTEGRATED OPTICS: CHARACTERISATION AND MODELLING OF OPTICAL WAVEGUIDES

S. PELLI and G. C. RIGHINI

1. Introduction

The first demonstration of the laser in 1960 opened the way to the development of lightwave technology; then the production of low-loss optical fibers in the 70s made guided-wave optical communication systems become a reality. One of the problems associated with the development of long-haul systems was obviously related to the introduction in the transmission line of a number of repeaters, able to recondition and to reamplify the optical signal. The solution offered by conventional optics was unsatisfactory, due to the size and electrical power consumption, as well as to the critical dependence on temperature variations, mechanical vibrations, and the presence of moisture. The alternative first suggested by S.E. Miller, a researcher at Bell Laboratories, was to miniaturise the repeater, integrating all the components onto a single chip and interconnecting them via optical waveguides: the concept of integrated optics was born. More than two decades have passed since then: innovative research has been carried out on a vast spectrum of waveguide devices, and in recent years the goal of performing useful optoelectronic functions in a number of commercial applications has eventually come to fruition.

The bases of linear integrated optics, as concerns both propagation theory and the most common manufacturing technologies, are generally well established, and we can refer the interested readers to a number of books on the subject.[1-5] There is, however, a lot of activity still going on and, as a consequence, an increasing need of fixing some standardisation, especially concerning the definition and measure of the operational parameters of integrated optical waveguides, components and devices. The knowledge of waveguide characteristics such as propagation constant, chromatic dispersion, propagation loss, in-plane and out-of-plane scattering, is fundamental for assessing waveguide quality; providing a feedback of the characterisation results to the designers and to the people in charge of the fabrication process is the key to improving both manufacturing throughput and device performance.

The scope of the present paper is to review the basic measurement techniques which are employed for waveguide characterisation and to discuss an example of a numerical modelling approach, in the case of gradient-index waveguides.

S. Pelli and G. C. Righini - Research Institute on Electromagnetic Waves (IROE), CNR via Panciatichi, 64 - 50127 Firenze, Italy

Advances in Integrated Optics
Edited by S. Martellucci *et al.*, Plenum Press, New York, 1994

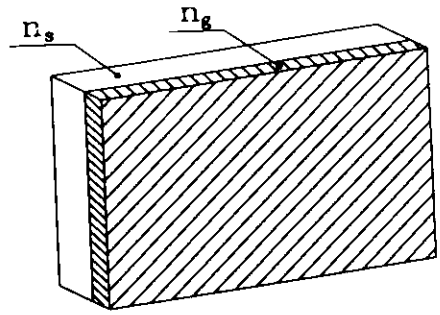

$n_s < n_g$

Fig. 1. The simplest structure of a planar waveguide; the guiding film has refractive index n_g higher than the substrate index n_s and the overclad index (here air, $n_c = 1$).

2. Waveguide Characterisation Using the Prism Coupler

The principle of optical confinement in a layer of dielectric material is based on the phenomenon of total internal reflection. The simplest planar waveguide, which is sketched in Fig. 1, is constituted by a three-layer structure: the guiding layer, with refractive index n_g , is supported by the substrate, having index n_s, and is covered by a cladding (which in this case is air, n_c=1). Provided that the refractive index of the film n_g is greater than n_s and n_c , any light ray entering the film in such a way that the angle Θ formed by the ray in the film with the normal to the film surface is greater than the critical angle for the interface with the smallest index difference, namely $\Theta > \arcsin(n_g / n_s)$, experiences total reflection at both the upper and lower interfaces: the light beam is thus trapped within the film. Those rays which, in addition, fulfill the phase condition:

$$2 k n_g d \cos\Theta - 2 \phi_a - 2 \phi_s = 2 m \pi \qquad (1)$$

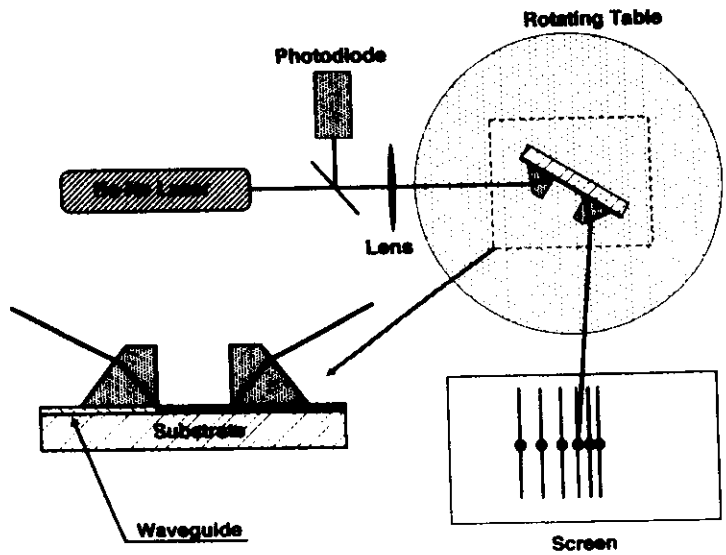

Fig. 2. Sketch of the two-prism experimental setup for the measurement of the effective index of guided modes from their optimum coupling angles (often referred to as m-line setup).

(where $k=2\pi/\lambda$, d is the film thickness, and m an integer which designates the mode number) correspond to stationary solutions and represent optical guided modes supported by the film. This is essentially a resonance condition; $-2\phi_a$ and $-2\phi_s$ are the phase changes suffered by the light beam at the film-air and film-substrate interfaces, respectively. Their values are given by the Fresnel coefficients and depend on the polarisation of the beam.[1b]

The practical excitation of a guided wave is one of the fundamental experimental procedures, both for the testing and for the real operation of an integrated optical device; the most straightforward methods are those of transverse coupling, in which the laser beam enters directly through an exposed cross-section of the waveguide (end-fire and end-butt coupling pertain to this class). When only the surface of the waveguide is accessible it is necessary to use longitudinal couplers such as prism, grating and taper couplers, in which the beam is incident obliquely onto the guide through a structure which provides the phase matching between the incident wave and a guided mode.

The prism-coupling technique[2b] is the most commonly used, because of some inherent advantages: high coupling efficiency (up to 80% for a Gaussian beam), applicability both to planar and to channel waveguides, and selective excitation of any of the guided modes. The main drawback is related to the critical effect on the coupling efficiency of a few factors: the form and position of the incident beam, and the adjustment of the air gap between the prism bottom base and the waveguide surface (gap thickness has usually to be less than 1 μm). The experimental setup includes a sample holder that allows the experimenter to regulate the pressure of the waveguide against the base of the prism in order to change the air gap thickness, and a precision rotating stage that allows the angle of the incident beam Θ' to be varied with respect to the waveguide.

In most cases, the excitation of the mode(s) of the waveguide is made evident by a visible streak along the propagation path, which is due to the guided light scattered out of the plane of the waveguide itself. Only in very low-loss guides, with attenuation below 0.2 dB/cm, will the streak be not so easily observed: a confirmation of the guided-wave excitation can be obtained by placing a second prism to outcouple light and by observing the light pattern onto a screen, as sketched in Fig. 2. If all the modes are excited at the same time (as occurs, for instance, when the incident beam is focused onto the prism), the pattern consists of *m-lines*, each one of them appearing as a brighter spot superimposed onto a weak line which extends along the direction parallel to the plane of the waveguide. Such a weak line is produced by in-plane scattering of the guided waves. By rotating the support table, one can preferentially excite one mode, so that the corresponding spot becomes the brightest one. If we do not use a focusing optical system, and the incident beam is collimated, we obtain the excitation of one mode at a time, and correspondingly a single line should be visible on the screen. Even in that case, due to scattering from topographical and/or index inhomogeneities, a portion of the power in the excited mode is coupled into the other modes and thus the entire set of m-lines is generally visible: the excited mode, however, produces a line on the screen which is much brighter than the other ones.

If the waveguide material is highly absorbing, the propagation length can be very short and it is not possible to use two prisms: a single symmetric, tent-shaped, prism is therefore used. In this case (see Fig. 3) we observe on the screen a bright spot corresponding to the reflected laser beam; when a waveguide mode is excited, part of the beam energy is coupled into the guide itself and absorbed so that a *dark line* appears in the centre of the spot.

Both of these experimental arrangements can be used to measure the propagation constants of the guided modes, since the propagation constant of the m-th mode is given by $\beta_m = k\, n_s \sin\Theta_m$, where Θ_m is defined according to Eq.(1) and it is correlated in a simple way to

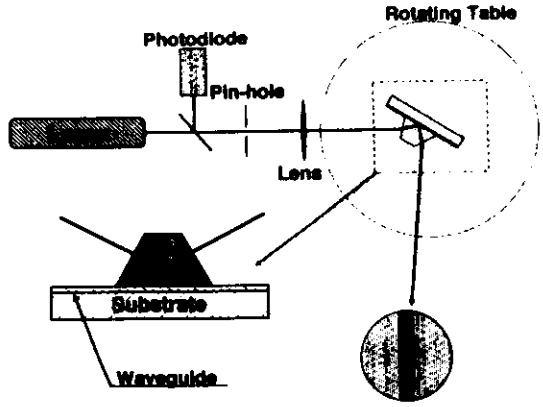

Fig. 3. Sketch of the single (tent-shaped) prism experimental setup for the measurement of the effective index of guided modes from their optimum coupling angles (often referred to as dark-line setup).

the external incidence angle Θ'. Thus, we can measure the angles Θ'_m corresponding to the excitation of the different modes and from these values calculate the respective propagation constants (or the effective indices $n_m = n_g \sin\Theta_m$). To have an idea of the measurement accuracy, the error in n_m is of the order of 10^{-4} when the synchronous coupling angles are determined with an accuracy of about 10^{-4} rad (20 seconds of arc).

In the case of a step-index waveguide, i.e. having a constant refractive index n_g , the refractive index and thickness of the guiding layer can be easily determined by measuring the effective indices of at least two modes and by using Eq.(1). When a waveguide is single-mode, one can solve the system of two equations in two variables by measuring either the TE and TM fundamental mode at the same wavelength, or the TE fundamental mode at two wavelengths. When the available measurements are more than two, iterative numerical procedures are generally used to increase the accuracy of the computation.

The same straightforward approach cannot be used for graded-index waveguides, namely those guides which are produced by diffusion processes (ion-exchange in glass, Ti-indiffusion in lithium niobate, ...) and have a refractive index distribution along the direction normal to the waveguide. This case is treated in Section 5.

3. Measurements of Other Waveguide Characteristics

A variety of specialised test and characterisation techniques can be employed in the evaluation of waveguides and components, especially when one is concerned not only with dielectric materials like glasses but with semiconductors as well. In the latter case the electronic properties are also very important, and measurements of the dopant profile, resistivity, carrier mobility etc. may be necessary. The techniques to be used include all the structural analysis developed for the characterisation of surfaces and solid-state materials (e.g. scanning and transmission electron microscopy, electron microprobe, ESCA, SIMS) plus optical techniques such as photoluminescence, Raman spectroscopy and so on.

Limiting ourselves to the most general problems, two simple and widespread measurements which are complementary to the prism-coupler characterisation are the direct observation of the mode profile and the evaluation of waveguide performance as a function of the wavelength. The setup for the former measurement is sketched in Fig. 4: the laser light is

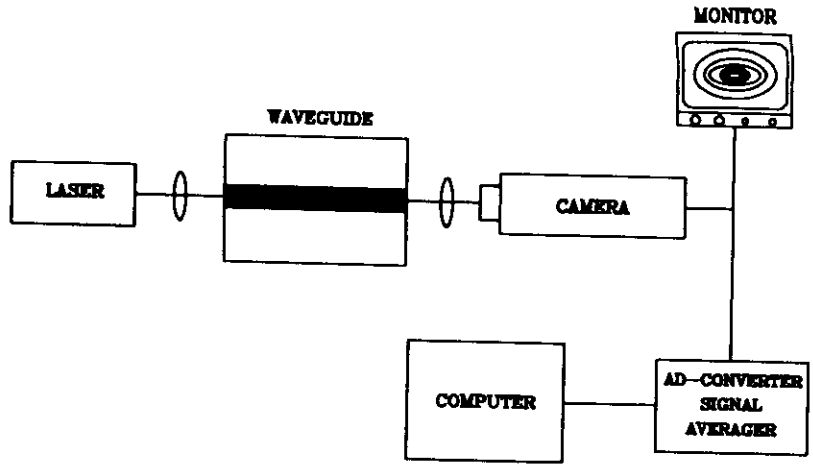

Fig. 4. Measurement of the modal field distribution in a channel waveguide.

end-fire coupled to the waveguide and the output face is imaged by an optical system onto a vidicon or CCD camera; a computer allows a detailed analysis of the image and therefore of the intensity profile of the mode. This knowledge is quite important to check the quality of the waveguide (this is especially true for channel waveguides) and also to properly model devices such as directional couplers and Mach-Zehnder interferometers; the mode profile is also a critical parameter for efficient coupling of the waveguide to external optical fibers. Moreover, from observation of the profile of the fundamental mode it is also possible to calculate the refractive index profile using the scalar wave equation.[6]

The experimental arrangement shown in Fig. 5 refers to the measurement of the transmission of the waveguide as a function of the propagating wavelength, using a white-light source and a monochromator in front of the detector. This measurement allows one to determine the range of wavelengths in which the given material structure has acceptable losses and can therefore be employed; it can also be important for analyzing whether the film has the same properties as the bulk material or if changes have been produced during the waveguide fabrication process. By the same technique, the spectra of species adsorbed on the film or of a fluid in contact with the film can be obtained.

Both these techniques have the common disadvantage that the waveguide end faces have to be accurately polished in order to permit efficient end-fire in/out coupling: the processing of the sample edges is often one of the most critical and time-consuming operations in the manufacture of waveguides and simple components.

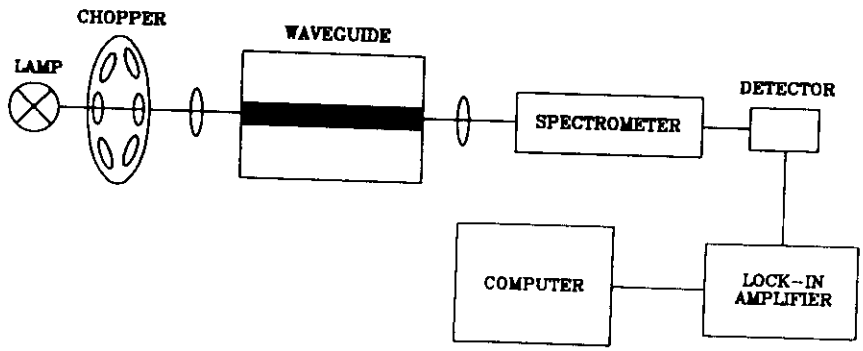

Fig. 5. Measurement of the spectral transmittance of a channel waveguide.

4. Measurements of Transmission Losses and Scattering

Visual observation of the light streak in the waveguide can give a quick but non-quantitative measure of the propagation loss coefficient a. As has already been said, the streak is very weak and difficult to observe in films with loss below 0.2 dB/cm, while in high-loss films ($\alpha > 5$ dB/cm) an approximate value of the loss can be inferred from the measurement of the length L (cm) of the streak itself. Since the dynamic range of the eye is of the order of 27 dB, the loss α in dB/cm can be evaluated as $\alpha = 27/L$. In the intermediate range of propagation losses it is necessary to perform a direct measurement; moreover, in order to provide feedback to the manufacturers it is often very useful to separate the contribution of the absorption from that of bulk or surface scattering. Most of the techniques briefly described in the following measure the total losses, i.e. due to both absorption and scattering. A very accurate measurement of absorption-only losses is possible by calorimetric techniques,[7] in which the temperature rise of a sample during laser irradiation is detected. The results of measurements in out-diffused lithium niobate waveguides show that absorption losses are of the order of 0.02 dB/cm, almost two orders of magnitude smaller than the total losses, thus demonstrating that, at least in the samples considered, scattering is the limiting mechanism in waveguide transmission. The authors have estimated that the minimum waveguide absorption coefficient measurable for samples with optimum geometry is on the order of 10^{-4} dB/cm.

4.1. Prism-Coupler Loss Measurements

One of the simplest and at the same time very effective methods of measuring the total loss is based on the use of two prisms,[8] according to the sketch depicted in Fig. 6. The intensity measured by the detector is plotted as a function of the propagation length Z, which can be varied by keeping prism 1 fixed and moving prism 2. The most critical factor of this nondestructive method is that the outcoupling efficiency should remain constant at all the different positions of prism 2: this aim is sometimes reached more easily by using between the prism and the waveguide a liquid with refractive index slightly lower than that of the guide. The limit of accuracy of the method is approached when the film has losses lower than 0.2 dB/cm, although some authors claim that the error can be kept down to ± 0.01 dB/cm. To achieve such results, however, the complexity of the measurement increases, and a good deal of operator skill is necessary.

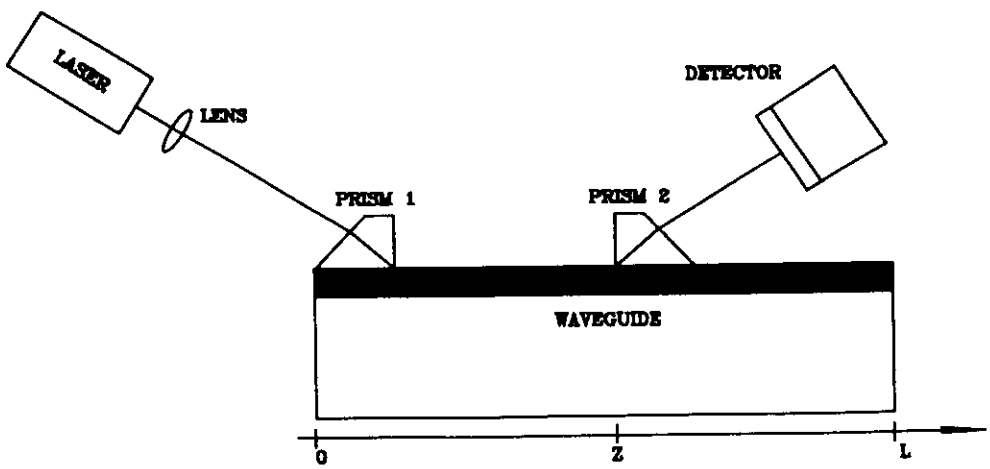

Fig. 6. Measurement of the transmission losses in a planar waveguide by the two-prism sliding method.

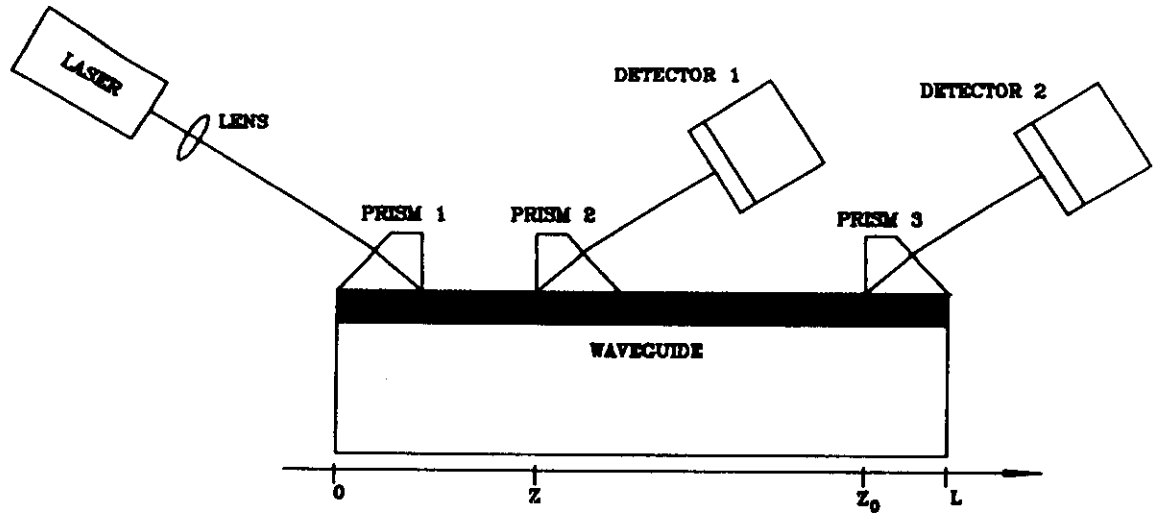

Fig. 7. Accurate measurement of the transmission losses in a planar waveguide by the three-prism sliding method.

A substantial relaxation of the constraints on the stability of the efficiency of the outcoupling prism is obtained when one uses the setup shown in Fig. 7, where three prisms are independently clamped to the guide. In this case both the prisms 1 and 3 are kept fixed, and prism 2 is moved along the guide. It has been shown[9] that, by measuring the intensity at detector 2 when prism 2 is removed and subsequently the intensities at detectors 2 and 1 for the various positions of the prism 2, an expression for the intensity of the guided light as a function of propagation length can be derived which is independent of the outcoupling efficiency of both prisms 2 and 3. Thus, even if in principle this technique is not any more accurate than the two-prism technique, it is more practical and rapid. An accuracy of the order of ± 0.01 dB/cm can now be achieved without taking particular care with the prism clamping pressure and without the use of matching fluids.

Another experimental arrangement, which is equivalent to the three-prism setup, is shown in Fig. 8; here, the light which was not coupled out by prism 2 and continued to

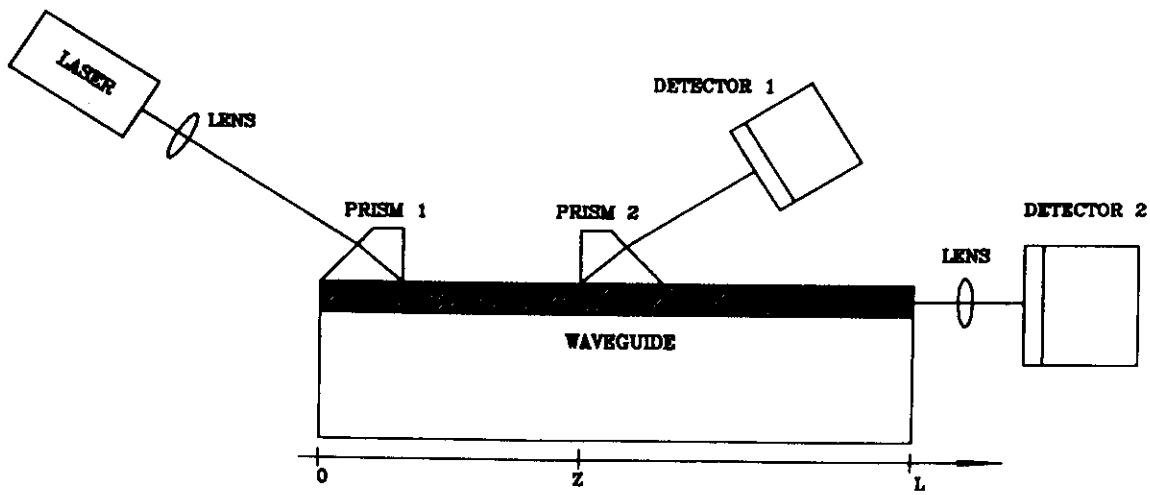

Fig. 8. Combination of the prism-sliding and end-fire techniques to measure the transmission losses of a planar waveguide.

propagate inside the waveguide is collected by a lens and measured by detector 2. This arrangement, which requires polishing of the output face of the guide, can be useful for short-length samples, where the positioning of three prisms and the movement of the intermediate one can be quite difficult.

4.2. Scattering-Detection Techniques

A simpler technique for measuring losses is one using a fiber optic probe,[10] according to the setup in Fig. 9. If we assume that the scattering centres in the waveguide are uniformly distributed and that the intensity of the scattered light in the transverse direction is proportional to the number of scattering centres, we can take the intensity of the scattered light along the guide (i.e. the brightness of the light streak) as proportional to the guided-light intensity at each point. Thus, to derive the plot of transmitted intensity versus propagation length it is sufficient to detect the scattered light by means of an optical fiber which is accurately moved along the streak, while keeping constant both its angular position and its distance from the waveguide. The use of the fiber probe in combination with a microscope allows better control of the distance, thereby improving the overall accuracy.

A variation of the method in which the distance does not need to remain constant, consists in moving the fiber probe normally to the guide until it just touches the guide surface and then withdrawing it until it just loses contact; the distal end of the fiber is connected to a detector, whose output goes to a chart recorder. By repeating this kind of measurement at several points along the streak and by analysing the resulting trace on the recorder chart, it is possible to measure attenuations as low as 0.3 dB/cm.[11]

The assumptions given above concerning waveguide uniformity are correct for most of the waveguides actually employed in device fabrication; an indication of the accuracy of a specific measurement can be given by the extent of the scatter of data points around the best-fit straight line (in a logarithmic-scale plot): the larger the extent, the lower the accuracy. By this method losses down to 0.2 dB/cm can be measured, with an error of ± 0.1 dB/cm.

All the previous techniques cannot be easily employed to measure losses of devices, be they Y-branches, directional couplers, or bidimensional components such as waveguide lenses. To overcome this difficulty, the scattering-detection method can be modified by using, instead of the fiber probe, a video camera onto which the image of the entire circuit is projected.[12]

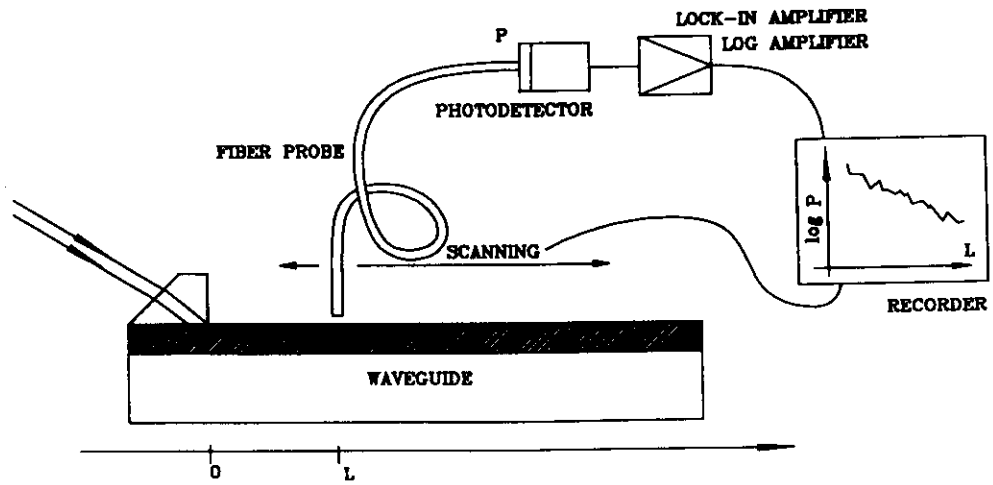

Fig. 9. Measurement of the waveguide transmission losses by the scattering detection method: here an optical fiber is used to collect the light scattered out of the guide.

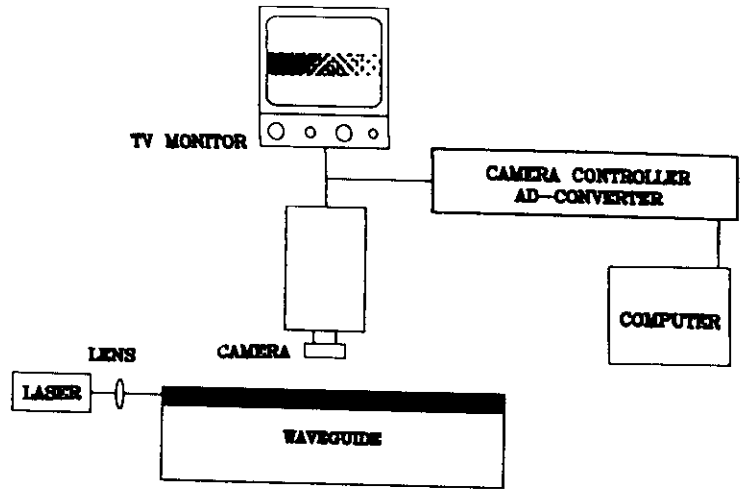

Fig. 10 This measurement technique is analogous to that sketched in Fig. 9, except that here a TV camera is used to collect scattered light instead of an optical fiber.

Easily available software allows the analysis of the image, as well as the evaluation of the propagation loss and the insertion loss of a component, if desired. In the setup of Fig. 10, end-fire coupling is assumed but the camera-detection technique can obviously also be used together with an input prism coupler. To improve the sensitivity of this technique, and to measure losses as low as 0.1 dB/cm, the use of a fluorescent overlayer has been suggested[13]; fluorescent light is emitted by the Nile Blue A perchlorate dye through the linear Stokes process, and therefore the fluorescent light intensity is proportional to the guided intensity. This method, however, requires special preparation of the sample and is not applicable to high-index materials; moreover, its use for measurements at near-infrared wavelengths would require the search for other suitable dyes.

A common advantage of all the scattering-detection methods is that they are not only nondestructive but also noncontacting; moreover, the optimum conditions for loss measurements have also been determined through an extensive set of measurements.[14]

Since scattering losses are usually dominant in dielectric waveguides, the assumption that absorption and radiation losses are negligible is acceptable, and in this approximation the above measurements of the scattered loss can be taken as equivalent to the measurement of the total loss. If, however, one is interested in deriving some specific information on the scattering characteristics of the waveguide, the fiber-probe or camera measurements can be repeated as a function of the mode and the collecting angle; in other words, for a given propagating mode one can move the detector in order to make an angular scanning in the plane containing the light streak and perpendicular to the guide surface: the position and size of the scattering centres, as well as the correlation length, can be thus evaluated.[15]

Additional useful information for the design of specific devices (e.g. for the design of an integrated optical spectrum analyser) is represented by the amount and the angular distribution of the in-plane scattering, namely of the light which is scattered by the waveguide inhomogeneities inside the plane at angles φ with respect to the propagation direction (see Fig. 11). For this measurement, the output beam is spatially Fourier-transformed by a lens, and the light distribution in the Fourier plane is measured by scanning it with a slit and photodetector (an image sensor can also be used to get the entire transform distribution): a plot of the scattered intensity vs the angle φ can be obtained, since the scanning coordinate y is related in a simple way to the angle φ.[16] Measurements on high-quality lithium niobate waveguides have shown that the scattering level can be as low as -55 dB at an angle $\varphi = 0.5°$ for a propagation length of 20 mm.

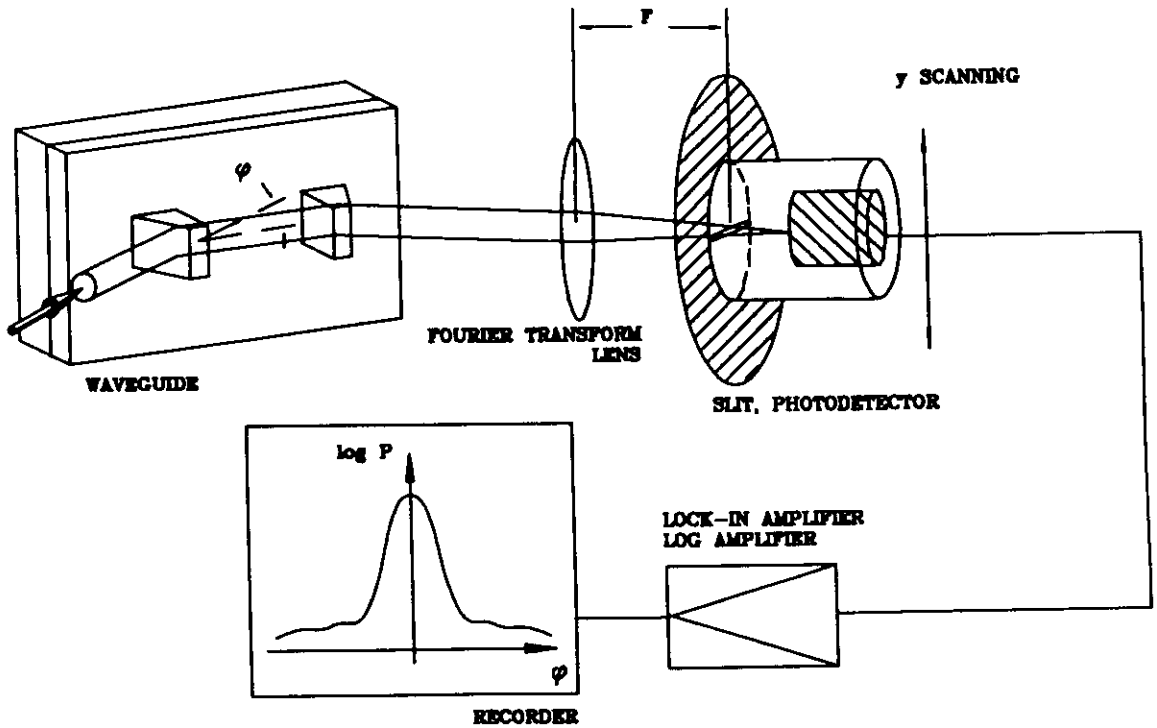

Fig. 11. Measurement of the in-plane scattering characteristics of a planar waveguide.

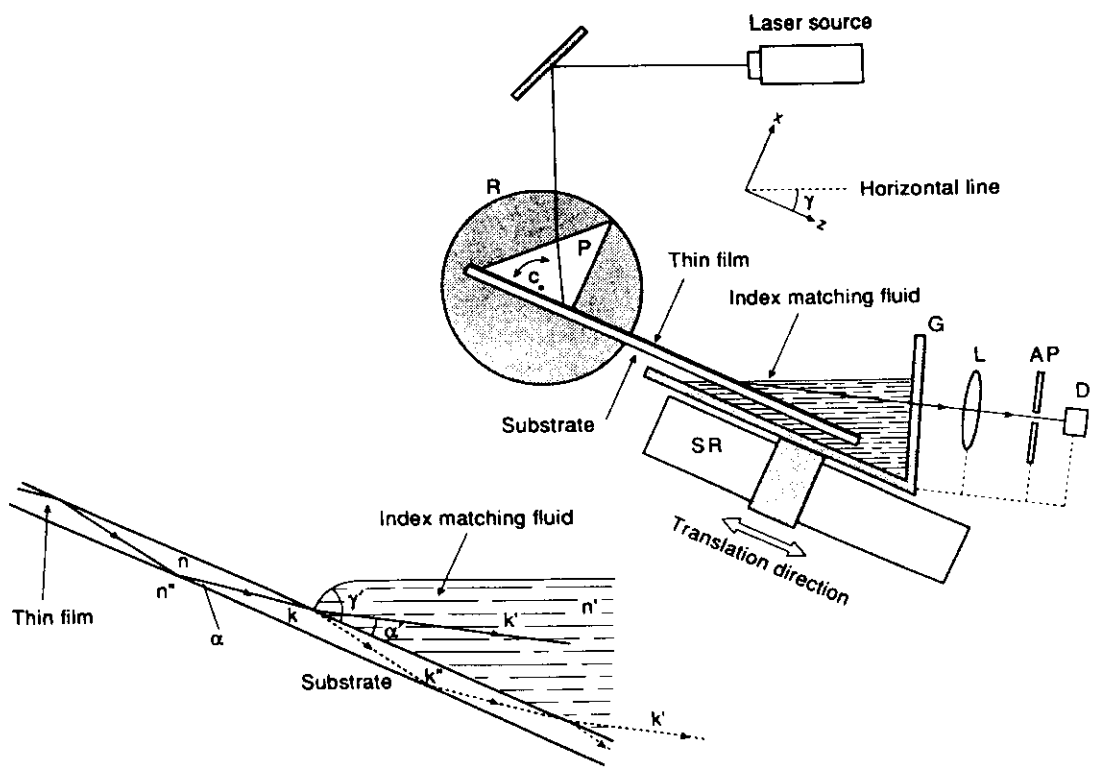

Fig. 12. Experimental setup for precision measurements of the optical attenuation in a waveguide, based on the outcoupling of guided light into a liquid with refractive index n' slightly higher than (n) of the guiding film. R, rotation stage; P, prism coupler; G, glass cell; L, focusing lens; Ap, aperture; D, photodiode; SR, sliding rail.

4.3. Precision Measurements of the Waveguide Losses

Because the quality of the materials and the fabrication processes have continued to improve, the propagation loss in a passive waveguide may well be quite small, below 0.1 dB/cm; it is therefore necessary to use more accurate measuring methods, without increasing their complexity. In a very recent paper an experimental technique has been reported, which is claimed to offer repeatability and accuracy of the measured attenuation typically better than 5%, even for measurements of losses below 0.1 dB/cm with less than 1cm-long guiding paths.[17] The experimental setup is shown in Fig. 12. A collimated laser beam is coupled into the thin-film waveguide by a prism coupler P which is mounted onto a rotation stage R. A V-shaped glass cell G, filled with a fluid having refractive index n' slightly higher than that of the guiding film, is mounted onto the sliding rail SR and can be moved in a direction parallel to the guide. As the film is immersed into the fluid, the guided beam does not undergo anymore total reflection at the upper interface and all the guided light is eventually outcoupled into the fluid, in the same direction (corresponding to the wave vector **k'**). The light emerging from the glass cell is focused by the lens L through the aperture AP and collected by the detector D. By translating the glass cell with respect to the sample, i.e. by immersing the waveguide for different lengths, it is possible to measure the guided-light intensity as a function of the propagation distance. Values of loss as low as 0.05 dB/cm have been measured, with standard deviation of the data below 0.01 dB.

4.4. Photothermal Deflection Technique

Another class of noncontacting loss measurement is that based on the photothermal deflection (PTD) effect. When some energy of a laser *pump* beam is absorbed by a material, a thermal gradient is produced, which in turn produces a refractive-index gradient in the absorbing and surrounding media. The PTD technique is based on the measurement of the refraction of a second laser beam, the *probe* beam, induced by such an index gradient.[18] Both crossed-beam and collinear-beam configurations are possible; in the former,[19] which is sketched in Fig. 13, the probe beam almost perpendicularly crosses the waveguide that is heated by the pump laser coupled into the waveguide itself. In the collinear configuration[20,21] the probe beam is parallel to the film surface and is refracted by the refractive index gradient induced in the gas (air) region close to the surface of the sample. The crossed-beam configuration was used[19] to measure the propagation loss of K-exchanged glass waveguides, which turned out to be 1.2 ± 0.2 dB/cm. Both the pump and probe beams were from He-Ne lasers at 633 nm: the probe beam was focused to a spot on the waveguide surface, and its deflection was detected by a bicell photodetector placed below the sample; the differential voltage of the bicell was amplified and separated from the noise by using a chopper and the lock-in detection. It was calculated that using 3 mW of pump power the induced index change was less than 10^{-5} : this gives an idea of the sensitivity of the method, which, according to some authors, in optimum conditions should be able to measure losses as low as 10^{-3} dB/cm.

5. Modelling of Graded-Index Optical Waveguides

Efficient numerical tools are necessary to simulate the operation of guided-wave components and devices, in order to properly design them and avoid "trial and error" steps towards their optimisation.

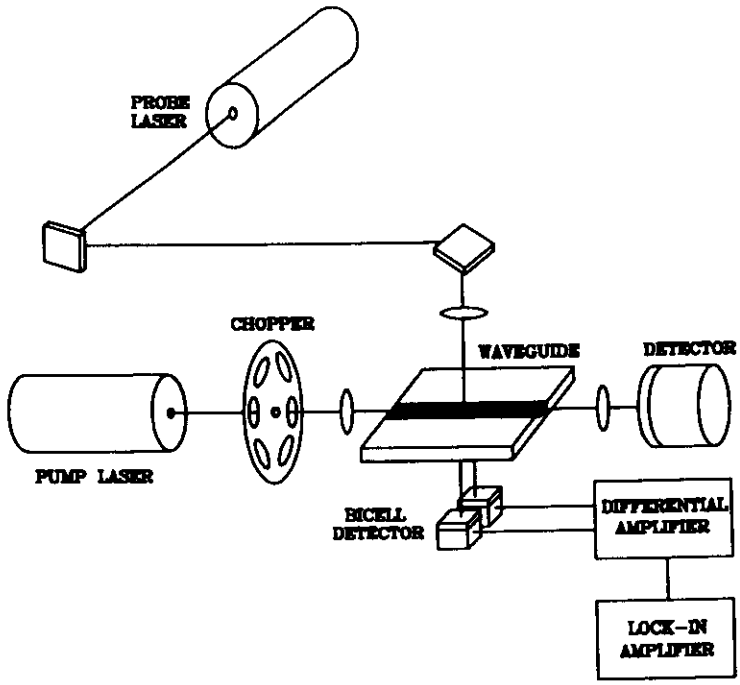

Fig. 13. Experimental setup for the photothermal deflection measurement in the crossed-beam configuration.

An example of a well known and widely used numerical algorithm for the modelling of integrated optical circuits is the one designated as the Beam Propagation Method,[22] which can be applied to both two- and one-dimensional guiding structures. In order to use these simulation tools, however, one of the most important parameters required is the refractive index profile of the guiding structure, which strongly affects the form of the guided field distribution; it can be of crucial importance especially in the design of nonlinear devices. It is therefore very important to determine the refractive index profile as a function of the process parameters used in the realisation of the waveguiding device. As mentioned in Section 2, the case of step-index waveguides permits a rather simple treatment; in the following discussion, we will consider some of the problems associated with the fabrication process of a very widely used class of graded-index waveguides, namely those produced by ion-exchange in glass, and with the reconstruction of the index profile from the experimental measurements of effective indices.

5.1. Characteristics of the Diffusion Process in Glass

Ion-exchange is the most widely used technique to obtain optical waveguides in various substrates such as glasses or lithium niobate.[23,24] Therefore it can be worthwhile to briefly recall the fundamental aspects of the dynamics of ion-exchange which can allow one, by assuming that the index distribution is proportional to the concentration of the exchanged ions in the substrate, to forecast the form of the refractive index profile.

The interdiffusion process between the metallic ions in the substrate and those in the salt melt is described by the Nernst-Planck equation[25]

$$F = -D\left(\nabla C - zC\frac{f}{RT}E\right) \tag{2}$$

where F is the ion flux, C is the concentration of any of the mobile ions normalised to the total concentration of the exchanged ions, E is the local electric field generated by the concentration gradient, D is the diffusion coefficient (assumed to be independent of the concentration), z is the ion valence, f is the Faraday constant, R is the gas constant and T is the temperature.

In one dimension, considering a one to one exchange of two ion species a and b, with $F_a=-F_b$ it can be proved that

$$\frac{\partial C_a}{\partial t}=\frac{\partial}{\partial x}\left(\frac{D_a\ \partial C_a}{1-\alpha C_a \partial x}\right) \tag{3}$$

with

$$\alpha=1-\frac{C_a}{D_a} \tag{4}$$

Under these assumptions the solution of Eq. (3) can be written as

$$C_a(x,t)=C_{\infty}\mathrm{erfc}\left(\frac{x}{2\sqrt{Dt}}\right) \tag{5}$$

where t is the diffusion time and D is defined by

$$D=\frac{D_aD_b}{D_aC_a+D_bC_b}=\frac{D_a}{1-\alpha C_a} \tag{6}$$

Hence, we would expect to find in most cases refractive index profiles of the form

$$n(x)=n_s+(n_0-n_s)\mathrm{erfc}\left(\frac{x}{d}\right) \tag{7}$$

where n_s is the substrate index, n_o is the surface index and d is the exchange depth parameter. However, it can be shown that this holds true only when the ion depletion of the salt melt near the substrate surface during the exchange process can be neglected; in any other case the expected profile form would be a half-gaussian profile. We will see in the next sections how these models can be compared with practical cases.

5.2. *WKB Method*

Analysis of the guided wave propagation can be carried out in the most complete way by starting from Maxwell equations, with the proper boundary conditions.

The resulting wave equation:

$$\frac{\partial^2 E_y}{\partial x^2}+\left[k_0^2\left(n_f^2-n_e^2\right)-k_0^2\left(n_f^2-n^2(x)\right)\right]E_y=0 \tag{8}$$

however, can be explicitly solved only for few special systems (among which are step-index waveguides); an approximate approach has to be followed for graded-index structures.

In particular, the WKB approximation (*Wentzel-Kramers-Brillouin*, developed first in quantum mechanics)[26,27] can be a useful tool to handle this kind of problem, provided that the term $k_0^2(n_f^2 - n^2(x))$ varies slowly over a distance λ.
Under the WKB approximation the modal dispersion equation becomes

$$k_0 \int_0^{x_t} \sqrt{n^2(x) - n_e^2(m)}\ dx = m\pi + \phi_a + \frac{\pi}{4} \tag{9}$$

$$n(x_t(m)) = n_e(m) \tag{10}$$

$$\phi_a = \sqrt{\frac{n_e^2 - 1}{n_f^2 - n_e^2}} \tag{11}$$

$n_e(m)$ being the effective index of the mode of order m, $n(x_t(m))$ being the so-called "turning points" (from their physical meaning of maximum penetration depth of the guided light in a ray optics description) and ϕ_a is half the phase shift caused by the reflection at the air-waveguide boundary.

In order to obtain the parameters that describe the refractive index profile of the waveguide, namely its mathematical form, the surface index n_o and the diffusion depth d, it is therefore necessary first to obtain the effective indices of the guided modes of the waveguide, given the substrate refractive index and the operational wavelength.

The effective indices can be measured by means of the experimental setup shown in Figs. 2 and 3, as already explained in Section 2.

Unfortunately, neither Eq. (9) cannot be solved analytically, so many numerical methods[28] have been proposed; here we will concentrate on two of them.

5.3. *Dispersion Curves Method*

This method, proposed by Yip and Albert,[29] requires the choice of a definite profile form, whose parameters must be fitted to the experimental data.
With the change of variable:

$$x' = \frac{x}{d} \tag{12}$$

Eq. (8) gives:

$$d = \frac{k\left(m\pi + \phi_a + \frac{\pi}{4}\right)}{\int_0^{x_t} \sqrt{n^2(x) - n_e^2(m)}\ dx} \tag{13}$$

This expression allows one to directly calculate the exchange depth, once the effective indices of the waveguide and all parameters of the index profile are given. Hence, in order to obtain the form of the index profile, it is sufficient to make the change of variable (12) and then, starting from a value slightly higher than that of the 0th-order effective index, increase the value of the surface index, until the sum of the squares of the differences between the

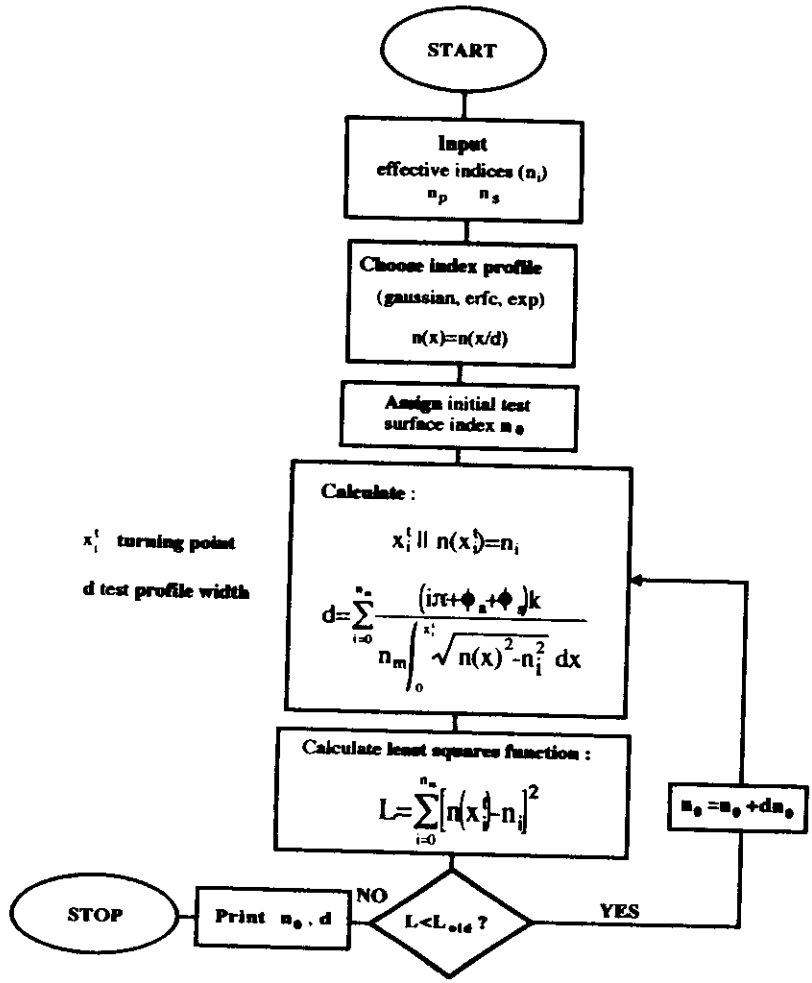

Fig. 14. Flow-chart of a program capable of computing the refractive index profile of a graded-index waveguide following the method proposed in Ref. 29.

experimental effective indices and the ones calculated by means of Eqs. (9-13) reaches a minimum. In Fig. 14 the flow-chart of a program capable of such a task is shown.

As trial profiles exponential, half-gaussian, erfc or second-order polynomial functions can be chosen. The most appropriate profile is usually the one which minimises the square sum mentioned above.

After this step, the modal dispersion curves are computed for a definite set of waveguides fabricated under the same conditions, using as surface index the mean of the surface indices of the whole set of waveguides considered. Agreement between the experimental data and the average dispersion curves is then checked as a final control on both the homogeneity of the set of waveguides and of the goodness of the fit process as a whole.

These dispersion curves are very important in the design of IO components, as they define the relationship between the effective indices and the thickness of the waveguides. Another relation which can be verified is the one between exchange depth and time, as shown in Fig. 15. As can be seen in the figure, the behaviour of the depth as a function of the exchange time follows quite well the theoretical square root function of Eqs. (5, 7), even for relatively long exchange times. The knowledge of this relation allows one to produce a waveguide of predetermined thickness and hence, by using the dispersion curves, with a priori well-defined propagation constants.

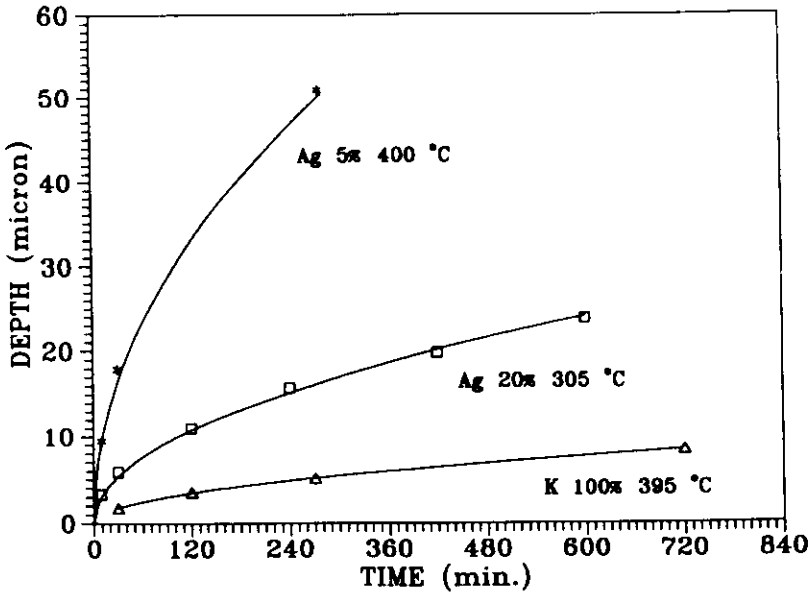

Fig. 15. Exchange depth vs. exchange time for various ion-exchange processes in a soda-lime glass.

5.4. Chiang Method

In this case, no profile is chosen at the beginning of the computation. The aim of this method, developed by K.S. Chiang,[30] is actually not to find any particular mathematical function as refractive index profile, but to determine through a recursive process an "empirical" index profile.

First of all, the experimental effective indices are interpolated with a polynomial function. This is a somewhat crucial step, because great care must be taken in the choice of the polynomial degree; too high a degree could for example lead to the enhancement of oscillation in the interpolated polynomial, caused by random errors in the experimental effective indices.

It is easy to show that by putting $x_i(m)=0$ in Eq. (8) the surface index is obtained as the effective index of the non-physical -0.75 order mode; thus, it is sufficient to extrapolate the interpolated polynomial to immediately obtain the surface index. Of course, as this parameter is the result of an extrapolation, it is very sensitive to the accuracy of the interpolation, but as this process is very straightforward this method becomes very attractive. In order to determine the entire index profile, the effective index profile is then approximated by a staircase function, which, once substituted in the integral of Eq. (9), transforms the integral into a series of sums, which are easier to deal with. In Fig. 16, where the flow chart of the whole process is shown, N_i's are successive sampling points of the interpolated effective index profile, whereas $\overline{N}_i$'s are the means between two successive sampling points. The recursive formula shown in Fig. 16 can then be derived and the whole profile computed. As a final step, the empirical profile can be fitted to a mathematical analytical function like the ones mentioned in the previous section, in order to have a result which is easier to treat in the following design processes.

5.5. Experimental Results

In order to provide an assessment of the agreement between the two numerical algorithms, the data for various ion-exchanged waveguides were processed using both methods, and the results are shown in Figs. 17 and 18.

The two figures correspond to different ion-exchange processes in the same soda-lime glass substrates, Fig. 17 referring to a 20% Ag^+/Na^+ exchange and Fig. 18 to a 100% K^+/Na^+ exchange.

In both figures the experimental data, the profiles obtained by the dispersion curve method, the "empirical" profile obtained by Chiang's method and the fit of an analytical function to the profile resulting from Chiang's algorithm are shown .

As it can be seen, the agreement between the two methods is fairly good, especially when considering the two fitted analytical profiles. In both cases, a gaussian profile seems to fit the experimental data best. This is not always the case, however; for example in Fig. 19, where the case of a Cs^+/K^+ exchange waveguide is considered, the proper choice consisted of a erfc type profile, as suggested by Eq. (5).

We compared the results in terms of surface index and exchange depth obtained by means of the two methods for a set of 20%, 5% Ag^+/Na^+ and K^+/Na^+ exchanged waveguides. Apart from a few exceptions the agreement is quite good.

In order to gain more confidence in these numerical methods, however, it is useful and sometimes necessary to make direct measurements either of the concentration of exchanged

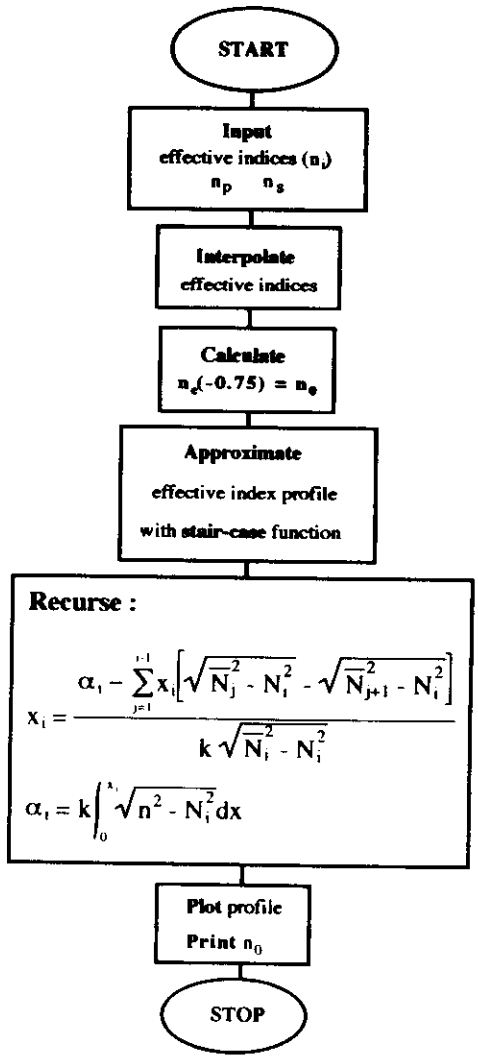

Fig. 16. Flow-chart of a program capable of computing the refractive index profile of a guided-index waveguide following the method proposed in Ref. 30.

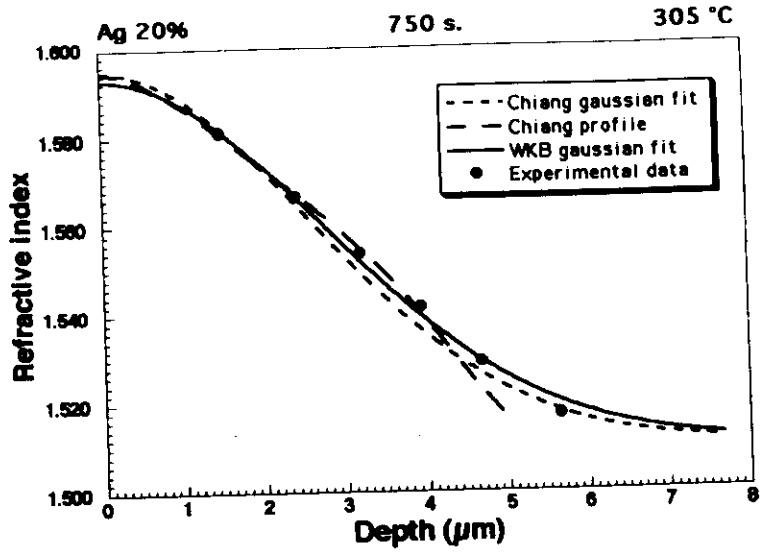

Fig. 17. Comparison of the reconstructed refractive index profiles of a waveguide produced by 20% Ag^+/Na^+ ion-exchange, as obtained by using the two numerical methods described in the text.

ions as a function of depth (which can be accomplished by such techniques as Rutherford Back Scattering or SIMS)[31, 32] or of the refractive index itself by interferometric techniques.[33] Unfortunately, these techniques are generally difficult of implementation; the limited number of tests we have been able to perform, however, tend to support quite well the simulation results.

6. Conclusions

A number of valuable characterisation techniques have been developed for the accurate measurement of the various parameters of an optical waveguide, from the thickness and refractive index to absorption and scattering losses. Most of the experimental techniques briefly

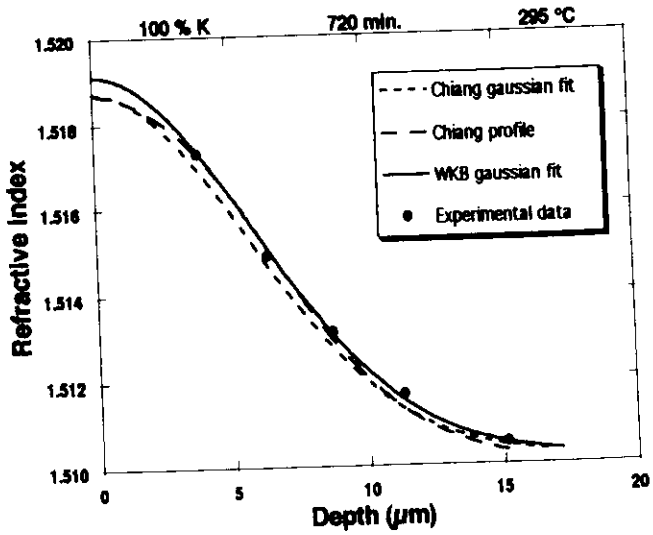

Fig. 18. Comparison of the reconstructed refractive index profiles: here the waveguide was obtained by 100% Cs^+/K^+ ion-exchange.

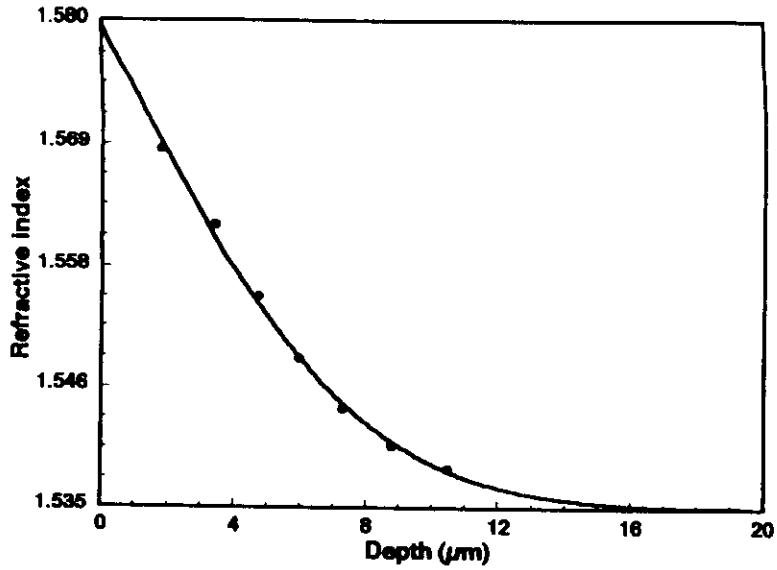

Fig. 19. Reconstructed refractive index profile of a 100% Cs^+/K^+ ion-exchanged waveguide, obtained by means of the dispersion curves method; in this case an erfc profile is used.

mentioned in the previous sections apply to any kind of waveguide structure, but it may be worthwhile to assess the best technique for the specific sample to be investigated.

It also should be emphasized that this summary is not at all inclusive, as the ingenuity of researchers has led to the development of a much larger number of measurement techniques, some of which, however, are suitable or cost-effective only in very specific cases.

Similar observations can be made concerning to the proposed modelling techniques. Here only two simple numerical techniques, easily implemented on a personal computer, have been summarised, which allow one to reconstruct the refractive index profile of graded-index waveguides. The results obtained by these methods, however, are accurate enough to give a good description of the realised waveguides and to be used as input data to more sophisticated modelling programs, e.g. based on the *Beam Propagation Method* or finite differences, which in turn allow one to optimise the design of discrete integrated optical components as well as to simulate the operation of more complex guided-wave circuits.

ACKNOWLEDGEMENTS. The financial support of the CNR Special Project TEO (Electro-Optic Technologies) is gratefully acknowledged.

References

1. T. Tamir, Editor, "Integrated Optics", Springer-Verlag, Berlin (1975); b) see Chapter 2 (Theory of dielectric waveguides).
2. R.G. Hunsperger, "Integrated Optics: theory and technology", Springer-Verlag, Berlin (1982); b) see Chapter 6 (Waveguide input and output couplers).
3. H. Nishihara, M. Haruna and T. Suhara, "Optical integrated circuits", McGraw-Hill, New York (1989).
4. M.A. Mentzer, "Principles of Optical Circuit Engineering", Marcel Dekker, New York (1990).
5. S.I. Najafi, "Introduction to glass integrated optics", Artech House, Norwood (1992).
6. L. McCaughan and E.E. Bergmann, J. Lightwave Techn. LT-1: 241-244 (1983).
7. S.D. Allen, E. Garmire, M. Bass and B. Packer, Appl. Phys. Lett. 34: 435-437 (1979).

8. H.P. Weber, F.A. Dunn and W.N. Leibolt, Appl. Opt. 12:755-757 (1973).
9. Y.H. Won, P.C. Jaussaud and G.H. Chartier, Appl. Phys. Lett. 37:269-271 (1980).
10. S. Dutta, H.E. Jackson, J.T. Boyd, R.L. Davis and F.S. Hickernell, IEEE J. Quantum Electron. QE-18:800-805 (1982).
11. N. Nourshargh, E.M. Starr, N.I. Fox and S.G. Jones, Electron. Lett. 21:818-820 (1985).
12. Y.Okamura, S. Yoshinaka and S. Yamamoto, Appl. Opt. 22:3892-3894 (1983).
13. Y.Okamura, S. Sato and S. Yamamoto, Appl. Opt. 24:57-60 (1985).
14. C. De Bernardi, A. Loffredo and S. Morasca, Proc. SPIE 651:259-262 (1986).
15. M. Imai, Y. Ohtsuka and M. Koseki, IEEE J. Quantum Electron. QE-18:789 (1982).
16. D.W. Vahey, Proc. SPIE 176:62 (1979).
17. C.-C. Teng, Appl. Opt. 32:1051-1054 (1993).
18. A.C. Boccara, D. Fournier, W. Jackson and N.M. Amer, Opt. Lett. 5:377 (1980).
19. R.K. Hickernell, D.R. Larson, R.J. Phelan, Jr. and L.E. Larson, Appl. Opt. 27:2636-2638 (1988).
20. H. Xue-bo and C. Wen-bin, Measurements of the absorption distribution of optical thin films by scanning photothermal microscopy, in "Photoacoustic and Photothermal Phenomena", P.Hess and J.Pelzl, Eds., Springer-Verlag, Berlin (1988).
21. C.Sibilia, M. Bertolotti, L. Fabry, G. Liakhou and R. Li Voti, Thermal diffusivity measurements in multilayers through photodeflection method: theory and experiments, in "Quantum Electronics and Plasma Physics: 6th Italian Conference", G.C.Righini, ed., Editrice Compositori, Bologna (1991).
22. J. van Roey, J. van der Donk and P. E. Lagasse, J. Opt. Soc. Am., 71:803 (1981).
23. T. Findakly, Opt. Eng., 24:780 (1985).
24. G. Stewart, C. A. Miller, P.J.R. Layboum, C.D.W. Wilkinson and R. M. de la Rue, IEEE Jour. Quan. El, 13:192 (1977).
25. J. Breton and P. Laborde,Proc. SPIE, 1128:80 (1989).
26. H.Nishihara, M. Haruna and T. Suhara, Optical waveguide theory, in: "Optical Integrated Circuits", McGraw Hill, USA (1985).
27. L. I. Schiff, Approximation methods for bound states, in: "Quantum Mechanics", Mc Graw-Hill, Singapore (1985).
28. J. M. White and P. F. Heidrich, Appl. Opt., 15:151 (1976).
29. J. Albert and G. L. Yip, Appl. Opt., 24:3692 (1985).
30. K.S. Chiang, Jour. Light. Tech., 3:385 (1985).
31. G. C. Righini, S. Pelli, R. Saracini, G. Battaglin and A. Scaglione, Proc. SPIE, 1513:418 (1991).
32. R. A. Betts, C. W. Pitt, K. R. Riddle and L. M. Walpita, Appl. Phys., A 31:29 (1983).
33. R. A. Betts, F. Lui and T. W. Whitbread, Appl. Opt., 30:4384 (1991).

MICROFABRICATION TECHNOLOGIES FOR INTEGRATED OPTICAL DEVICES

G.C. Righini and M.A. Forastiere

Optoelectronics and Photonics Department (IROE CNR)
"Nello Carrara" Electromagnetic Waves Research Institute
Via Panciatichi 64, 50127 Florence, Italy

1. INTRODUCTION

Microelectronics and Integrated Optics (IO) share most of the microfabrication technologies, in particular micropatterning. Fabrication processes of IO devices, however, are subject to specific requirements, imposed by the nature of light confinement, which are often tighter than the ones usually adopted in microelectronics.

As a matter of fact, optical waveguiding structures are usually a few centimeters long, but at the same time their transverse dimensions must be of the order of the guided-light wavelength (i.e. ~ 1 μm); this generates a number of problems, mainly connected with the necessity of keeping propagation losses as low as possible. As an example, low propagation loss and highly tolerant fabrication processes are generally not easily compatible with high-Δn structures (i.e. structures where the refractive index difference between the guiding layer and the surrounding media is larger than 0.1), because this implies a further reduction in waveguide dimensions (e.g. down to sub-micrometer size). While this may be an advantage from the point of view of compatibility with microelectronics IC technology (especially in view of integrated optoelectronics silicon wafers), it is clear that high-Δn guides suffer very high coupling loss (even larger than 3 dB/facet) with input/output fibers. On the other hand, in low-Δn structures (where the index change may vary between 0.001 and 0.01) the bending loss can be very high unless the curvature radius of the guide is kept above a certain value, typically of the order of centimeters: this puts therefore a strong limit to the integration capability.

Much work is therefore currently devoted to the development of fabrication processes which could at the same time guarantee high compatibility with electronic LSI and yield integrated optical devices with low insertion loss; low cost and high flexibility are other two key factors for a process to be adopted in industrial production of IO components and devices.

The choice of the material structure and of the fabrication process of course depend also on the functional requirements of the device to be realized; since planar structures are

Diffractive Optics and Optical Microsystems
Edited by Martellucci and Chester, Plenum Press, New York, 1997

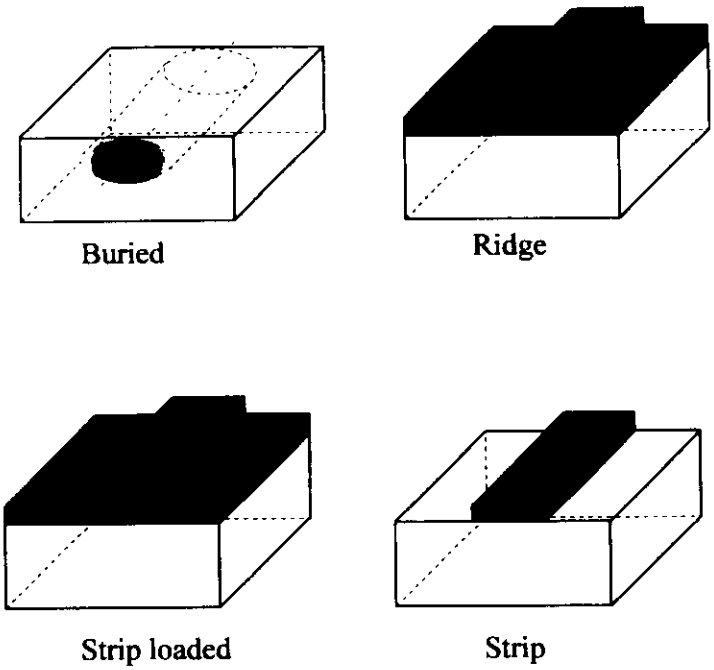

Fig. 1 Different types of channel waveguides. Light is confined transverse in the shaded regions.

being used only in very few cases, however, a common need is that of patterning the guiding layer and/or the cladding layer in order to create 2D guides. Various index or topographic configurations can be used, such as the ones sketched in Fig. 1, where darker shading indicates higher refractive index. Buried waveguides are generally obtained by diffusion processes (such as ion-exchange in glass, Ti-diffusion or proton exchange in lithium niobate, ion implantation or electron bombardment), while the other structures (ridge, strip, or strip-loaded waveguides) are produced in deposited layers. Accordingly, transverse light confinement is achieved by increase of the effective refractive-index of a limited dielectric region with respect to the surrounding regions: in most cases this is achieved by coating the substrate (or the guiding layer) with a mask material, which is then patterned lithographically with waveguide features. The following step consists of diffusion through the mask openings or of material removal, by wet or physical etching, respectively. In some cases, direct fabrication of 2D guides may be obtained, e.g. by laser or electron-beam writing.

In this Chapter a brief overview of the most important fabrication processes is presented, with particular attention devoted to glass material systems [1, 2] and to silica-on-silicon integrated optics.[3, 4]

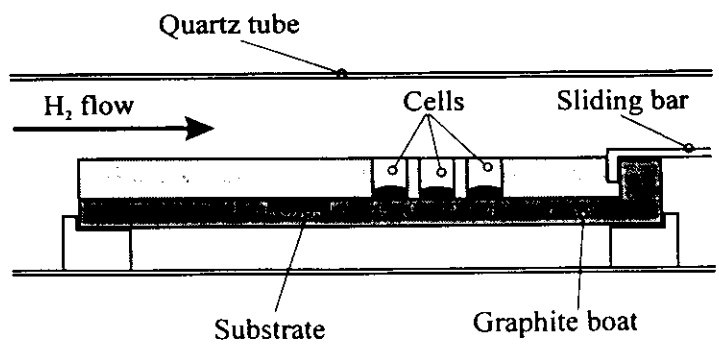

Fig. 2 Fabrication of thin films by Ar-plasma sputtering: behaviour of refractive index as a function of pressure and RF power (inset).

2. THIN FILM DEPOSITION TECHNIQUES

Most guided-wave optical devices are based on dielectric multilayer structures, obtained by successive deposition of thin films having tightly controlled thickness and refractive index. At this time, several deposition techniques are available. Some of them (such as e-gun evaporation, radio-frequency and magnetron sputtering) are definitely mature, having been borrowed from the classical area of optical coatings. Others were originally developed for semiconductors or optical fibers, and include for example Chemical Vapor Deposition (CVD), Flame Hydrolysis Deposition (FHD), and epitaxial growth techniques like Liquid Phase Epitaxy (LPE), Metal-Organic Chemical Vapor Deposition (MOCVD), and Molecular Beam Epitaxy (MBE). Recently, production processes have been implemented which exploit the power and selectivity of laser sources: as an example, Pulsed Laser Deposition (PLD) is becoming a widespread technique.[5] Finally, a deposition process which appeared only recently in IO is the so-called "sol-gel" technique:[6] its potential has yet to be fully exploited, but the prospects are quite appealing.[7]

2.1. Radio-frequency (RF) sputtering

Among the various vacuum thin-film deposition techniques, RF-sputtering is probably the most popular method for producing low-loss glassy planar waveguides. Sputtering is based on the use of positive highly accelerated ions to eject particles - usually atomic clusters or neutral atoms - from a target made of the material to be deposited. The ions are generated by injecting an electron current into an inert gas plasma (usually argon) at a pressure of $10^{-3} \div 10^{-2}$ Torr. RF-sputtering was first used in IO to deposit films of Corning 7059 glass (bulk refractive index about 1.53) onto ordinary soda-lime slides.[8] Several authors have since investigated the effect of various operating parameters on the deposition rate and composition of deposited films.[9-12]

A drawback of RF-sputtering is its slow deposition rate: as an example, in a diode sputtering system with a single 6"-diameter target the average deposition rate of Corning 7059 glass is about 1 nm/hour per Watt of RF electric power applied to the electrodes.

The quality of films is generally quite good, with propagation losses repeatedly lower than 0.8 dB/cm, for applied power less than 400 W. At higher sputtering powers, however, waveguide quality worsens and some yellow-brown discoloration of the films may occur.

The composition and optical characteristics of sputtered films vary as a function of the power level and gas pressure at which the deposition is made. This is likely due to the loss of oxygen caused by dissociation of the oxides of glass during the impact of ions onto the target. Introduction of a percentage of oxygen in the plasma (reactive sputtering) and application of a little potential to the anode (bias sputtering) can help reduce these effects. On the other hand, the possibility of varying the refractive index according to the sputtering parameters is also interesting because it can be used to increase flexibility in the design of the deposited films. As an example, a variation in the index of a 7059 glass film from 1.53 to 1.585, at 0.633 μm wavelength, was measured [9] for a corresponding change of the RF sputtering power density from 0.5 W/cm^2 to 4.0 W/cm^2. For the same type of glass, a series of measurements were carried out on the refractive index as a function of pressure in a pure argon plasma at 300 W: the results are reported in Fig. 2, where a significant decrease of the index with increasing pressure can be observed. In the same figure, the inset shows how the refractive index increases with increasing RF power, becoming much larger than the index of the bulk material itself. In the same working conditions, the addition of oxygen produces a further decrease of the refractive index, of the order of -2×10^{-3} for a 60% Ar - 40% O_2 mixture. One can easily conclude that the RF-sputtering process permits us to tailor quite accurately the optical properties of the deposited film.

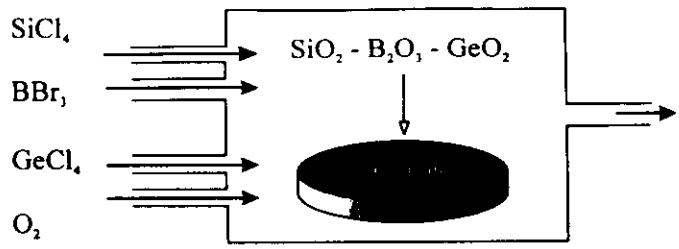

Fig. 3 Schematic diagram of apparatus for chemical vapour deposition (CVD).

RF-sputtering has also been applied for the deposition of active and/or nonlinear guiding layers: for instance, rare-earth-doped [13, 14] and semiconductor-doped [15] glass waveguides have been produced using a co-sputtering technique.

2.2. Chemical Vapor Deposition (CVD)

The CVD method was originally developed for the production of preforms of optical fibers, but it can be advantageously applied to planar waveguides as well. The classical CVD plant is sketched in Fig. 3: the silica (or silicon) substrate is placed in a reaction chamber, where accurately controlled flows of oxygen (carrier gas), $SiCl_4$, BBr_3 and $GeCl_4$ gases are introduced. The reaction with oxygen at a temperature higher than 1200 °C causes reagent oxidation and the deposition of a thin oxide layer (with SiO_2-B_2O_3-GeO_2 composition) onto the substrate. The waveguide is then obtained by vitrification of the soot at a temperature around 1700 °C. A lower-index cladding layer can be finally deposited on the waveguide by reducing the flowing rate of $GeCl_4$.

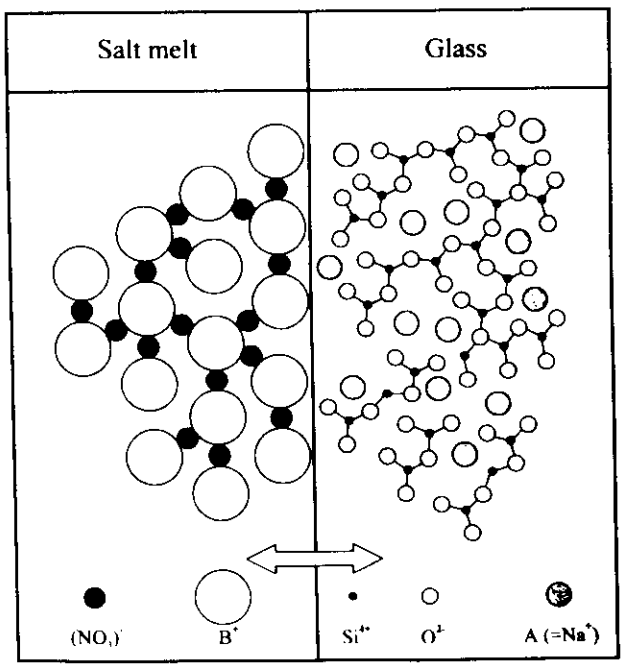

$$A_{glass} + B_{source} \longleftrightarrow A_{source} + B_{glass}$$

Fig. 4 Diagram of a setup for liquid phase epitaxy (LPE).

The resulting CVD-deposited glass films usually show absorption loss lower than 0.1 dB/cm at 0.633 μm wavelength. Low-loss channel waveguides can also be formed by this technique, using suitable grooves previously formed by any reactive etching procedure.

The CVD process lends itself to many modifications, which have been developed in different laboratories with the aim of optimizing both the quality and the yield of the process. Among the most common types of CVD-derived fabrication processes used to make IO devices we can cite: flame hydrolysis deposition (FHD), [16-19] low-pressure (LPCVD), [20] plasma enhanced (PECVD), [4,21] and atmospheric pressure (APCVD) [22] processes.

2.3. Liquid Phase Epitaxy (LPE)

This technique is the simplest one among the epitaxial growth processes, and consists of the deposition of a solid phase from an over-saturated solution of the material to be grown. In the case of III-V semiconductors, the solvent is the same metal which is present in the compound (for example, Ga in GaAlAs). A sketch of the equipment for epitaxial growth is shown in Fig. 4. Schematically, it consists of a graphite boat placed in a quartz tube where H_2 flows. Several cells are present in the boat itself, each of them containing a different solution. The bottom of each cell is a slide containing a slot for the substrate, which therefore can be put in contact successively with the various solutions. Temperature is around 750 to 900 °C and must be tightly controlled (within ±0.01 °C) in order to assure the required uniformity. Mechanical tolerances are obviously very strict, but the equipment is altogether very simple.

The LPE technique has mostly been used to produce waveguiding structures for laser diodes operating at wavelengths in the range from 0.7 μm to 1.5 μm, such as $Ga_{1-x}Al_xAs$ layers grown on GaAs,[23] but LPE has also been used to grow waveguides in ferromagnetic materials, e.g. $Y_3Sc_{0.7}Fe_{4.3}O_{12}$ grown on $Gd_3Ga_5O_{12}$,[24] and in magneto-optical materials.

Channel waveguides, multilayer structures and various passive integrated optical components can be obtained by using the LPE technique combined with photolithographic and reactive etching procedures.

2.4. Sol-gel

The sol-gel process is a glass deposition technique based on the hydrolysis and polycondensation of metal alkoxides.[6,25] The procedure undergoes three steps: 1) hydrolysis of the different metal alkoxides in a mutual solvent (formation of the *sol*); 2) polycondensation and subsequent polymerization to form a highly porous solid network (the *gel*); and 3) drying of the gel and final heat-treatment to produce a stable and compact glass.

A number of features make the sol-gel method inherently attractive. First, this technique is based on liquid solutions, and therefore allows easy fabrication of fibers and waveguiding films. Moreover, it is a low-temperature process, so that special multicomponent compositions can be obtained without risk of phase-separation and crystallization; thus, many dopants can be introduced in the matrix, allowing for production of non-linear or active optical materials. Finally, the optical characteristics of the final glass can be varied by simply changing the initial sol composition.

Fig. 5 schematically illustrates how bulk, fiber and thin film materials can be produced by the sol-gel technique, through the careful control of process parameters (viscosity, drying and heating conditions).

Channel waveguides can be realized, as in most film deposition techniques, by the use of photolithography and a suitable etching procedure. However, since the sidewalls may remain quite rough, thus heavily contributing to scattering loss, a reflow treatment may be necessary.[26]

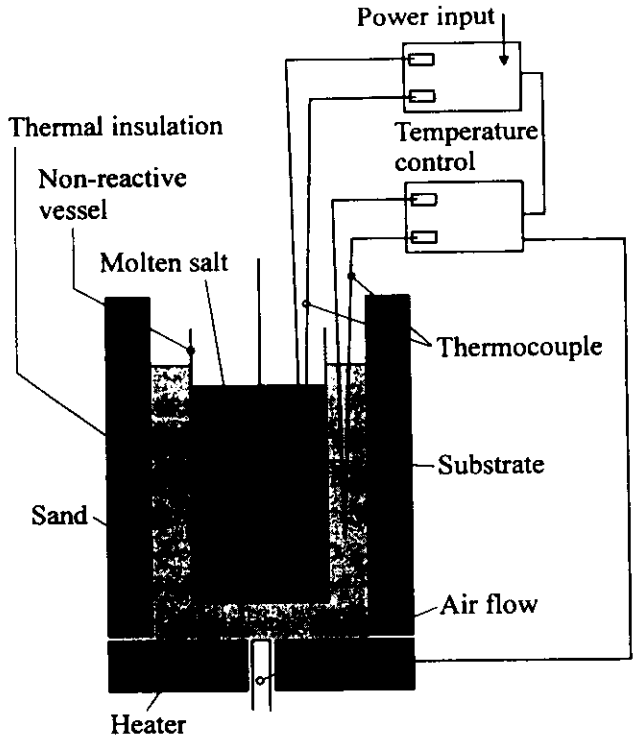

Fig. 5 Different material configurations obtainable by the sol-gel technique.

Recently, a great deal of work has been reported concerning sol-gel preparation of semiconductor-doped [27,28] and rare-earth-doped waveguides.[29-31]

3. ION DIFFUSION AND ION IMPLANTATION TECHNIQUES

Although thin-film deposition techniques are widely practiced, and some of them are also easy to implement, nevertheless it is sometimes more convenient to exploit the properties of a bulk material and create a guiding structure in it by locally modifying its refractive index. In this case one mainly uses diffusion techniques: a very common and effective one for glass and some crystals (such as lithium niobate, KTP and a few others) is ion-exchange, while a more general approach is that of inducing the thermal diffusion of a dopant in the bulk material. Another possibility is that of using high energy ion beams to implant a large variety of ions into a material.

Here, we will principally discuss the ion-exchange technique in glass; only a short description of the ion implantation approach will be given.

3.1. Ion implantation

The apparatus for ion implantation consists of a generator of ions, an accelerator, an ion separator and a deflector. Ions having energy ranging from 20 to 300 KeV can be implanted in various substrates, causing lattice modifications and the formation of impurities. These in turn produce an increment in the refractive index within a thin layer close to the surface, and therefore the creation of an optical waveguide.

As an example, the first experiments with this kind of technology were carried out on fused-silica substrates, bombarded by H^+ ions at 1.5 MeV [32] and by Li^+ ions at energies between 32 and 200 KeV.[33] The most reproducible results were obtained by using Li^+, for

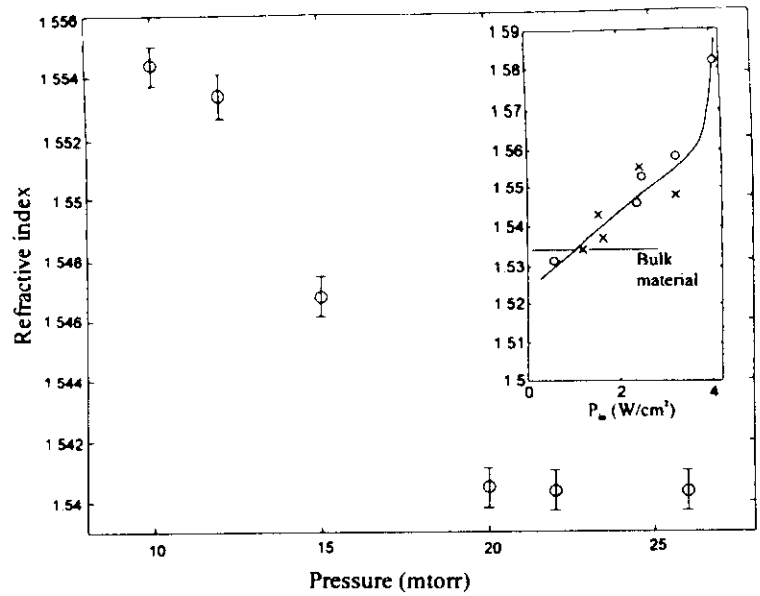

Fig. 6 Diagram of the ion-exchange process in a molten salt. The ionic species A is Na^+ in soda-lime glasses.

which a proportionality between refractive index increase and dose of implanted ions was verified. Propagation loss in ion-implanted waveguides can be as low as 0.2 dB/cm at 0.633 μm wavelength.

Unfortunately, ion implantation requires very large and expensive equipment, although it has the advantage of allowing very precise control of fabrication parameters. The interested reader is referred to a recent review of current developments for waveguide formation as used in electro-optics, lasers or nonlinear optics applications; economic factors related to implantation have also been analyzed there.[34]

3.2. Ion exchange in glass

The suitability of ion-exchange technology to produce integrated optical components in glass has been recognized since the early 1970's, when a few pioneering studies demonstrated how to take advantage of the refractive index increase produced in the glass by replacing the sodium ions with other ions having higher electronic polarizability (such as silver or potassium).[35, 36] One of the greatest advantages of the ion-exchange technique is the extreme simplicity and low cost of the process, which can also be easily transferred to batch production.[1, 37]

In order to understand the principle of the method, one needs first of all to remember that the so-called "network modifier" ions, i.e. alkali ions such as Na^+ which may occur in the silicate network of a glass, have a temperature-dependent mobility following an exponentially decreasing behavior with inverse temperature. At sufficiently high temperatures (typically a few hundred degrees Celsius), and in the presence of a melt solution containing other ions with similar chemical properties, the alkali ions of the glass can leave the silicate lattice, being readily substituted by similar ions from the melt solution. A sketch of the thermal ion-exchange process is shown in Fig. 6.

In a qualitative way, the exchange proceeds as follows. The glass substrate, containing for example Na^+ ions, is immersed in a molten solution of $MeNO_3$ in $NaNO_3$, where *Me* can be Ag, K or any other metal chemically similar to Na. Since a gradient exists in both ion concentrations, a diffusion process will take place, being essentially driven by thermal agitation. Random collisions will therefore cause replacement of Na^+ ions by the Me^+ ones in

the glass matrix, which gradually forms a thin layer close to the surface. The process terminates when the substrate is allowed to cool down to room temperature.

The exchange temperature is usually slightly higher than the melting point of the salt (ranging from about 200 °C to 550 °C). Excessive heating may in fact cause damage of the surface due to nitrate decomposition and thermal relaxation of glass.

The index change resulting from ion exchange can be easily determined from the fact that the ions taking part in the exchange have different electronic polarizabilities and that they occupy a different volume in the glass lattice.[38] Quantitatively, the refractive index variation Δn can be expressed as

$$\Delta n \approx \frac{\chi}{V_0}\Delta R - \frac{R_0}{V_0}\Delta V \qquad (1)$$

where χ is the concentration of the new ions in glass, V_0 is the volume of glass per mole of oxygen atoms, R_0 the refraction per mole of oxygen atoms and ΔV, ΔR are the changes of these quantities due to the ion exchange.

The above model, though a very simple one, holds very well for bulk changes of composition. For surface ion-exchange, as is the case with IO, one should also take into account the effects of stress, due to the substrate resisting the localized volume change. As a consequence, the estimation of ΔV may not be accurate. Nevertheless, the model provides very useful information, giving at least the correct order of magnitude of the index change.

As an example, the predicted maximum index change in Ag^+-Na^+ exchange is 0.09, in good agreement with experimental results. In some cases, such as that of K^+-Na^+ ion-exchange, a birefringence effect also arises, due to anisotropic stress. Therefore, the index change for TM polarized modes is different from that of TE polarized modes. By taking into account volume variations induced by stress one can calculate a correction to Eq. (1) and find, for the K^+-Na^+ exchange, $\Delta n_{TE} = 0.0089$, $\Delta n_{TM} = 0.011$. The experimental results agree fairly well with the theory, being approximatly $\Delta n_{TE} \approx 0.008$ to 0.009 and $\Delta n_{TM} \approx 0.0095$ to 0.011.[39] The refractive index profile resulting from the ion-exchange method depends on the particular ions involved. For example, the Ag^+-Na^+ index profile for planar waveguides is well approximated by a complementary error function:

$$n(x) = n_{sub} + \Delta n \ \mathrm{erfc}\frac{x}{\sqrt{D_e t}} \qquad (2)$$

where n_{sub} is the substrate index, Δn the maximum index change, D_e an "effective diffusion coefficient" and t the exchange time. Since the process is diffusion driven, the D_e coefficient has the following temperature dependence:

$$D_e = C_1 \exp\left(-\frac{C_2}{T}\right) \qquad (3)$$

where C_2 is proportional to the activation energy of the process. For the Ag^+-Na^+ ion-exchange process the salt used as the source of ions, $AgNO_3$, is usually diluted in $NaNO_3$, with concentrations varying from 5% to 20%; the temperature is kept around 300 °C (the melting point of $AgNO_3$ is 212 °C), while exchange times are of the order of a few minutes to obtain mono-modal waveguides. Dilution is advisable in the case of Ag^+-Na^+ ion-exchange because it both increases the reproducibility of the process and relaxes the tight constraints necessary for undiluted melts.

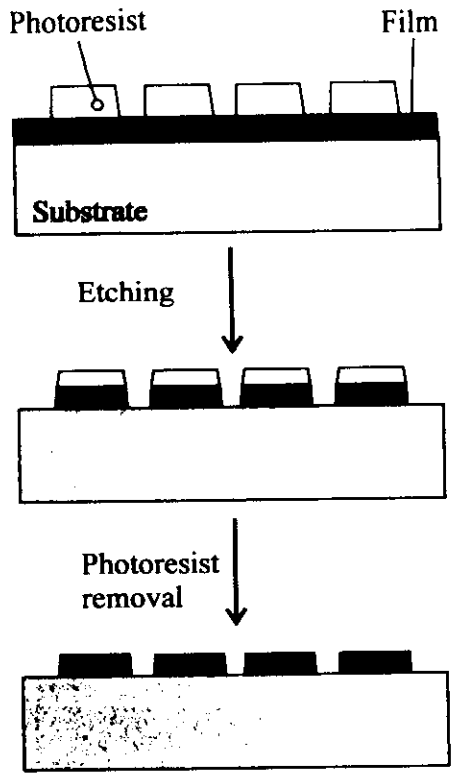

Fig. 7 Schematic setup for the production of glass waveguides by the ion-exchange technique.

A typical, economical laboratory setup for the production of waveguides by the ion-exchange technique is shown in Fig. 7 ; it consist mainly of an oven (a fluidised-bath furnace, in the case depicted in the figure, where the air flow through the sand gives rise to very good heat convection and therefore produces homogeneous heating of the reactor vessel) with accurate temperature controls in order to guarantee reproducibility of the process.

4. MICROSTRUCTURE FABRICATION

Fabrication of a guided-wave device, as already mentioned, requires not only having the proper refractive-index distribution but also in most cases creating a topographic structure. This means that some material has to be deposited or removed through a suitable mask. Etching, either chemical or physical, is the best process to produce these microstructures. The minimum size of the features which can be produced depends mainly on the resolution of the photoresist, which is the basic material in almost any lithographic process: currently, the minimum line width with negative resists (i.e. resists where exposure to light causes polymerization of the material, making the exposed regions insoluble in the developer) is larger than 1 μm, and a bit smaller (around 0.5 μm) in positive resists (where exposed areas become soluble and therefore removable in the proper developer).[40]

While microlithography is still the most widespread and effective tool to produce nanostructures,[41] in less demanding applications locally-selective processing can be done by direct laser-writing: the applicability of the method obviously depends also on the choice of the material system. As an example, 2D waveguides may be produced in sol-gel films by direct laser densification, or other structures may be obtained by removing material through laser ablation.

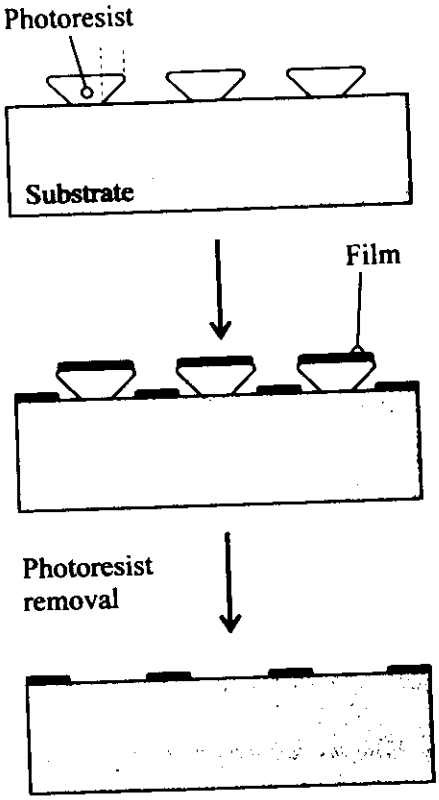

Fig. 8 Patterning of thin films by the lift-off technique (schematic).

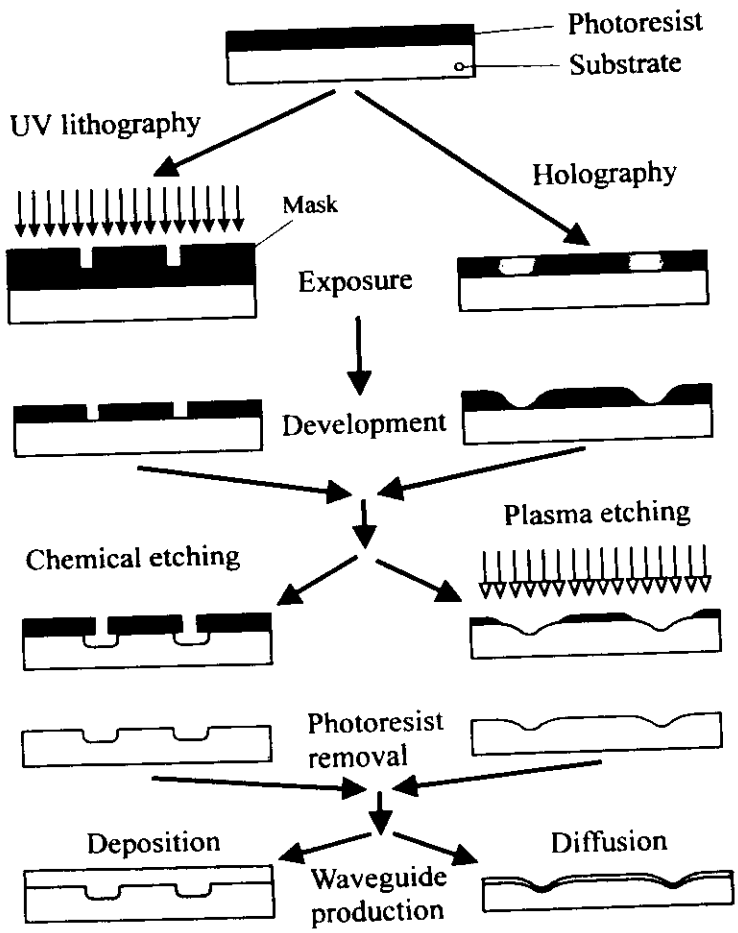

Fig. 9 Patterning of thin films by the etching technique (schematic).

4.1. Lift-off technique

The principle of operation of the lift-off technique, which is an alternative to the conventional etching process, is indicated in Fig. 8. A pattern is formed in the photoresist layer, previously deposited onto the substrate by spin-coating, by means of the photolithographic technique. As illustrated in the figure, an overhang is formed in the resist during development, if suitable thickness, exposure and development conditions are provided. Moreover, it is necessary that the resist thickness be larger than the thickness of the film to be deposited; the masking film is in most cases a metal film, which is deposited by means of vacuum evaporation or sputtering. Finally, the sample is immersed in a suitable solvent which dissolves the resist and thus causes the removal of the film directly deposited on it. In this way, the desired pattern is replicated in the masking film.

A few requirements have to be met in order to obtain good results by the lift-off technique: 1) an appropriate overhang must exist; 2) the resist layer must be completely removed from the patterning windows before film deposition; and, 3)good film adhesion must be guaranteed.

In order to enhance film adhesion, one can slightly ash the resist with oxygen plasma after development; another possibility is to post-bake the substrate at a temperature which does not cause resist deformation (100 to 150 °C). When using Al films for the mask, their adhesion to the substrate can be improved by previously depositing an underlayer of Cr or Ti on the substrate.

4.2. Etching techniques

Fig. 9 shows a schematic representation of a conventional etching procedure. The resist may operate as a masking material itself (in such a case the film indicated in the figure is the guiding layer), or instead it may be used to transfer the features from the master mask to the masking film for the waveguide fabrication process. If the resist cannot withstand the etching process, a masking underlayer must first be deposited on the substrate.

Etching processes can be divided into two classes: *chemical* (or *wet*) *etching*, which makes use of liquid chemicals, and *dry etching*, which uses gaseous etchants.

Wet etching can be achieved by a variety of substances, such as aqueous solutions of acids (HF, H_3PO_4, HNO_3), alkalis (NaOH), and salts (NaCN, $FeCl_3$). The sample is immersed in the appropriate etchant after development, kept at a certain temperature and stirred in order to remove air bubbles. The process can be monitored by observation through a microscope. Although wet etching requires extremely simple equipment and is thus very attractive, good results are rarely obtained, primarily because of the difficulty in achieving acceptable reproducibility of etch rate.

The term dry etching includes in fact a number of quite different techniques. Many of them are commercially available, being extensively used in the semiconductor industry. As an example, the basic *plasma etching* consists of an apparatus which produces plasma by RF discharge in a reactive gas (e.g. CF_4) at a 0.1 to 10 Torr pressure; chemical reactions with the resultant neutral radicals produce the etching of both silicon and silicon compounds.[42] *Sputter etching* is based on an ordinary sputtering apparatus, the only difference being that the samples are placed at the target position and undergo physical bombardment by Ar^+ ions, which cause the etching of the substrates. Variations or combinations of these two basic processes, based on physical-chemical and purely physical actions, respectively, include dry-etching configurations known as *reactive ion etching (RIE)*, *ion beam etching (IBE)*, and *reactive ion beam etching (RIBE)*. [43]

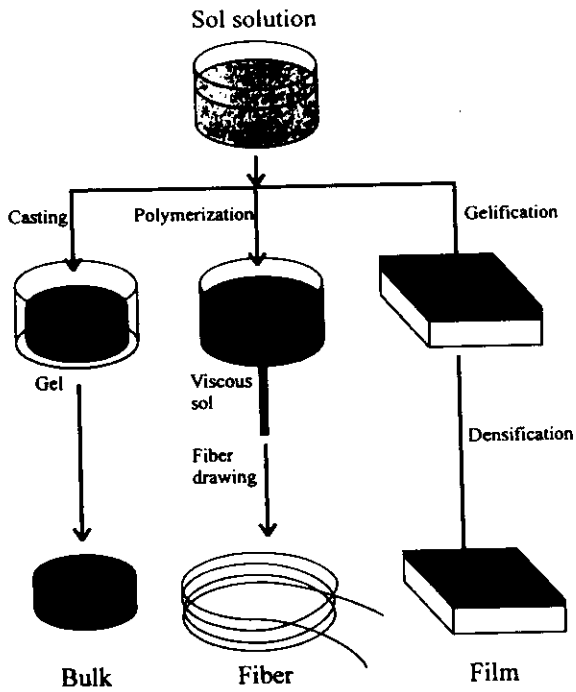

Fig. 10 Illustration of the procedure for realisation of waveguide patterns (such as gratings).

Fig. 10 summarizes some of the possible procedures to be followed for the fabrication of topographic waveguides and IO devices. When the aim is to fabricate a periodic structure, such as a grating coupler or filter, instead of using the conventional photolithographic process one can also exploit holographic techniques to produce the desired modulated pattern in the photoresist; using this approach it is easier to produce sinusoidal gratings.

4.3. 2D-waveguide fabrication by direct laser writing

Writing of integrated circuit masks is often done by electron-beam exposure of suitable resists (usually, PMMA), because this method offers very high resolution and dimensional precision. Laser writing, however, may also be used as an effective tool for mask production in all the cases where geometrical tolerance constraints are relaxed.[44] Both methods can also be used for direct writing of the waveguides through an induced change of refractive index or of material thickness.

Early demonstrations of direct laser writing included fabrication of guides in Kodak KPR photoresist films, [45] in sensitizer-doped polymers by the so-called *photolocking* mechanism, [46] and in SiO_2-TaO_2 films by CO_2-laser irradiation.[47] More recently, laser writing has been widely used in conjunction with the sol-gel deposition technique, either through local densification of the still-porous film or through UV-irradiation of a sensitizer introduced in the starting solution.

The formation of topographic structures in sol-gel films is possible by laser-induced selective densification.[48 - 50] Strip waveguides with propagation loss below 1 dB/cm have been produced in silica-titania sol-gel films by exploiting the localized heating of sol-gel material due to the absorption of laser light by the film itself and by the substrate.[50] A schematic representation of the selective densification process induced by a focused CO_2 laser is given in Fig. 11: the sol-gel film is spin-deposited and baked at a temperature below 200 °C, in order to leave it quite porous. The strip of the material which is irradiated by the

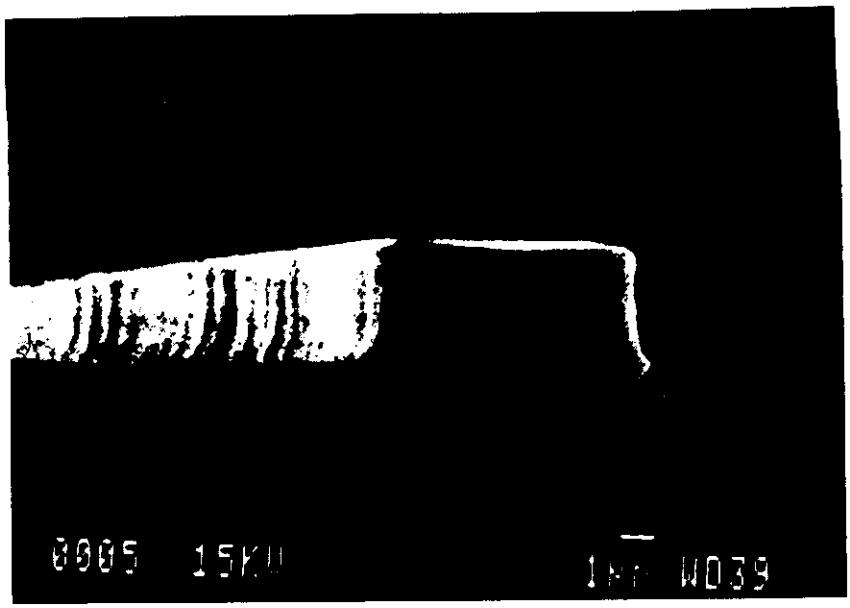

Fig. 12 SEM photograph of a strip waveguide in sol-gel glass.

focused scanning beam from a cw CO_2 laser (the power actually delivered onto the strip is in the range 50 to 60 mW) heats up and shrinks; the unexposed, and therefore undensified areas of the film are removed by immersing the sample in a buffered and diluted HF solution, which almost has no effect on the densified strip, due to the much slower etching rate of the dense material.

Another recently developed procedure uses UV light imprinting in a photosensitive hybrid organo-silicate film produced by a dip-coating sol-gel process. The good optical quality of a ridge optical waveguide fabricated by this procedure can be seen in Fig. 12, which shows a scanning electron microscope photograph of a 5-μm wide and 4-μm high ridge waveguide deposited onto a silicon wafer.[51] Propagation losses as low as 0.1 dB/cm at λ = 1.55 μm have been measured. A set of passive integrated optical devices, including directional couplers,[52] power splitters and wavelength-division-multiplexers, have been fabricated by this process.

5. CONCLUSIONS

A quick overview of the most common fabrication processes in integrated optics has been given, with particular attention devoted to practical problems in the production of passive components in glass materials and in silica-on-silicon structures.

The basic requirements for any process are the capability for very accurate control of the refractive index and thickness of the guiding layer, freedom from scattering defects and smoothness of surfaces. Moreover, in order to facilitate the commercialization of fabricated components and devices, the process should not be highly expensive nor very critical, and should be suitable for batch production. A significant role in the optimization of the processes and in the development of IO devices is obviously played on the one hand by modeling and design techniques, and on the other hand by the characterization and quality-assessment techniques, some of which have been developed specifically for use in optical waveguides.[53]

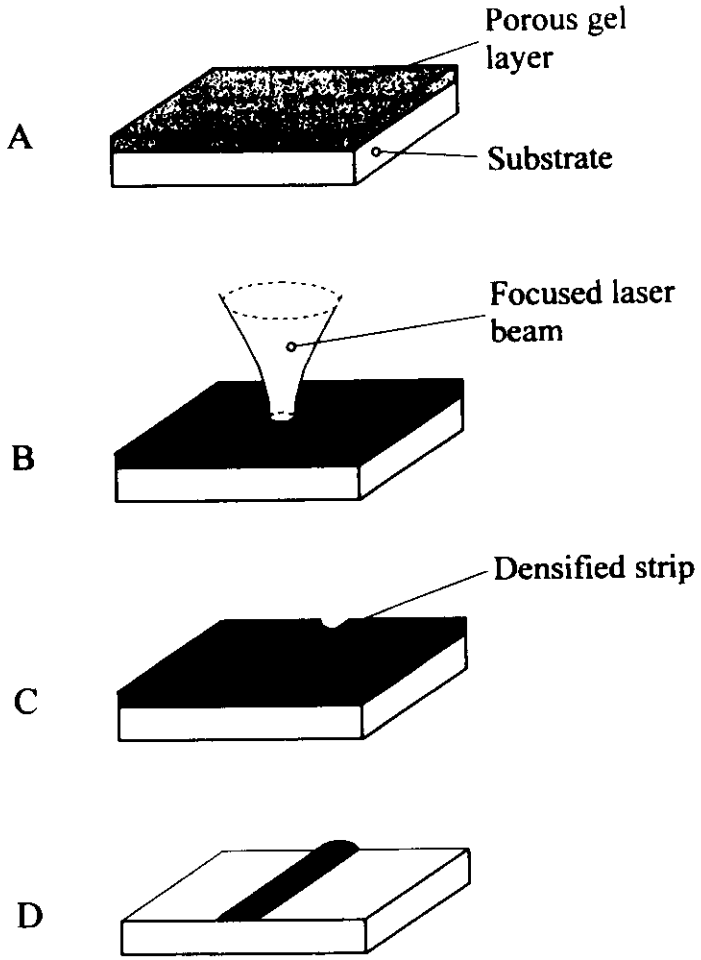

Fig. 11 Schematic of the laser densification method. A: deposition of the sol-gel layer; B: laser densification; C: densified strip; D: removal of the undensified layer by chemical etching.

ACKNOWLEDGMENTS. The authors wish to thank Dr. S. Pelli and Dr. A. Verciani for useful discussions. Financial support by the CNR Strategic Project on *Materials and Devices for Optoelectronics* and by the CNR Special Project on *Glass Waveguides for Non-Linear Optics* is also acknowledged.

REFERENCES

1. S.I. Najafi, Ed., *Introduction to Integrated Optics* (Artech House, Boston, 1992).
2. P. Mazzoldi and G.C. Righini, Glasses for Optoelectronic Devices, in *Insulating Materials for Optoelectronics*, F. Agulló-López, Ed. (World Scientific, Singapore, 1995) 367-392.
3. R.R. Syms, Silica on Silicon Integrated Optics, in *Advances in Integrated Optics*, S. Martellucci et al. Eds. (Plenum Press, New York, 1994) 121-150.
4. S. Valette, Integrated Optics on Silicon: IOS Technologies, in *Advances in Integrated Optics*, S. Martellucci et al. Eds. (Plenum Press, New York, 1994) 151-164.
5. C.N. Afonso, Pulsed Laser Deposition of Fibers for Optical Applications, in *Insulating Materials for Optoelectronics*, F. Agulló-López, Ed. (World Scientific, Singapore, 1995) 1-28.
6. C.J. Brinker and G.W. Scherer, *Sol-Gel Science* (Academic Press, San Diego, 1990).
7. M.P. Andrews, An Overview of Sol Gel Guest-Host Materials Chemistry for Optical Devices, *Proc. SPIE* vol. 2997, 48 (1997).
8. J.E. Goell, and R. D. Standley, Sputtered glass waveguide for integrated optical circuits, *Bell System Techn.* J. 48, 3445 (1969).
9. C. W. Pitt, F.R. Gfeller, and J.R. Stevens, RF-sputtered thin films for integrated optical components, Thin Solid Films 26, 25 (1971).

10. W. M. Paulson, F.S. Hickernell and R.L. Davis, Effects of deposition parameters on optical loss for RF-sputtered Ta_2O_5 and Si_3N_4 waveguides, *J. Vac. Sci. Technol.* 16, 307 (1979).
11. H. Terui, M. Kobayashi, Refractive-index-adjustable SiO_2-Ta_2O_5 films for integrated optical circuits, *Appl. Phys. Lett.* 32, 666 (1978)
12. G. C. Righini, G. Margheri and L. Mancinelli Degli Esposti, Glass waveguides for integrated optical circuits, *Rivista Staz. Sper. Vetro* no. 6, 109 (1986).
13. B. Chen and C.L. Tang, Nd-glass thin-film waveguide: An active medium for Nd thin-film laser, *Appl. Phys. Lett.* 28, 435 (1976).
14. J. Shmulovich, A. Wong, Y.H. Wong, P.C. Becker, A.J. Bruce, and R. Adar, Er^{3+} glass waveguide amplifier at 1.5 μm on silicon, *Electron. Lett.* 28, 1181 (1992).
15. H. Nasu, K. Tsunetomo, Y. Tokumitsu, and Y. Osaka, Semiconducting CdTe Microcrystalline-Doped SiO_2 Glass Thin Films Prepared by Rf-Sputtering, *Jap. J. Appl. Phys.* 28, L862 (1989).
16. H. Yanagawa, S. Nakamura, I. Ohyama, and K. Ueki, Broad-Band High-Silica Optical Waveguide Star Coupler with Asymmetric Directional Couplers, *IEEE J. Lightwave Technol.* 8, 1292 (1990).
17. G. Barbarossa and P.J.R. Laybourn, High-silica low-loss three waveguide couplers on Si, *Proc. SPIE* vol. 1513, 37 (1991).
18. C.J. Sun, W.M. Myers, K.M. Schmidt, S. Sumida, and K.P. Jackson, High Silica Waveguides on Alumina Substrates for Hybrid Optoelectronic Integration, *IEEE Photon. Technol. Lett.* 4, 630 (1992).
19. S. Kobayashi, Recent Development on Silica Waveguide Technology for Integrated Optics, *Proc. SPIE* vol. 2997, 264 (1997).
20. C.H. Henry, G.E. Blonder, and R.F. Kazarinov, Glass Waveguides on Silicon for Hybrid Optical Packaging, *IEEE J. Lightwave Technol.* 7, 1530 (1989).
21. A.M. Fiorello, E. Giannetta, M. Valentino, A. Vannucci, and M. Varasi, Co-doped silica-on-silicon waveguides fabricated by PECVD technique, *Proc. SPIE* vol. 2954, 124 (1996).
22. T. Hanada, M. Kitamura, and S. Nakamura, *Proc. OECC'96*, 18C2 (July 1996).
23. E. Garmire, Optical waveguides in single layers of $Ga_{1-x}Al_xAs$ grown on GaAs substrates, *Appl. Phys. Lett.*, 23, 403 (1973).
24. P. K. Tien, R. J. Martin, S. L. Blank, S. H. Wemple, and L. J. Varnerin, Optical waveguides of single-crystal garnet films, *Appl. Phys. Lett.* 21, 207 (1972).
25. B. Zelinski, C. Brinker, D. Clark, and D. Ulrich, Better Ceramics Through Chemistry IV, *Mat. Res. Soc. Symp. Proc.*, vol. 180 (1990).
26. A.S. Holmes and R.R.A. Syms, Fabrication of low-loss channel waveguides in sol-gel glass on silicon substrates, in *Advanced Materials in Optics, Electro-optics and Communication Technologies*, P. Vincenzini and G.C. Righini Eds. (Techna, Faenza, 1995) 73.
27. E.J.C. Dawnay, J. Fick, M. Green, M. Guglielmi, A. Martucci, S. Pelli, G.C. Righini, G. Vitrant, and E.M. Yeatman, Nonlinear properties of semiconductor-doped sol-gel thin films for photonic application, in *Advanced Materials in Optics, Electro-optics and Communication Technologies*, P. Vincenzini and G.C. Righini Eds. (Techna, Faenza, 1995) 15.
28. T.A. King, D. West, D.L. Williams, C. Moussu, and M. Bradford, Nonlinear optics in thin films and waveguide sol-gel composites, in *Advanced Materials in Optics, Electro-optics and Communication Technologies*, P. Vincenzini and G.C. Righini Eds. (Techna, Faenza, 1995) 21.
29. D. Barbier, X. Orignac, X.M. Du, and R.M. Almeida, Spectroscopic properties of Neodymium doped sol-gel planar waveguides, in *Advanced Materials in Optics, Electro-optics and Communication Technologies*, P. Vincenzini and G.C. Righini Eds. (Techna, Faenza, 1995) 33.
30. G. Milova, S.I. Najafi, A. Skirtach, D.J. Simkin, and M.P. Andrews, Erbium in photosensitive hybrid organoaluminosilicate sol-gel glasses, *Proc. SPIE* vol. 2997, 90 (1997).
31. X. Orignac and D. Barbier, Potential for fabrication of sol-gel-derived integrated optical amplifiers, *Proc. SPIE* vol. 2997, 271 (1997).
32. E.R. Schineller, R.P. Flam, and D.W. Wilmot, Optical waveguides formed by proton irradiation of fused silica, *J. Opt. Soc. Am.* 58, 1171 (1968).
33. R.D. Standley, W.M. Gibson, and J.W. Rodgers, Properties of ion bombarded fused quartz for integrated optics, *Appl. Opt.* 11, 1313 (1972).
34. P.D. Townsend, Application of Ion Implantation for Optoelectronics and Photonics, in *Insulating Materials for Optoelectronics*, F. Agulló-López, Ed. (World Scientific, Singapore, 1995) 393-420.
35. T. Izawa and H. Nakagome, Optical waveguide formed by electrically induced migration of ions in glass plates, *Appl. Phys. Lett.* 21, 584 (1972).
36. T.G. Giallorenzi, E.J. West, R. Kirk, R. Ginther, and R.A. Andrews, Optical waveguides formed by thermal migration of ions in glass, *Appl. Opt.* 12, 1240 (1973).
37. G.C. Righini, Ion-exchange process for glass waveguide fabrication, in *Glass Integrated Optics and Optical Fiber Devices*, S.I. Najafi Ed., vol. CR53 (SPIE, Bellingham, 1994) 24.

38. S.D. Fantone, Refractive index and spectral models for gradient-index materials, *Appl. Opt.* 22, 432 (1983).
39. J. Albert and G.L. Yip, Stress-induced index change for K^+- Na^+ ion exchange in glass, *Electron. Lett.* 23, 737 (1987).
40. R.A. Bartolini, Photoresists, in *Holographic Recording Materials*, H.M. Smith, Ed. (Springer-Verlag, Berlin, 1977) 209-228.
41. S.P. Beaumont, Today's microlithography, in *From Galileo's occhialino to optoelectronics*, P. Mazzoldi Ed. (World Scientific, Singapore, 1993) 419.
42. D.M. Manos and D.L. Flamm, *Plasma Etching* (Academic Press, New York, 1989).
43. see for instance H. Nishihara, M. Haruna and T. Suhara, *Optical Integrated Circuits* (McGraw-Hill, New York, 1987), pp. 172-184.
44. G.M. Lad, G.M. Naik, and A. Selvarajan, Laser patterning system for integrated optics and storage applications, *Opt. Eng.* 32, 725 (1993).
45. H.P. Weber, R. Ulrich, E.A. Chandross, and W.J. Tomlinson, Light-Guiding Structures of Photoresist Films, *Appl. Phys. Lett.* 20, 143 (1972).
46. E.A. Chandross, C.A. Pryde, W.J. Tomlinson, and H.P. Weber, Photolocking - A new technique for fabricating optical waveguide circuits, *Appl. Phys. Lett.* 24, 72 (1974).
47. H. Terui and M. Kobayashi, Fabrication of channel optical waveguide using CO_2 laser, *Electron. Lett.* 15, 79 (1979).
48. B.D. Fabes, Laser processing of sol-gel coatings, in *Sol-Gel Optics: Processing and Applications*, L.C. Klein, Ed. (Kluwer Academic Publishers, USA, 1994) 483.
49. M. Guglielmi, P. Colombo, L. Mancinelli degli Esposti, G.C. Righini, S. Pelli, and V. Rigato, Characterization of laser densified sol-gel films for the fabrication of planar and strip optical waveguides, *J. Noncryst. Solids* 147&148, 645 (1992).
50. S. Pelli, G.C. Righini, A. Scaglione, M. Guglielmi, and A. Martucci, Direct laser writing of ridge optical waveguides in silica-titania glass sol-gel films, *Opt. Materials* 5, 119 (1996).
51. S.I. Najafi, M.P. Andrews, M.A. Fardad, G. Milova, T. Tahar, and P. Coudray, UV-light imprinted surface, ridge and buried sol-gel glass waveguides and devices on silicon, Proc. SPIE vol. 2954, 100 (1996).
52. C.Y. Li, J. Chisham, M.P. Andrews, S.I. Najafi, J.D. Mackenzie, and N. Peyghambarian, Sol-gel integrated optical couplers by ultraviolet light imprinting, *Electron. Lett.* 31, 271 (1995).
53. S. Pelli and G.C. Righini, Introduction to Integrated Optics: Characterization and Modeling of Optical Waveguides, in *Advances in Integrated Optics*, S. Martellucci et al. Eds. (Plenum Press, New York, 1994) 1-20.

ELSEVIER

January 1996

Optical Materials 5 (1996) 119–126

OPTICAL Materials

Direct laser writing of ridge optical waveguides in silica-titania glass sol-gel films

Stefano Pelli [a], Giancarlo C. Righini [a], Antonio Scaglione [b], Massimo Guglielmi [c], Alessandro Martucci [c]

[a] *Optoelectronic Technologies Group, Istituto di Ricerca sulle Onde Elettromagnetiche "N. Carrara" (IROE-CNR), 50127 Firenze, Italy*
[b] *Laboratorio di Ottica, Dip. di Ingegneria Elettronica, Facoltà di Ingegneria, Università di Salerno, Salerno, Italy*
[c] *Dip. Ingegneria Meccanica-Sez. Materiali, Università di Padova, Padova, Italy*

Received 24 January 1995; accepted 18 August 1995

Abstract

Sol-gel process is attracting a growing attention as a rather simple technology with potential for low-cost batch manufacture of integrated optical waveguides. Here experimental results are presented on the fabrication of silica-titania sol-gel films and on their laser densification, a technique which may be very useful for rapid circuit prototyping. Transversally multimode waveguides with propagation loss around 1 dB/cm have been produced by selective densification using a CO_2 laser. Data from optical and structural analysis of the sol-gel strips are reported and discussed.

1. Introduction

The realisation of integrated optical devices requires the patterning of the guiding layers in order to obtain the appropriate structures for the circuit. In most cases conventional photolithographic techniques borrowed from the electronics industry are employed in this crucial step of circuit fabrication; however, other routes are also exploited in order to find solutions which could lead to a higher yield or simply to be more convenient in specific applications.

Direct writing of patterns in the guiding films is one viable solution in order to avoid the need for photolithographic steps, and has been pursued by several groups using different materials and techniques. This approach may be particularly useful in the prototyping stage of the device, since it makes possible an optimisation of the structures after the design process by simply changing the software that controls the writing equipment. The same action using photolithographic techniques would require the production of a new mask each time the design changed, even if by only a small amount. In large-scale production, other time and economic considerations might have an influence on the choice between direct writing and photolithographic techniques, but in the optimisation process direct writing may definitely have an advantage over lithography.

Direct writing of masks [1] or waveguide structures by means of laser irradiation have already been demonstrated in silicon dioxide [2] and nitride [3], lithium niobate [4,5], polymers [6] and also sol-gel glass [7].

As far as materials for integrated optics are concerned, the sol-gel process is emerging, thanks to its flexibility and to its capacity to produce films (especially glass films) with a controlled composition and

SSDI 00925-3467(95)00049-6

almost free of contamination. This capacity makes it extensively possible to fine-tune the film characteristics to the particular needs met by the design. Variations in the refractive index or dopants, added in order to confer to the material special (e.g. nonlinear or active) properties, are achieved simply by changing the composition of the starting solution.

In this paper we report on the fabrication of silica-titania sol-gel layers suitable for direct laser densification and in general for integrated optics applications, and on the results of laser writing in these films.

2. The sol-gel process

The steps which have to be followed to produce bulk or thin-film silica glass by the sol-gel process are summarized in Fig. 1. First of all, a silicon alcoxide is hydrolised in an alcoholic solution. Subsequently, it can react with the organic or hydroxyl group of the surrounding ones creating an O–Si–O bond. If the same reaction is repeated for all the molecules present in the solution, a porous silica network enclosing a liquid is obtained.

After the solution has been poured into a suitable vessel (to produce bulk glass) or deposited onto a substrate (to produce a glass thin film), a baking treatment burns out the organic content and the grid relaxes into a state of minimal energy, which corresponds to the shrinking (about 40%) of the sol-gel material. This stage must be accomplished with care, since irregular or excessively rapid baking may cause stress in the material, leading to undesired cracks which would completely impair its optical characteristics.

At the end of the process, a material that is substantially indistinguishable from the corresponding bulk glass can be obtained.

2.1. Preparation of sol-gel films

We have been preparing sol-gel films starting from an alcoholic (ethanol) solution of the silicon alcoxide tetraethoxysilane (*TEOS*); 30% relative titanium butilate is also added to the solution as the precursor of titania in order to increase and control the refractive index of the resulting film. The total concentration of the solution, expressed as the total weight of final oxides per liter, was 50 or 100 g/l.

The pH of the solution may have a strong influence on the final structure of the sol-gel glass, since a basic environment increases the tendency of the molecules to produce clusters, whereas an acidic

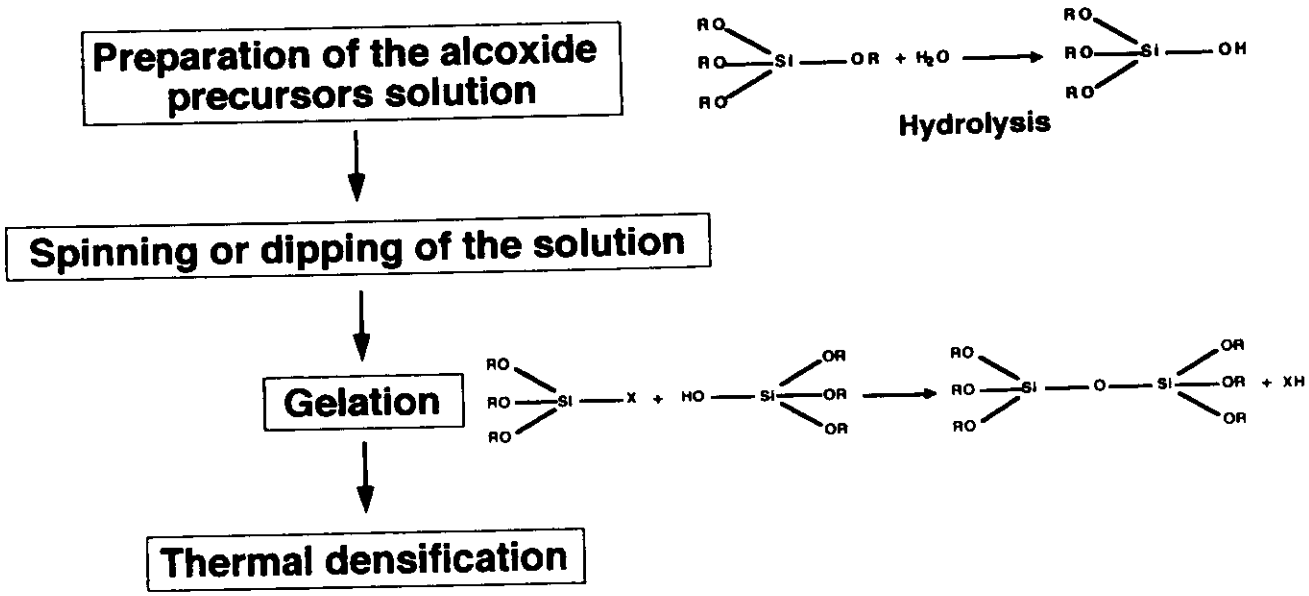

Fig. 1. Sketch of a typical sol-gel process for the production of glasses. In the chemical equations shown RO represents an alcoxide group and X indicates an OH or alcoxide group.

environment helps the hydrolysis of the molecules and produces more branched polymers. In order to obtain the right pH, 0.01 mol HCl per mol TEOS was added to the solution.

The films were deposited on soda-lime glass (Chance Propper "Gold Star" microscope slides) by using the *dipping* technique, which consists of immersing the substrate in the sol-gel solution and subsequently removing it at a constant speed. The removal speed influences the final thickness of the film: the thickness is greater when the speed is higher.

Gelation of the solution, in contact with the air, occurs a few seconds after the substrate has emerged from it.

The parameters of the subsequent baking process depend on the results that we want to achieve: when denser films ready for waveguiding are desired, the samples are baked at 500°C for 4 hours; otherwise, if more porous films are needed to be used for laser writing processes, baking is carried out at temperatures ranging from 60 to 200°C to obtain sufficient mechanical properties.

The maximum thickness which can be obtained by the deposition of a single layer without experiencing cracking effects is about 0.15 μm (measured after baking at 500°C). Greater thicknesses can in any case be obtained by superimposing several layers of sol-gel, till the desired thickness is reached. We have produced multilayer structures with thickness larger than 1 μm; but in this case great attention must be paid to the cleanliness of the environment, since any dust particles included between the layers would strongly worsen the quality of the film. The refractive index of the resulting films, with 30% titania content, is 1.65.

Before any serious attempt at producing strip or channel waveguides was made, much attention was devoted to optimising the characteristics of the sol-gel films, especially in order to achieve low propagation loss. So far, we have obtained films with losses of the order of 0.5 dB/cm, low enough to allow the fabrication of devices.

3. Preparation of laser-written strip waveguides

The laser writing of sol-gel films to obtain strip waveguides exploits the localised heating of sol-gel due to the absorption of laser light by the film itself and/or the substrate, which substitutes the heating usually performed in an oven during the sintering stage of the sol-gel process (see Fig. 2).

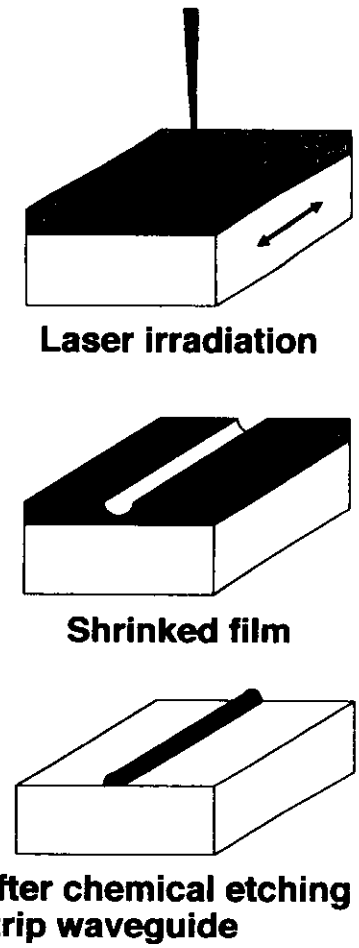

Fig. 2. Schematic representation of the selective densification process induced by a focused laser beam.

Obviously, in order to heat the film sufficiently, it is necessary that the laser irradiation be carried out at a wavelength that is strongly absorbed by the film and/or the substrate. In the case of silica glasses this means working in the ultraviolet or infrared region of the spectrum, as the material is completely transparent to visible light.

Alternatively, a thin cladding layer, which absorbs at a convenient wavelength, may be deposited on the sol-gel layer. The heat absorbed by the cladding can then be transmitted to the sol-gel film, producing its densification. Experiments with metal claddings and a Nd:YAG laser source have been

performed by various groups [8].

In our case we used a continuous-wave CO_2 laser operating at 10.6 μm. The choice was motivated by the fact that the CO_2 radiation is absorbed both by the substrate and by the sol-gel film, thus fulfilling the requirements of having sufficient heating of the sol-gel material at a low laser power. The wide availability and reasonable cost of such a laser system were further advantages offered by this choice, while its major inconvenience derives from the long wavelength of the radiation, which due to diffraction limits prevents obtaining a writing spot smaller than 30 μm. This fact limits the use of CO_2 laser writing to the production of highly-multimode or tapered guiding structures.

In our case, the laser processing was carried out on porous films baked at 60–200°C. When working with low-temperature baked films, the superimposition of a large number of layers is not possible since it would lead to the cracking of the film, even before the actual writing process. We have thus limited ourselves in general to the superposition of a couple of layers, reducing in this way the maximum final thickness of the waveguides to about 0.3 μm.

After passing through proper attenuators, the beam from a 12 W cw Synrad CO_2 laser was focused on the surface of the sample, mounted on a translation stage moved by a step-motor. The translation speed was 2 mm/s.

The power of the incident laser light is a very crucial parameter in the whole process, since insufficient power density produces too little or no effect on the sol-gel layer, whereas excessive irradiation leads to damage of the film and even to fusion of the substrate. Since the right amount of power irradiated on the sample depends, of course, also on the spot size of the laser beam, the right balance is very critical. Nevertheless, it is possible to find a range of values (not very broad, but large enough to allow a sufficient control of the parameters) which make possible a correct densification of the layer. We found the best incident power to be 50–60 mW, at which the spot size was about 100 μm.

A good control of the focusing conditions is very important as well. We therefore tried to obtain reproducible focusing of the laser beam on the surface of the sample, by using a micrometric translation stage for the focusing optics and with our looking at the burning effect of the beam on paper positioned precisely in the place of the sample. Though very simple, this system proved to be quite effective. We used focusing lenses having 50 and 100 mm focal length: of course, the best results in terms of minimum spot size were obtained with 50 mm lenses,

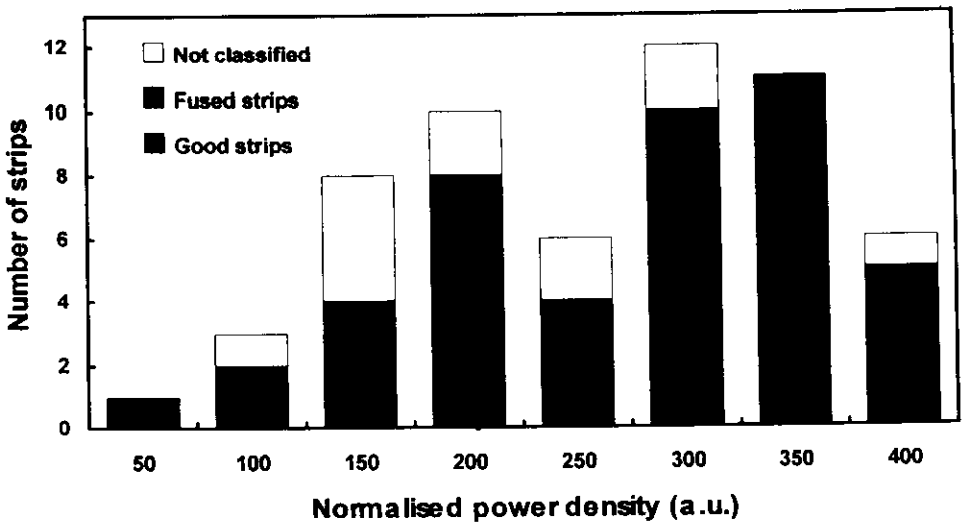

Fig. 3. Quality assessment of silica-titania strip waveguides as a function of the incident power density. Evaluation is made by optical inspection through a microscope, with typical magnification of 200. The "not classified" label indicates stripes where, despite of the lack of evident defects, the operator was feeling that the structure was not truly good (e.g. because of a weak appearance). The optimum value of the incident energy density (corresponding to values in the range 50–100 in the graph) was found to be about 6 W/mm^2.

although in this case the smaller depth of focus made control of the best focusing distance more difficult.

In order to assess the reproducibility of the process as a function of the laser power, a statistical analysis was made of the quality of the strips obtained. In Fig. 3 we show a representation of the quality of the waveguide as a function of the power density that is incident on the sol-gel layer. It is evident how quickly the relative amount of "burned" waveguides increases as the power exceeds the optimal value. The damages that excessive irradiation can create on the sample are shown in Fig. 4. In this case, the boundary of the region of the substrate melted by the laser beam is clearly visible in the SEM picture.

During the writing process, the films experience the usual shrinkage caused by the material sintering; this is now localised in the area heated by the laser light, as shown in Fig. 5, where the transversal profile of an irradiated sol-gel film measured by means of a stylus profilometer is shown.

The undensified areas of the film must then be removed, in order to eliminate unstable material, which may deteriorate in the course of time. Its removal is achieved by immersing the samples in a buffered and diluted solution of HF ($HF:NH_4 = 1:6$ diluted 1:1 in water). An etching time of 1 minute is enough to remove all the undensified sol-gel, leaving the densified strips practically unaffected, thanks to

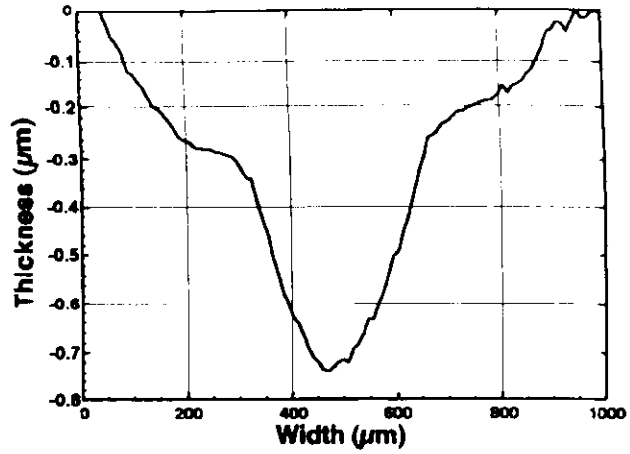

Fig. 5. Depth profile, as measured by means of a stylus profilometer, of a transversal section of a laser-heated sol-gel strip before the etching process which removes the unexposed part of the film. The zero-thickness level corresponds to the surface of the original (unexposed) layer: the shrinking of the sol-gel film due to the laser densification (80 mW laser power, 50 mm focal length lens) is evident.

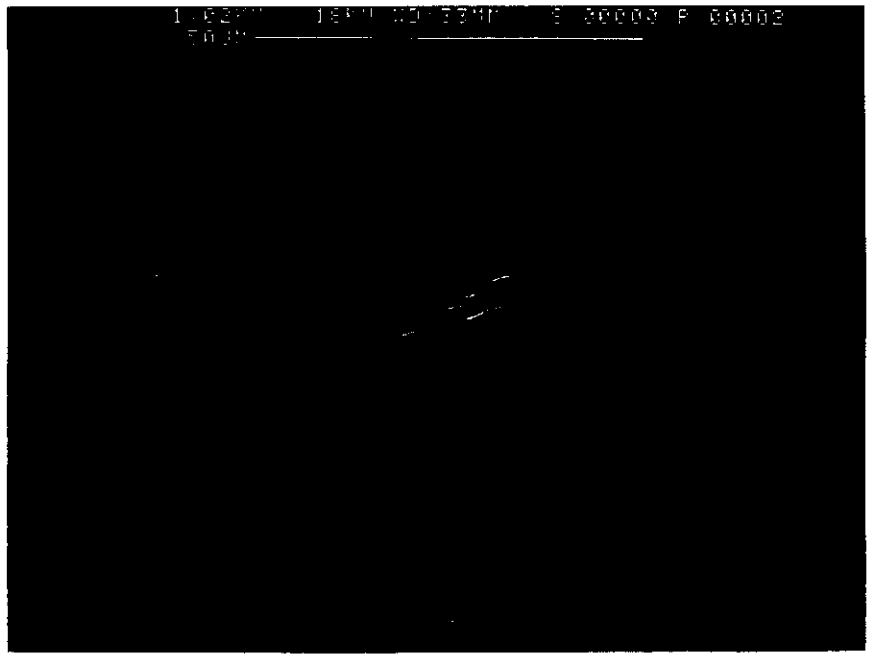

Fig. 4. SEM picture showing a typical damage induced on the sample by excessive laser irradiation. The boundary between the melted part of the substrate and the intact part is clearly visible.

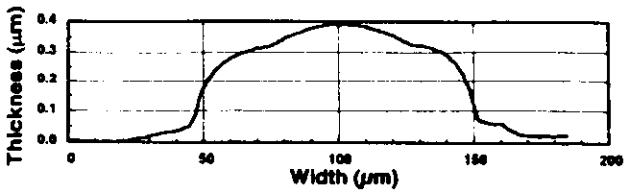

Fig. 6. Typical profile of a strip obtained by laser densification after the removal of the unexposed portion of the sol-gel film.

the high difference in etching rates between the two materials.

At the end of the process sol-gel glass strips are obtained. Their width is obviously dependent on the spot size achieved during the writing process; on an average, we have obtained strips about 100 μm wide. In Fig. 6 we show the transverse profile of a typical strip.

As noted above, this value is too high for normal waveguides, but may be of interest for tapered structures; further optimisation of the focusing system should make the production of 50-μm-wide waveguides possible, comparable with standard multimode optical fibres (even if the thickness remains very different).

4. Optical and structural characterisation

The most relevant step in the characterisation process is constituted by the measurement of light propagation loss along the produced waveguide. A scattering detection technique has been used, which employs a semiautomatic system with a Vidicon camera collecting the light scattered out of the plane of the waveguide. If we assume that the light inside the waveguide is proportional to the light scattered outside the waveguide, as is usually true, from this measurement we can readily obtain the decay of the radiation inside the strip.

The light was injected into the waveguides both by end-fire and prism coupling., since the width of the strips permitted this latter technique, thus making it possible to avoid the endface polishing step.

So far, the measurements have given average values of about 1 dB/cm propagation losses, with best values (in very few, and unfortunately not yet reproducible, cases) of 0.7 dB/cm. These values are very interesting, because they are very close to those obtained by other methods and represent a substantial improvement compared to our earlier results, that were obtained with much higher incident power

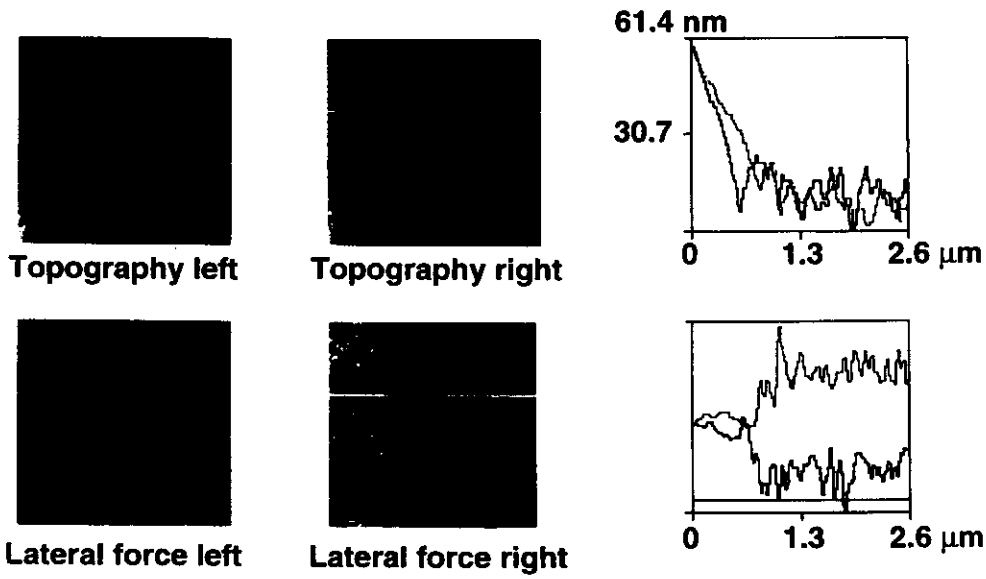

Fig. 7. The upper AFM pictures show the topographic map of the area at the border between the substrate and the edge of a strip waveguide, taken in the two senses of the transversal scan direction; lower pictures indicate the friction measured by the stylus during the scan. The plots on the right represent the topographic and friction data respectively as measured along the highlighted line. An inversion of white/dark areas in the lateral force pictures has to be attributed to the difference in the material structure.

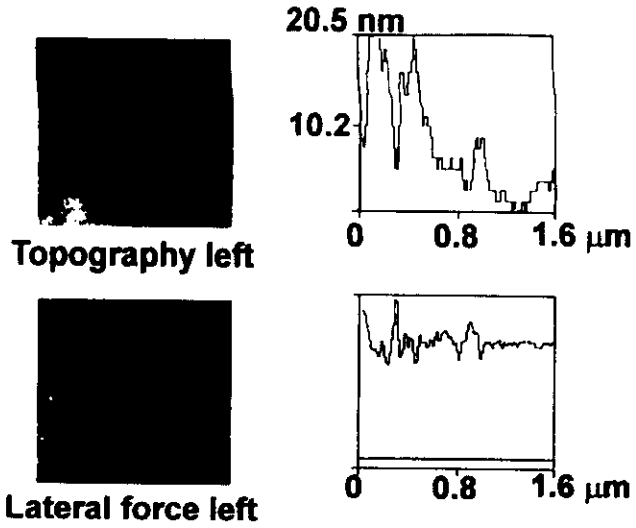

Fig. 8. The upper AFM picture shows the enlarged topographic map of an area close to the strip edge; the lower picture shows the corresponding friction measured by the stylus during the scan. The plots on the right represent the topographic and friction data respectively as measured along the highlighted line. The inhomogeneity of the film in this area (due to some clusters of what is considered to be partially densified material) is evident.

(about 0.3–0.4 W on 250 μm focal spots), and which had shown propagation losses of the order of 6 dB/cm.

In order to obtain more information on the quality of the laser-densified sol-gel strips, and possibly to compare them with films obtained by conventional oven densification, structural analyses were also performed.

As a first step, we performed a series of Atomic Force Microscope (*AFM*) measurements in order to determine the surface porosity and rugosity of the sol-gel strips. In Fig. 7 is shown the edge of a strip waveguide as taken by AFM: the border of the edge is clearly visible, especially in the friction pictures where the material difference between the strip and the glass substrate is clearly visible. No clear evidence of residual porosity exists, as in the case of oven-densified waveguides; there seems, however, to be a little roughness, possibly caused by stresses that arose during the laser irradiation. This type of defect could be reduced by carrying out a reflow process after the etching, in order to relax the stresses. The quality of the waveguides would also be improved by the subsequent deposition of a low-index cladding layer.

In Fig. 8 the AFM picture shows some small residuals of undensified strips still remaining near the strip edge after the chemical etching process. The

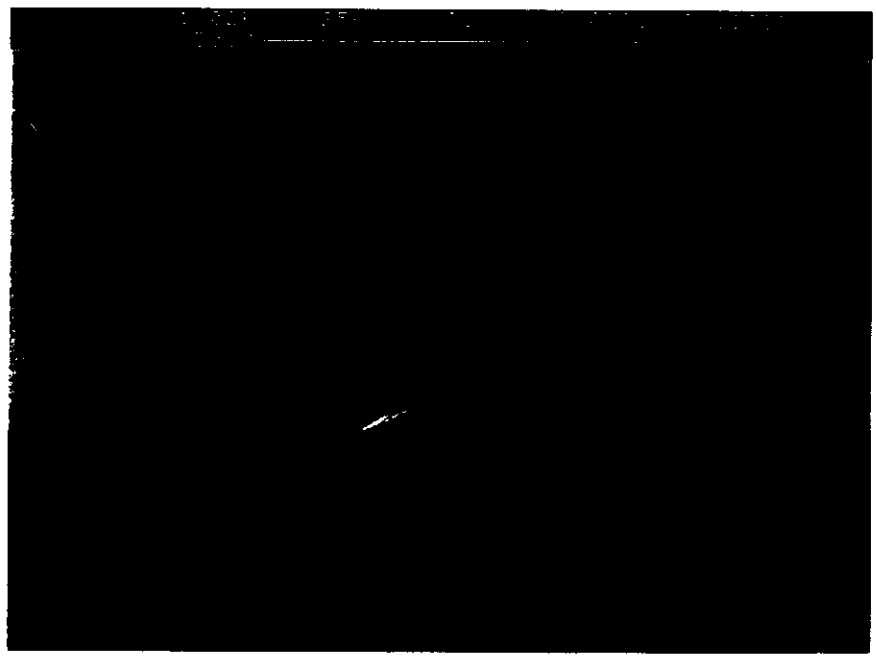

Fig. 9. SEM microphotograph of the entrance face of a laser densified strip. Apart from the very poor quality of the edge itself, which had not been properly polished, the overall quality of the waveguide appears to be quite good.

extent of this defect is very small and should not heavily affect propagation.

Fig. 9 is a picture taken by Scanning Electron Microscope (*SEM*) of a laser-densified strip. Apart from the poor edge polishing, the overall good quality of the strip is visible, as well as its very asymmetric aspect ratio, since it is much wider than it is higher. To overcome this limitation, work is in progress to obtain thicker monolayers, e.g. by leaving higher organic content in the film.

Another concern was the residual carbon left in the strip after the laser irradiation. Actually, the rapid heating of the sol-gel layer and burning of the organic content during the laser-densification process can hinder the release of combustion products outside the film, leading in the end to higher propagation losses due to absorption by the residual carbon. In our first trials using nuclear techniques (Rutherford Back Scattering) we indeed found a higher content of carbon compared to that present in oven-densified samples [9]: at that time we attributed part of the contribution to the higher losses measured on laser-densified waveguides to this effect. However, later measurements, obtained by means of microprobe spectroscopy, have shown that in the most recent, low-loss samples, the carbon content is very low; therefore in the current samples propagation losses can be attributed mostly to the roughness of the strip edges.

The problem of high losses in laser-densified waveguides has been discussed in detail also by Faber [10], who carried out a comparative analysis of different results reported in the literature. So far it has not been possible to assess quantitavely the various causes of losses, but there are indications that a better choice and a more accurate control of laser heating conditions could lead to achieving loss values almost equal to those in oven-heated films.

5. Conclusions

The applicability of laser-writing techniques to the selective densification of silica-titania glass sol-gel layers was investigated. Laser-densified sol-gel strip waveguides were produced and characterised.

Although achieving low-loss waveguides appears to be difficult, as this requires an accurate control of both the environmental conditions and laser-writing parameters, our recent results, with propagation losses below 1 dB/cm, are very promising. Moreover, since the main source of loss seems to be related to the residual roughness of the strip walls rather than to carbon content or titania crystallization, effective improvements can be obtained by inducing glass reflow and/or by depositing a pure silica glass layer.

Further attention has to be devoted to the design and realization of the waveguide structures, both by optimizing the laser-writing optical system, in order to obtain almost diffraction-limited focal spots, and by using thicker sol-gel films, in order to obtain strips with a better height/width ratio.

Acknowledgements

The collaboration of Dr. P. Boffi (Centro Laser, Bari) for SEM pictures and microprobe analysis and of Dr.s C. Cecconi (Ist. Biofisica, Pisa) and A. Verciani (CEO, Firenze) for AFM analysis is gratefully acknowledged. The support of EEC through the ESPRIT project N. 6993, "NODES" is also acknowledged.

References

[1] G.M. Lad, G.M. Naik and A. Selvarajan, Opt. Eng. 32 (1993) 725.
[2] R.R. Krchnavek, H.H. Gilgen and R.M. Osgood Jr., J. Vac. Sci. Technol. B2 (1984) 641.
[3] M. Ohtani and M. Hanabusa, Appl. Optics 31 (1992) 5830.
[4] M. Haruna, T. Kato, K. Yasuda and H. Nishihara, Appl. Optics 33 (1994) 2316.
[5] C. Lavoie, M. Meunier, S. Boivin, R. Izquierdo and P. Desjardins, J. Appl. Phys. 70 (1991) 2343.
[6] R.R. Krchnavek, G.R. Lalk and D.H. Hartman, J. Appl. Phys. 66 (1989) 5156.
[7] D.J. Shaw and T.A. King, Proc. SPIE 1328 (1990) 474.
[8] B.D. Fabes, D.J. Taylor, L. Weisenbach, M.M. Stuppi, D.L. Klein, L.J. Raymond, B.J.J. Zelinski and D.P. Birnie III, Proc. SPIE 1328 (1990) 319.
[9] M. Guglielmi, P. Colombo, L. Mancinelli degli Esposti, G.C. Righini, S. Pelli and V. Rigato, J. Noncrist. Solids 147&148 (1992) 645.
[10] B.D. Fabes, in: Sol-Gel Optics: Processing and Applications, ed. L.C. Klein (Kluwer Academic Publishers, USA, 1994) p. 483.

Sol–gel glasses for nonlinear optics

Giancarlo C Righini†‖, Alessandro Vercianì†‖, Stefano Pelli†‖, Massimo Guglielmi‡¶, Alessandro Martucci‡¶, Jochen Fick§+, Guy Vitrant§+

† Optoelectronic Technologies Group, IROE-CNR 'Nello Carrara', via Panciatichi 64, I-50127 Firenze, Italy

‡ Dipartimento Ingegneria Meccanica, Sezione Materiali, Università di Padova, via Marzolo 9, I-35131 Padova, Italy

§ LEMO-ENSERG, Institut National Polytechnique de Grenoble, Grenoble, France

Abstract. In recent years a large amount of activity has been carried out searching for novel or advanced materials which exhibit large nonlinear third-order susceptibility $\chi^{(3)}$. Emphasis has been put on materials suitable for integrated optical circuits, since the guided-wave format can provide additional routes to the conception and realization of photonic devices. The preparation of nanoparticle-doped glass by the sol–gel technique represents one of the most promising approaches: here we give a short overview of alternative processes to control the size of semiconductor clusters and we present experimental results from CdS- and PbS-doped silica–titania sol–gel films.

1. Introduction

Current developments in optical telecommunications are leading to demand in the near future for devices capable of ultrafast signal switching and routing, in order to cope with an increased volume of transmitted data. These functions, presently carried out mainly by electro-optical circuits, will have to be performed by all-optical integrated devices to guarantee sufficiently fast response times. In order to realize such devices, new optical materials, exhibiting strong nonlinear properties, must be developed. Research has been moving along several directions, ranging from polymers to semiconductors, from organic to inorganic materials; in this paper a brief survey is provided of the properties of a particular class of materials, namely that of semiconductor-doped glasses (SDG) produced by the sol–gel technique.

SDGs offer the advantages of glass as a cheap and robust material for integrated optical circuits, together with the nonlinear properties of semiconductors; the aim of many researchers has been the increase of their nonlinearity, as required for all-optical switching devices [1] and the assessment of an easy and reliable production process. The sol–gel method, on the other hand, has gained considerable attention in recent years, since it allows low process temperature and easy manufacture of glassy materials, combined with the possibility of inserting in the glass matrix a huge variety of dopants, which can confer special properties to it.

‖ E-mail address: righini@iroe.fi.cnr.it, alex@suniroe.iroe.fi.cnr.it, pelli@suniroe.iroe.fi.cnr.it

¶ E-mail address: maxgugl@ipdunidx.unipd.it, material@ipdunivx.unipd.it

+ E-mail address: fick@enserg.fr, vitrant@enserg.fr

0963-9659/96/050655+12$19.50

While reporting on current efforts in the development and characterization of SDG films obtained by the sol–gel technique, particular reference here will be given to our work, carried out in the framework of a European Commission's ESPRIT project.

2. Sol–gel glasses

The sol–gel method allows the synthesis of inorganic networks at low temperature. A solution of specific chemical precursors is hydrolysed and, through a polycondensation process, is transformed into a gel. The drying of the gel, which is constituted by interconnected solid and liquid phases, eliminates the liquid and thus produces a porous xerogel. Finally, by a proper heat treatment, densification occurs and the xerogel transforms into a solid material: an amorphous one, i.e. a glass, or, if crystallization takes place along with sintering, a ceramic one.

Sol–gel bulk materials and coatings are not new, but only at the end of the 1980s was a significant amount of work being focused onto the deposition of sol–gel layers to be used as optical waveguides and onto the possibility of doping amorphous glasses, either in bulk or in film format, with organic and inorganic compounds in order to produce novel nonlinear or active optical materials.

Silicate sol–gel glasses, in particular, are often obtained by hydrolysing monomeric, tetrafunctional alkoxide precursors such as tetraethoxysilane (or tetraethyl orthosilicate, TEOS), $Si(OC_2H_5)_4$. The hydrolysis reaction replaces alkoxide groups OR (where R indicates an alkyl group, C_xH_{2x+1}—in this case the alkyl is ethyl, C_2H_5) with OH hydroxyl groups; subsequent condensation reactions produce siloxane bonds (Si–O–Si) which in turn start forming a porous solid network. The gelation stage can be carried out in a vessel, thus obtaining a bulk sample, or by depositing the solution onto a substrate (by spinning or dipping), which leads to the formation of a film with quality suitable for integrated optics applications. A first drying process, typically at temperatures around or below 100 °C, eliminates most of the solvents still present in the porous gel, and a further process at higher temperature (300–500 °C) densifies the material, producing a dense glass with only 5–10% porosity left.

Several parameters may seriously affect the process and therefore the optical quality of the resulting glass: they include the choice of the solvent and catalyst, the pH of the solution and the process temperature [2].

The addition of other compounds gives the process great flexibility; thus, for instance, if titanium butoxide $Ti(n\text{-}Obu)_4$ is added to the solution as a precursor of titanium dioxide, the refractive index of the resulting glass can be tailored in a wide range by controlling the relative quantity of the two precursors.

Much effort is currently being put toward producing novel or advanced glassy materials by the sol–gel route and to developing suitable patterning techniques for direct fabrication of integrated optical circuits [3].

3. Semiconductor-doped glasses

The inclusion of semiconductor microcrystals such as CdS, CdS–Se, ZnS, PbS, CuCl, CdTe and PbTe in a glass matrix host represents an effective way of producing a material with enhanced nonlinear properties. Moreover, it is well known that if the dimension of the semiconductor clusters is of the order or smaller than the exciton Bohr radius (about 20 Å for CdS), the quantization of the energy levels due to size quantization can lead to a strong

improvement of the nonlinear characteristics of the material itself [4, 5].

Research has initially concentrated on commercially available SDGs, commonly used as sharp-cut optical filters [6]; though this first approach has been important for the understanding of some basic mechanisms of the nonlinear properties enhancement, these materials were not optimized either for integrated optical applications or for optimal performance in terms of nonlinear response [7, 8].

The first problem which had to be addressed to optimize these materials was the size distribution of the clusters, which in the early samples, obtained by usual melting processes, was too broad to obtain a sharp, strong enhancement of the nonlinearity [8].

The second problem was constituted by the darkening of the glasses when exposed to light beams (*photodarkening*). This phenomenon, probably caused by photochemical reactions which take place at the boundary between the semiconductor and the glass matrix, although usually improving the time response of the glass, also increases its absorption, which of course harms light propagation.

While optimization of the production of SDGs by the melting processes is still considered, other processes have been explored, such as RF-sputtering deposition [9, 10] and sol–gel deposition, which offer better prospects especially for the control of size of nanocrystals.

An advantage of the sol–gel route is that the glass synthesis through chemical reactions can start from ultrapure components: thus, the problem of photodarkening can be strongly reduced, since the possibility of impurities located at the cluster–glass matrix interface is reduced. The high purity of the glass and the complete control of the material composition also allows an increase in the dopant concentration, which can, in turn, further improve the special characteristics of such glasses.

Several techniques can be applied to the process in order to effectively control the size of the clusters, obtaining narrower size distributions of the crystallites; even subsequent thermal treatments for drying and densification, at temperatures usually lower than 500 °C, do not induce unwanted effects of growth of the nanocrystals and broadening of the size distribution, as occurs in SDGs produced by standard melting processes. In contrast, the particle size can be controlled by applying appropriate heat-treatment schedules [11, 12].

Two main approaches are being investigated in order to efficiently control the size of the semiconductor clusters: the first one takes advantage of the porosity of the sol–gel matrix to put an upper limit to the growth of the crystallites (*pore doping*), while the second one uses chemistry to control the cluster surface and to terminate it by capping groups which prevent further aggregation and growth of nanoclusters (*surface capping*).

3.1. Nanocrystal control by pore doping

Many recent papers describe good results achieved by this approach [13–23]. Herron and Wang [15], for instance, explored different routes to the preparation of semiconductor nanoparticulates; in particular, they prepared porous silica glass starting from tetraethoxysilane and introduced semiconductors into the pores, the average size of the pores being controlled by the pH of the starting solution. If a metal (e.g. Cd) precursor had been previously added to the starting solution, the samples were annealed in an H_2S atmosphere (the size of the cluster is also controlled in this case by the annealing time); otherwise, Cd could be inserted into the porous glass by impregnation, soaking the substrate in a cadmium nitrate solution and then obtaining CdS by carrying out the annealing process. The latter technique may lead to very high density of semiconductor clusters in the glass pores, but the authors realized that it is very difficult to achieve a uniform dispersion of the

dopant throughout a large substrate using an impregnation approach. They also made use of MOCVD-type chemistry to introduce III–V semiconductors such as GaAs into a glass.

The impregnation approach was also followed by Choi and Shea [16] who used Na_2S instead of H_2S for the sulphidation step.

Yeatman *et al* [17] investigated thoroughly the influence of the sol–gel process on the pore size distribution and obtained CdS crystals with an average size of 4 nm by annealing a silica gel in an H_2S atmosphere where Cd had already been dispersed in the gel by adding cadmium acetate to the starting solution. They found that the higher the annealing temperature, the smaller the crystal obtained. Nonlinear m-line measurements using low and high intensities (0.76 μJ/pulse and 8.41 μJ/pulse, respectively) were performed on a film obtained by the process described: from these results the nonlinear refractive index at the wavelength of 0.532 μm was estimated to be $n_2 = -5.5 \times 10^{-9}$ cm^2 kW^{-1} [18]. However, the higher values of n_2 obtained for thinner films, e.g. 3.2×10^{-8} cm^2 kW^{-1} in [19], suggest that substantial improvements are possible. Such values of nonlinear refractive index n_2, defined according to the expression $n = n_0 + n_2 I$, can be transformed into values of third-order nonlinear susceptibility $\chi^{(3)}$ by using the numerical relation n_2 (cm^2 kW^{-1}) $= (4\pi^2/n_0^2)\,\mathrm{Re}\,\chi^{(3)}$ (esu) [20]. Thus, corresponding values of $\chi^{(3)}$ are 3.2×10^{-10} esu and 1.8×10^{-9} esu, respectively.

Using a similar technique, Minti *et al* [21] obtained CdS clusters with sizes mostly in the range 2–5 nm, but going up to 20 nm; despite this rather broad size distribution, third-harmonic generation signals were observed when the sample was laser irradiated at 1.06 μm and observed at 0.355 μm: the corresponding $\chi^{(3)}$ was evaluated to be about 10^{-12} esu.

3.2. Nanocrystal control by surface capping

The approach described in the previous section corresponds to introducing a physical size restriction, but more flexibility can be provided by nanochemistry itself. The basic problem is how to prevent aggregation of the nascent crystallites into larger clusters and eventually into a macroscopic bulk solid, as required by the system's thermodynamics: an effective answer is to use a terminating agent, i.e. a molecule which attaches to the growing cluster surface and thus controls the size to which it can grow. Research efforts have therefore focused on the selection of the best ligands and on the optimization of the entire process: the development of a synthetic methodology to prepare monodisperse nanoclusters is important not only for optical devices, but also for catalysis (e.g. for the preparation of size-selective photocatalysts), for chemical sensing or novel magnetic devices (nanoscale magnetic particles exhibit new physical properties and have potential for application to information storage and colour imaging) [22].

To mention some examples, Mackenzie and co-workers [23] developed CdS-doped glass samples by combining the previous technique with the use of chemical agents to control the cluster growth. They started producing a porous organically modified silica gel containing CdO clusters and carried out an annealing under an H_2S atmosphere to obtain CdS clusters, as described above. By introducing 3-aminopropyltriethoxysilane (APTES) as a ligand functional to the solution they obtained a narrow distribution of the cluster size (2.8 nm on average, 0.9 nm standard deviation). The ligand anchors the Cd to the gel-glass matrix, avoiding its precipitation during the drying step and thus improving the homogeneity of the film. A huge nonlinearity, with $\chi^{(3)}$ of about 10^{-6} esu, is claimed from preliminary measurements on these samples but its repeatability has yet to be checked.

A different approach based on the production of colloidal particles and the control of

their size through surface capping independently of their incorporation in sol–gel media has been used by several authors [16, 21, 24, 25]. For example, Gacoin *et al* [22] produced semiconductor nanoclusters capped with phenylthiol, which were then dispersed in a sol–gel precursor solution.

Herron and Wang [26] also obtained CdS clusters of size up to 40 Å by using thiophenolate as a capping agent. In this case the clusters were in acetonitrile solution and showed a $\chi^{(3)}$ of around 10^{-14} esu. Since the clusters are easily soluble in a wide range of solvents, the authors suggest either to produce pure CdS films by spray pyrolysis or to incorporate them in polymeric films like PMMA.

4. Preparation of CdS- and PbS-doped sol–gel films

In our experimental work we have concentrated on the preparation of silica–titania glasses doped with CdS and PbS semiconductor clusters. Our approach has been similar to the last method described in the previous section: we first prepared a colloidal suspension of semiconductor microcrystals and then we added it to the solution used for the sol–gel synthesis of a pure silica–titania film. The latter was an ethanol (EtOH) solution, prepared by mixing TEOS and methyltriethoxysilane (MTES) in 1:1 molar ratio, plus titanium butoxide as a precursor of titania. The other compounds added to the solution are: water for the hydrolysis, HCl as a catalyst to the reaction and acetylacetone in order to stabilize titanium alkoxide against fast hydrolysis. Usually a molar ratio of 7:3 was used between MTES + TEOS and titanium butoxide. The other components were mixed in the following molar ratios: $H_2O/(TEOS + MTES) = 2$, $HCl/(TEOS + MTES) = 0.01$, $(TEOS + MTES)/EtOH = 1$.

MTES was used in order to obtain thicker coatings by a single deposition run. Colloidal solutions of CdS and PbS were produced by dissolving cadmium and lead acetate, respectively, in methanol (where the solubility is higher than in ethanol) together with surface capping agents. A second solution of thioacetamide, as a source of sulphur, was prepared and thereafter mixed with the former solution. As a result of the reaction between the metal acetate and thioacetamide a colloidal suspension of CdS or PbS was obtained at room temperature.

Various surface capping agents were tested for their efficiency in controlling the crystal growth: acetylacetone, 3-aminopropyltrimethoxysilane (APT and 3-mercaptopropyltrimethoxysilane (MPTMS). The best results were obtained with MPTMS, which was thus chosen for the production of all the films. By changing the molar ratio M = MPTMS/cadmium (or lead) acetate, different growth rates and dimensions of the clusters were obtained. As an example, CdS particles having 3.5 nm and 7.5 nm size were obtained by using $M = 2$ and $M = 0.5$, respectively; these values were deduced, using the Scherrer equation [27], from x-ray diffraction analysis of the powders obtained by the corresponding sols.

The colloidal suspension produced was added to the TEOS–MTES–$Ti(n\text{-}Obu)_4$ solution (with the molar ratio between semiconductors and silica + titania equal to 0.05) and almost immediately deposited by dipping on soda-lime microslides. The samples were dried at 60 °C and densified at 300–500 °C for 1 hour in a nitrogen atmosphere to prevent the oxidation of sulphides and the consequent decrease in the optical properties of the films. The typical refractive index of the films produced was around 1.54.

5. Characterization of the samples

5.1. Spectroscopic measurements

Spectroscopic characterization is very important, since the appearance of the characteristic absorption edge confirms the presence of semiconductor clusters in the films. Also, the shift of the edge with respect to the bulk value gives an indication of the crystallite size, as the quantum confinement shifts the edge toward higher energies (and hence shorter wavelengths) for smaller clusters. According to Kayanuma [28], the relationship between the band gap energy shift ΔE_g and the cluster radius R is given by

$$\Delta E_g = \frac{h^2}{8R^2}\left(\frac{1}{m_e} + \frac{1}{m_h}\right) - \frac{1.786e^2}{\varepsilon R}$$

where m_e and m_h are the reduced masses of the electron and the hole, respectively.

The blue shift is evident in figure 1, where the comparison between the spectra of CdS films obtained with two different MPTMS concentrations is shown. The film with higher MPTMS concentration ($M = 2$) has the absorption edge shifted toward shorter wavelengths, as expected. This shift indicates values of cluster size which are quite a lot smaller than the ones measured by x-ray diffraction in the powders.

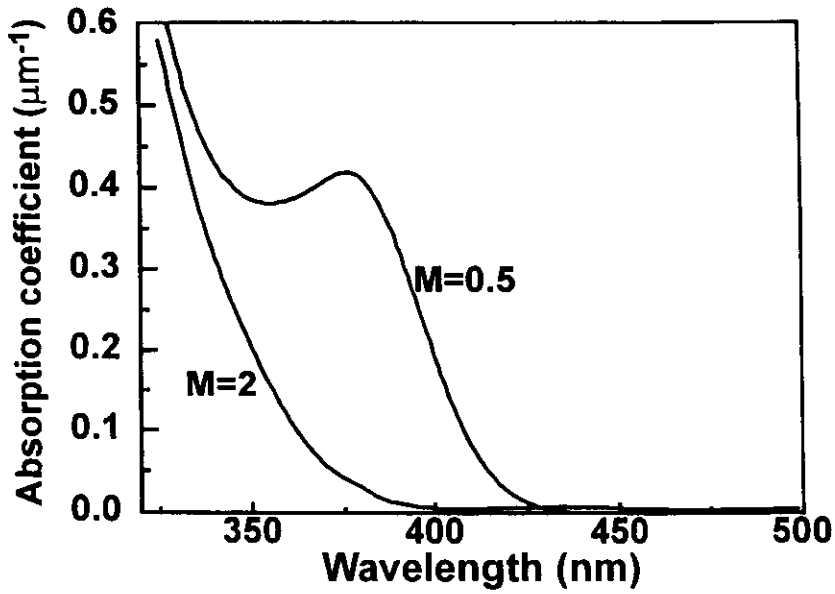

Figure 1. Absorption spectra of CdS-doped pure silica films dried at 60 °C; $M = 0.5$ and $M = 2$ refer to MPTMS/Cd ratios of 0.5 and 2, respectively. In the sample with $M = 2$, clusters are likely to be so small as to shift the absorption edge below 320 nm, where the substrate itself is highly absorbing.

In figure 2 the broadening and decreasing of the resonance upon higher temperature heat treatment for a CdS-doped film is noticeable. While the shift and the broadening can be attributed to the increase in size of the clusters and to the likely increase in size dispersion, respectively, the overall decrease of the effect with the increase in temperature may well be due to oxidation of a number of sulphide clusters and to evaporation of sulphur.

Figure 3 shows two absorption spectra of PbS-doped films, corresponding to two different MPTMS/(lead acetate) molar ratios. All of the PbS spectra taken in films showed featureless absorption edges: various explanations of this behaviour are possible and further investigations are therefore necessary for a better understanding of it. According to Wang

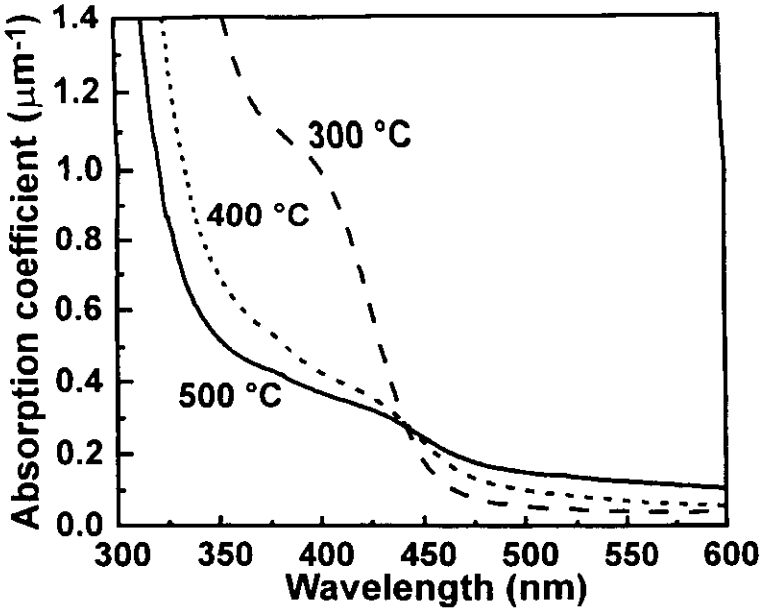

Figure 2. Absorption spectra of CdS-doped silica–titania films heat treated at different temperatures in a nitrogen atmosphere. The red shift of the absorption edge makes evident the effect of higher temperature treatment on the particle growth and on the broadening of the size distribution.

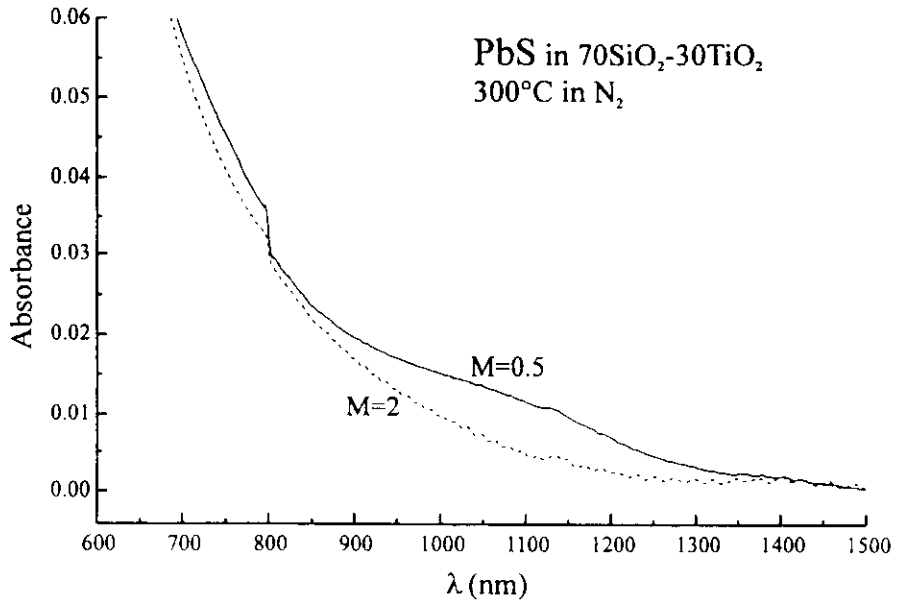

Figure 3. Absorption spectra of PbS nanoparticles in silica–titania sol–gel films. Analogously to figure 1, *M* indicates the molar ratio between MPTMS and lead acetate.

et al [29], for instance, the absence of excitonic structures may be attributed to the weak exciton binding energy due to strong Coulomb screening and/or to broad size distributions.

5.2. X-ray diffraction measurements

XRD measurements carried out on powders obtained either directly from the precipitation of the metal–thioacetamide solution or from bulk or film samples of the final composite gel have allowed us to make a direct evaluation of the dimensions of the semiconductor

crystals. The analysis of thin films was performed using a Philips diffractometer, Cu K_α Ni filtered radiation at 40 kV and 50 mA and glancing-incidence x-ray optics. The average crystallite size was calculated from the Scherrer equation by fitting the experimental profiles.

Thus it was confirmed that, by suitably changing the MPTMS concentration, we were able to produce particles with dimensions ranging from 2 to 20 nm. An interesting effect is the fact that PbS particles measured from powders of bulk gel glass are larger than those obtained from films: we measured 8 nm in powders and 2.5 nm in films treated at 300 °C [30]. The same situation was also observed for CdS particles, even if it could not be quantified (at least by XRD only) due to the fact that the peaks of CdS in the films, although clearly present, were too broad and weak to enable the size calculation. The different particle sizes of the precipitates produced from the colloidal sol and of the particles in the films indicate that the history of the particle growth is different in the two cases. With the conditions used for the preparation of the colloidal sol, the particle growth rate was strongly decreased, but not stopped, by the presence of the capping agent. In films this growth was 'frozen' by the sol-to-gel transition, differently from what occurs in the colloidal sol, thus giving smaller particles.

5.3. Nonlinear optical measurements

Apart from the structural characteristics, the most relevant parameter to be measured in such films is constituted by the value of the nonlinear refractive index n_2 or, equivalently, the third-order nonlinear susceptibility $\chi^{(3)}$.

In order to accomplish such a measurement a guided optics configuration has been chosen, since it is a sufficiently sensitive technique and we had produced good quality sol–gel waveguides, having a typical propagation loss below 1 dB cm^{-1}.

The technique is based on the fact that the optimum coupling condition of a light beam to a waveguide is determined by all the parameters constituting the waveguide. If any parameter changes (in particular, the index of the guiding film) the coupling angle changes as a consequence. Our experimental technique allows us to detect quite small variations of the optimum coupling angle caused by the index change induced by the nonlinear Kerr effect in the doped film [31].

The experimental set-up is shown in figure 4; the light from a frequency tripled mode-locked Nd:YAG laser (8 ns pulse length, 10 Hz repetition rate) pumps an OPO source, which allows tunability over a wide range of wavelengths (400–3000 nm). This is then aimed onto a holographic grating realized by us on the surface of the film or on the substrate, which acts as a light coupler to insert light into the waveguide. The optimal coupling condition depends on the incidence angle of the laser beam on the grating. The intensity of reflected beam has a minimum when the optimal coupling is met; by tracking the position of this minimum, any change of the refractive index of the film is detected. By fitting the experimental reflectance versus coupling angle data to a theoretical model curve an evaluation of the guiding layer index is possible.

In figure 5 two measured reflectance curves, corresponding to the fundamental mode coupling m-line in a CdS-doped film are reported, one of them corresponding to low laser intensity, the other to high intensity (the energies were 5.5 μJ/pulse and 60 J/pulse, respectively). The deduced value of the nonlinear coefficient at a wavelength of 532 nm is, in this case, $n_2 = -3 \times 10^{-9}$ cm^2 kW^{-1} (corresponding to $\chi^{(3)} = 1.8 \times 10^{-10}$ esu). The measurements could be repeated several times without change in the m-line patterns, demonstrating the repeatability and reliability of the measurement process.

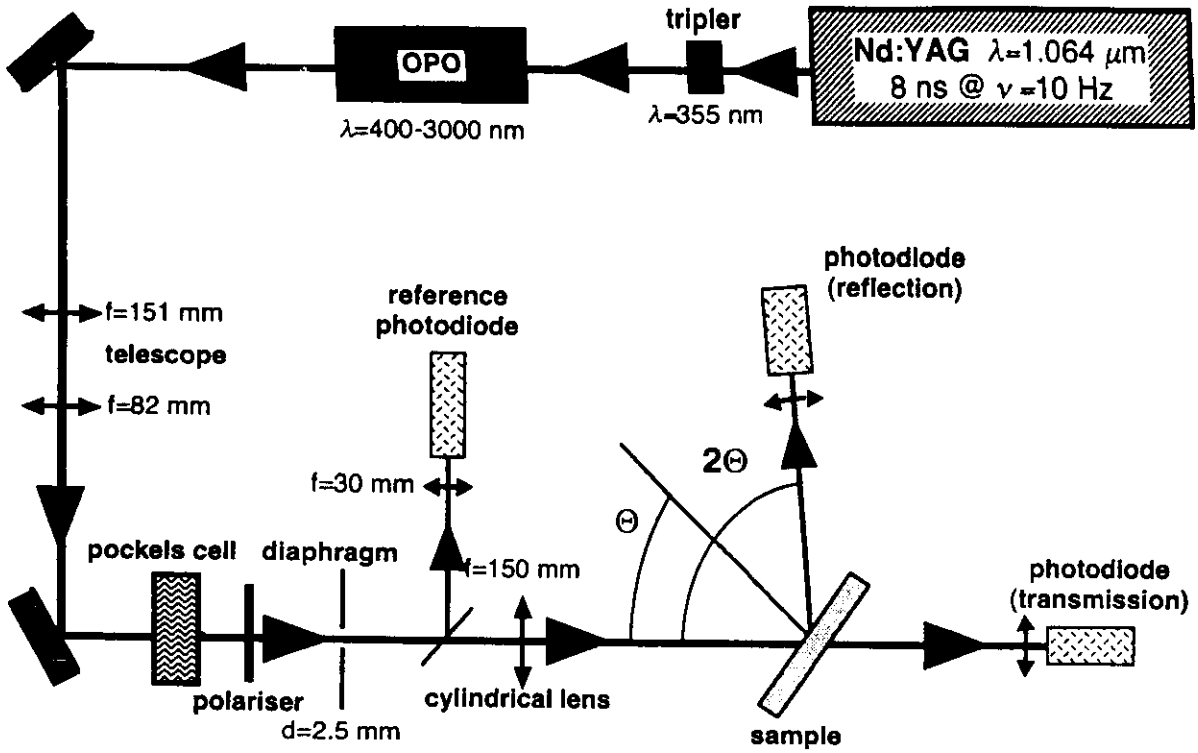

Figure 4. Experimental set-up of the nonlinear *m*-line measurements: the sample has a grating coupler built into the substrate or the guiding film itself.

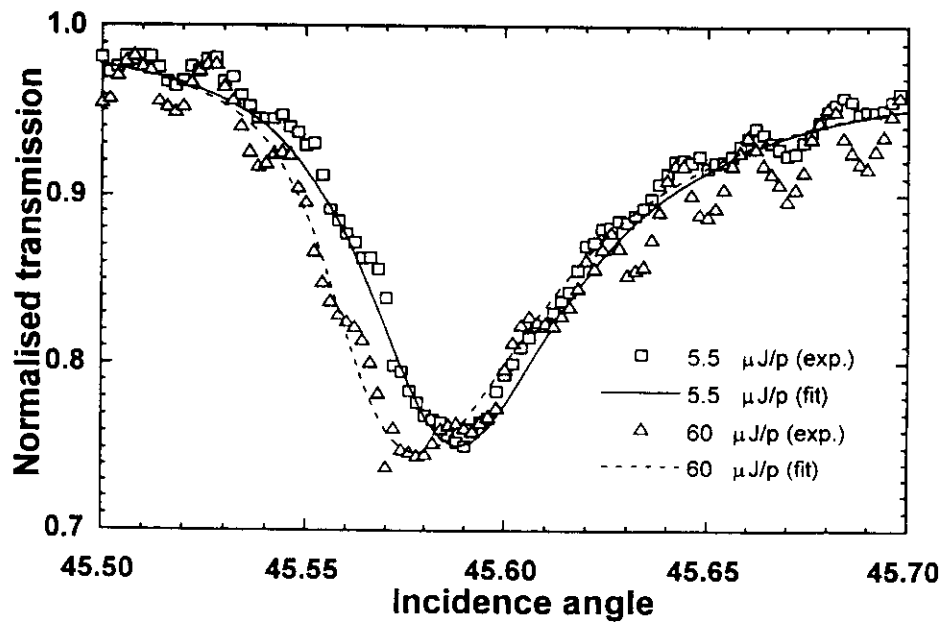

Figure 5. Resonant coupling curves showing the normalized intensity transmitted through the grating coupler as a function of the incidence angle, as measured by the corresponding photodiode in figure 3. The curves, both at low and high incident laser energy, show the expected behaviour according to a theoretical model: it can be seen that the fit between experimental data and the theoretical curves is quite good. These nonlinear measurements refer to a CdS-doped sample heat treated at 300 °C in nitrogen.

A similar measurement on a PbS-doped sample, carried out [illegible] coupling the light of the Nd:YAG laser into the waveguide through an isosceles prism instead of a grating, gave as a preliminary result the very promising value of $n_2 = -4.6 \times 10^{-9}$ cm^2 kW^{-1}. This value, equivalent to $\chi^{(3)} = 2.8 \times 10^{-10}$ esu, compares favourably with other results, such as the one obtained by Pellegri *et al* [32] who measured by degenerate four-wave mixing a $\chi^{(3)} = 1.95 \times 10^{-11}$ esu at 532 nm in PbS-doped gels prepared by reverse micelle and sol–gel routes.

Figure 6 shows the time decay of the nonlinear properties of a CdS-doped sample during a six month period. The nonlinearity is rather stable and in any case we expect to further reduce or cancel the decay of the nonlinear coefficient, which is probably caused by the oxidation of CdS molecules, by depositing a protective pure silica cladding layer on top of the guiding layer.

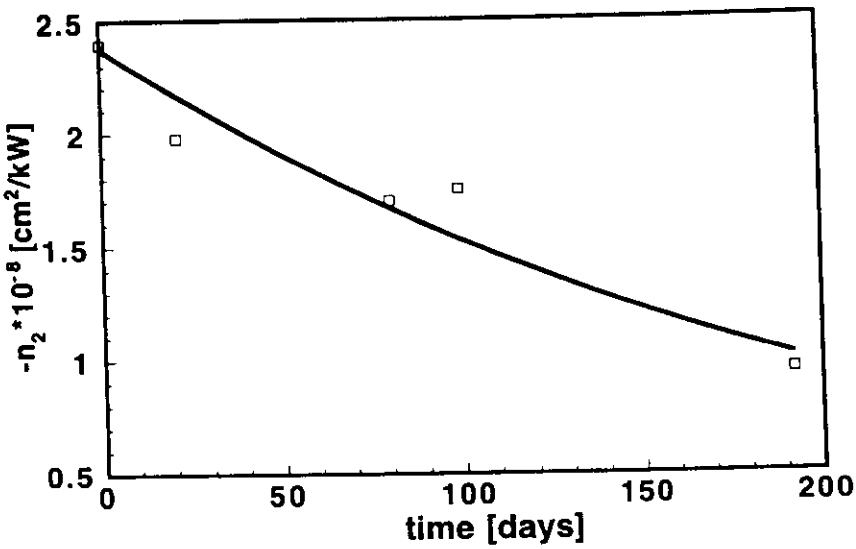

Figure 6. Evolution of the nonlinear refractive index of a CdS-doped sample as a function of storage time in the laboratory.

Further work is now being carried out on the inclusion into a silica–titania glass matrix of other semiconductors such as HgS and HgSe in order to find even higher nonlinear coefficients at longer wavelengths.

6. Conclusions

The unique features of the sol–gel method—primarily the capability of material synthesis at low temperature—make it ideal for the preparation of many nonlinear optical materials. The technique has been successfully applied to the preparation of many composite glasses, doped with nanoclusters of II–VI semiconductors such as CdS, CdSe, CdTe, ZnS, HgS or of other semiconductors like PbS, CuBr and also GaAs. All of these materials exhibit interesting third-order nonlinear properties. Sol–gels, however, also have the capability of producing another class of highly promising nonlinear optical materials, namely that of organic–inorganic hybrids, which can also exhibit second-order nonlinearities.

Referring to SDGs, a good control of size and dispersion of semiconductor clusters has already been obtained by using either the pore doping process or the surface capping nanochemistry; however, there is still room for further improvement.

In our experiments we worked mostly on CdS-doped sol–gel films, but we are also producing and studying films doped with PbS, (Cd, Pb)S systems, HgS and HgSe, searching for composite materials exhibiting a high nonlinearity in the near infrared region. The control of size of semiconductor clusters in the range 2–20 nm was achieved. The quality of CdS-doped films, having a typical refractive index of around 1.54, is good for application to integrated optics, as demonstrated by measured propagation losses, always within the range of 1–1.9 dB cm^{-1} at 633 nm wavelength. Nonlinear optical measurements on both CdS- and PbS-doped films, based on the difference in high- and low-intensity laser coupling into the waveguide through a grating etched in the substrate, showed values of the nonlinear refractive index n_2 in the range 10^{-9}–10^{-8} cm^2 kW^{-1}, corresponding to a third-order nonlinear susceptibility $\chi^{(3)}$ of the order of 10^{-10}–10^{-9} esu. Samples of CdS-doped films exhibited high nonlinearity over the entire region 450–570 nm, with a best value of $n_2 = -2.9 \times 10^{-7}$ cm^2 kW^{-1} [33]. These results appear so far to be among the best ever achieved for SDGs, independently of the manufacturing technique used, and are closely approaching the value of about 10^{-7} cm^2 kW^{-1} considered necessary for practical all-optical switching integrated optical devices.

Acknowledgments

We acknowledge the support of the European Commission through the ESPRIT Project NODES (contract no 6993). Partial support from CEO, Firenze and from CNR Progetto Strategico 'Material Innovativi' is also acknowledged.

References

[1] See for instance Stegeman G I, Burke J J and Seaton C T 1987 Nonlinear integrated optics *Integrated Optical Circuits and Components* ed L D Hutchinson (New York: Dekker) ch 9
[2] Brinker C J and Scherer G W 1990 *Sol–Gel Science: the Physics and Chemistry of Sol–Gel Processing* (San Diego, CA: Academic)
[3] See for instance Mackenzie J D (ed) 1994 *Sol–Gel Optics III (SPIE Proc. 2288)* (Bellingham: SPIE)
[4] Takagahara T 1987 *Phys. Rev.* B **36** 9293
[5] Brus L 1986 *IEEE J. Quantum Electron.* **22** 1909
[6] Borrelli N F, Hall D W, Holland H J and Smith D W 1987 *J. Appl. Phys.* **61** 5399
[7] Righini G C, Banfi G P, Degiorgio V, Nicoletti F and Pelli S 1991 *Mater. Sci. Eng.* B **9** 397–403
[8] Cingolani R, Moro C, Manno D, Striccoli M, De Blasi C, Righini G C and Ferrara M 1991 *J. Appl. Phys.* **70** 6898–901
[9] Yumoto J, Shinojima H, Uesugi N, Tsunetomo K, Nasu H and Osaka Y 1990 *Appl. Phys. Lett.* **57** 2393
[10] Nasu H, Yamada H, Matsuoka J and Kamiya K 1995 *J. Non-Cryst. Solids* **183** 290–6
[11] Li G and Nogami M 1993 *J. Sol–Gel Sci. Technol.* **1** 79–83
[12] Hui Y, Dijie H, Zhonghong J and Yong D 1994 *J. Sol–Gel Sci. Technol.* **3** 235–9
[13] Nogami M, Nagasaka K and Kotani K 1990 *J. Non-Cryst. Solids* **122** 101–9
[14] Hummel D C, Torriani I L, Ramos A Y, Craievich A F, De La Rosa Fox N and Esquivias L 1994 *Mat. Res. Soc. Symp. Proc.* **346** 673–8
[15] Herron N and Wang Y 1994 *Mat. Res. Soc. Symp. Proc.* **346** 887
[16] Choi K C and Shea K J 1994 *Mat. Res. Soc. Symp. Proc.* **346** 763
[17] Yeatman E M, Green M, Dawnay E J C, Fardad M A and Horowitz F 1994 *J. Sol–Gel Sci. Technol.* **2** 711
[18] Fardad M A, Yeatman E M, Dawnay E J C, Green M, Fick J, Guntau M and Vitrant G 1996 *Proc. IEE* to be published
[19] Dawnay E J C, Fick J, Green M, Guglielmi M, Martucci A, Pelli S, Righini G C, Vitrant G and Yeatman E M 1995 *Advanced Materials in Optics, Electro-Optics and Communication Technologies* (Faenza: Techna Slr) 15–20
[20] Butcher P N and Cotter D 1991 *The Elements of Nonlinear Optics* (Cambridge: Cambridge University Press)
[21] Minti H, Eyal M and Reisfeld R 1991 *Chem. Phys. Lett.* **183** 277–82

[24] Spahnel L 1992 *J. Non-Cryst. Solids* **147–148** 657
[25] Gacoin Y, Boilot J P, Chaput F and Lecomte A 1992 *MRS Proc.* **272** 21
[26] Herron N and Wang Y 1994 *Mat. Res. Soc. Symp. Proc.* **346** 887
[27] Guglielmi M, Martucci A, Righini G C and Pelli S 1994 *SPIE Proc. Sol–Gel Optics III* **2288** 174
[28] Kayanuma Y 1986 *Solid State Commun.* **59** 405
[29] Wang Y, Suna A, Mahler W and Kasowski R 1987 *J. Chem. Phys.* **87** 7315–22
[30] Guglielmi M, Martucci A, Menegazzo E, Righini G C, Pelli S, Fick J and Vitrant G 1996 Control of semiconductor particle size in sol–gel thin films *J. Sol–Gel Sci. Technol.* at press
[31] Vitrant G and Reinisch R 1993 *5th Int. Topsoe Summer School on Nonlinear Optics (Aalborg, 1992)* ed O Keller (Commack: Nova)
[32] Pellegri N, de Sanctis O and Kadono K 1995 Fabrication of PbS nanoparticles in silica gel by reverse micelles and sol gel routes *8th Int. Workshop on Glasses and Ceramics from Gels (Faro)*
[33] Fick J, Vitrant G, Martucci A, Guglielmi M, Pelli S and Righini G C 1995 *Nonlinear Opt.* **12** 203–9

ERBIUM-DOPED GLASS WAVEGUIDES FOR INTEGRATED OPTICAL AMPLIFIERS AND LASERS

Giancarlo C. Righini[1], Simone Capecchi[1], Stefano Pelli[1], Alessandro Verciani[1], Carmen N. Afonso[2], Yingchao Yan[3], Anne Jans Faber[3], Henk der Waal[3]

[1]IROE-CNR "Nello Carrara", Optoelectronic Technologies Group
via Panciatichi 64, I-50127 Firenze, Italy

[2]Instituto de Optica, CSIC, Serrano 121, 28006 Madrid, Spain

[3]TNO - Institute for Applied Physics, P.O.Box 595, 5600 AN Eindhoven, The Netherlands‡

ABSTRACT

Integrated optical lasers and amplifiers are attracting large attention for their use in optical sensing as well in optical communication systems. Here we present preliminary results on the characterisation of optical waveguides fabricated in Er-doped phosphate glasses either by ion-exchange or by pulsed laser deposition. It is shown that spectroscopic features of the waveguides are fully suitable to the implementation of active guided-wave devices.

INTRODUCTION

Since very shortly after the discovery of laser, glasses have been used to host a number of active compounds and especially of rare-earth ions.[1] Later on, the advantages offered by guided-wave format, namely the small size, the high pump power density, and the larger flexibility in design and fabrication, led to the development of fibre lasers and subsequently of erbium doped fibre amplifiers (EDFAs): the latter devices, which exploit the radiative transition from excited to ground state of erbium at about 1540 nm, find large use in long-haul optical communication systems.

More recently, a growing activity was aimed at achieving optical gain in Er-doped planar waveguides, having in mind the single-chip realisation of integrated optical amplifiers and lasers as well as of lossless splitters to be employed in particular in the distribution of an optical signal to single users in their homes (*fibre to the home*). Some remarkable results have been already achieved using various technological routes, from doping of bulk glasses and later fabrication of the guiding layer by ion-exchange to the deposition of active layers by co-sputtering, CVD, FHD, sol-gel techniques.[2-7] but further work is still necessary to exploit all the potential of active glass waveguides. Material requirements, in fact, are much more stringent for integrated optics than for fibres, due to the different fabrication technologies and to the resulting much higher losses of planar or channel waveguides.

Here we describe some preliminary results concerning the characterisation of erbium-doped glass waveguides produced by ion-exchange in both commercial and experimental glasses or by pulsed laser deposition of the active material.

ION-EXCHANGED Er^+-DOPED GLASS WAVEGUIDES

Ion-exchange is a quite simple, low-cost and effective process to produce optical waveguides in glasses containing a sufficient percentage of alkali ions;[8] in silicate glasses, a sodium oxide content higher than 7% in weight is usually regarded as fully

‡ [1] Fax: + 39 55 412878, e-mail: righini@iroe.fi.cnr.it; [2] Fax: +34 1 5645557, e-mail: afonso@pinar1.csic.es ; [3] Fax: + 31 40 449350, e-mail: jyan@tpd.tno.nl

satisfactory. As to laser glasses, nowadays many efforts are focused onto the production of low-phonon-energy materials, such as germanate or fluoride glasses, suitable also for hosting Pr^+ ions: the manufacture of these glasses, however, is not yet a mature technology and often the realisation of optical waveguides (integrated optical or fiber guides) is a difficult process. Among the easily produced and potentially useful glasses, silicates and phosphates are the most widely employed; their phonon energy is similar, but phosphates have larger values of both oscillator strength and peak stimulated emission cross section for the transition at 1.5 μm.[9]

Thus, we started investigating a number of different phosphate glasses, including commercial glasses produced by Kigre (U.S.A.) and experimental aluminophosphates developed by some of the authors at TNO.[10] Table I shows the main components of some of the glasses investigated; stars (*) indicate that exact quantities are unknown. A common requirement for experimental glasses was a relatively high sodium oxide content, in order to make easy the realisation of optical waveguides by the ion-exchange process. Several batches of alumino-phosphates were produced, changing slightly the chemical composition and/or using different thermal treatments: all these samples are indicated here with the label PG, followed by a letter (A to E) which corresponds to a different batch. Erbium content is quite high in PGs, with atomic concentration ranging from 0.4 to 4%. Co-doping with Ytterbium, which absorbs light at the same wavelength as Erbium (i.e. 980 nm) and then transfers energy to Erbium, is also very high in some samples.

Table I - Main components of some Er-doped glasses (weight %)

Glass	label	P_2O_5	Al_2O_3	Li_2O	Na_2O	Er_2O_3	Yb_2O_3
Kigre Q89	K-Q89	*	*	4		2	4
Kigre Special Melt	K-SM	67	5	3		1	
Phosphate glass C	PG-C	54	19		23	7.1	
Phosphate glass E	PG-E	54	*		7.91	2.71	17

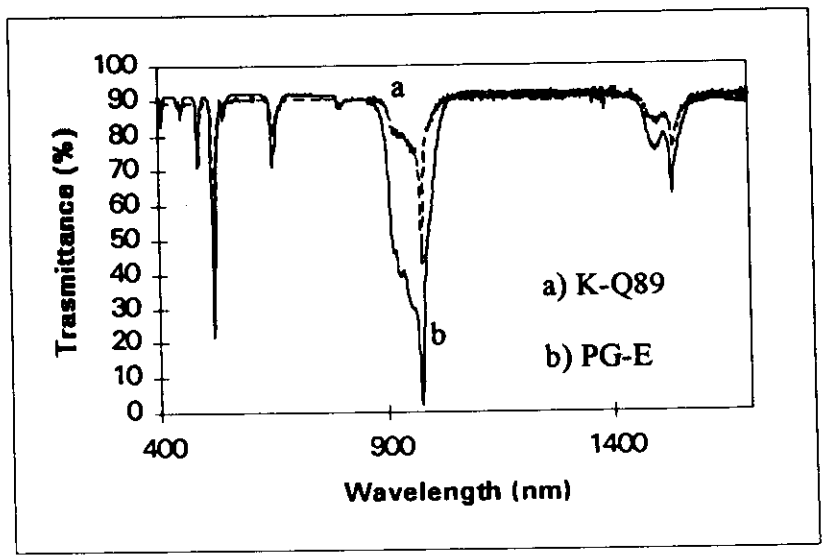

Figure 1. Absorption curves of a commercial (a) and an experimental (b) phosphate glass doped with Er^+ and Yb^+ ions.

First of all, the characterisation of bulk samples was carried out, and typical results are reported in Figures 1 and 2: the former one presents the absorption curves of two samples (K-Q89 and PG-E), while the latter shows the fluorescence curves of three samples. For that measurement the beam at 514.5 nm from an argon laser was used as a pump, so that the Er^{3+} ions were excited at the $^2H_{11/2}$ level; from there they first decay non-radiatively to the $^4I_{13/2}$ level and then to the $^4I_{15/2}$ level emitting radiation at around 1540 nm: radiated light was collected by a Jobin-Ivon Spex 270-M spectrophotometer using a InGaAs photodiode as detector.

Table II reports the spectroscopic characteristics of some samples, while the lifetimes experimentally measured in several of our samples are presented in Table III.

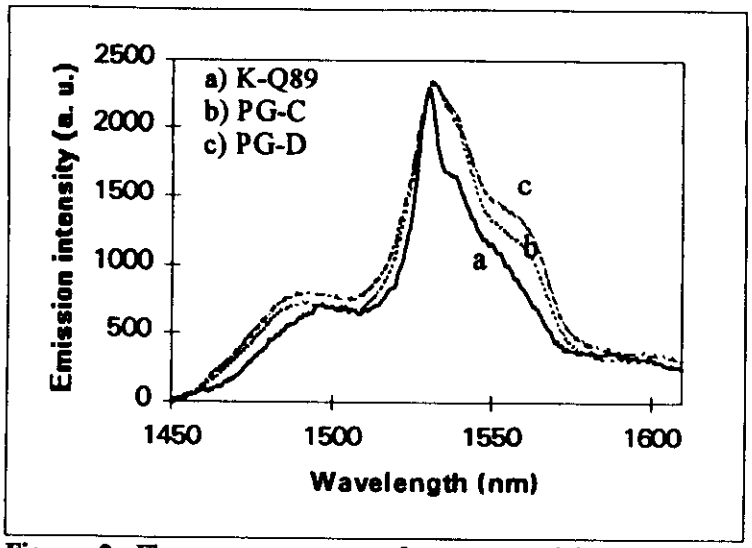

Figure 2. Fluorescence curves of a commercial (a) and two experimental (b, c) Er-doped phosphate glasses, exhibiting typical emission peak at around 1540 nm.

The overall characteristics of these doped glasses are very good, as we have doping levels, absorption and emission cross sections, and lifetimes comparable with the best results already reported in literature. For instance, the lifetime of about 8 ms for the samples having 2% atomic Er concentration (glass type PG-A) appears to be suitable for device applications. The reduction to about 4 ms of the fluorescence lifetime in the samples doped with 4% atomic erbium (as in glass type PG-C and PG-D) indicates that in this case there might be some quenching effects, as it could have been expected due to the very high Er concentration.

After these measurements on bulk glasses, we started trying to produce optical waveguides in them, first of all by using the ion-exchange technique.

The Kigre glasses, however, contain only lithium as an alkali ion and our attempts of fabricating optical waveguides (that require a local increase of the refractive index) by Li-Ag exchange were not satisfactory because of the poor repeatability of the results. Thus, the production of ion-exchanged waveguides was carried out only using the aluminophosphate glasses, which include a suitable quantity of sodium. In these samples, having in mind the achievement of low propagation losses, Na^+/K^+ ion-exchange was tested first: the stresses caused by the large difference in ionic radius of sodium and potassium, however, led to significant damage of the surface of the sample, where the maximum concentration of K-ions occurs. We therefore moved to Na^+/Ag^+, using diluted melts of $AgNO_3$ in $NaNO_3$. The dilutions ranged from 5% down to 0.5 % molar, while the melt temperature was kept at 325 °C. The process proved to be very efficient, with exchange times of the order of 1 minute leading to waveguides supporting several modes at 633 nm. The propagation constants were thereafter measured by dark-line spectroscopy and the refractive index profile derived from the experimental data. In the case of 0.5 % silver nitrate molar dilution, that was eventually chosen as the best process for these glasses, we found an erfc profile, with a surface refractive index change of 0.03 at 633 nm (the refractive index of PG samples at that wavelength is around 1.495). The typical propagation losses measured by detecting the decaying light scattered out of the plane of the waveguide by means of a Vidicon camera[11] were slightly under 1 dB/cm at 633 nm, sufficiently good to enable the production of optical devices.

Table II - Spectroscopic characteristics of some Er-doped glasses

Glass	Erbium atoms (cm^{-3})	Emission peak (nm)	Absorption peak (nm)	Emission cross section ($*10^{-21}$ cm^2)	Absorption cross section ($*10^{-21}$ cm^2)
K- Q89	$1.98*10^{20}$	1530.5±0.5	974±1	6.5±0.5	7.3±0.5
K- SM	$8.9*10^{19}$	1530±0.5	977±1	8.3±0.5	4.6±0.5
PG - A	$3.1*10^{20}$	1531±0.5	976±1	4.8±0.3	2.4±0.5

Table III - Lifetimes of various Er-doped glasses

Glass	label	Er_2O_3 weight %	Lifetime (ms)
Kigre Q89	K-Q89	2	9.5
Kigre Special Melt	K-SM	1	8.4
Phosphate glass A	PG-A	3.6	8.1
Phosphate glass B	PG-B	3.6	5.5
Phosphate glass C	PG-C	7.1	4.5
Phosphate glass D	PG-D	7.1	3.0

Since the host matrix of the glass can influence the decay rate of the fluorescence, we checked if the ion-exchange process had caused any change under this respect. Thus, the chopped pump beam was coupled into an ion-exchanged waveguide and care was taken to collect the fluorescence produced by the guided pump beam and only this, by shielding the parts of the sample out of the guided light path. The fluorescence lifetime was of the same order, if not longer, than the one measured in bulk samples, thus indicating that the ion-exchange process did not affect the spectroscopic properties of the glass.
We also checked the existence of possible ageing effects; thus, measurements of the fluorescence were performed on fresh as well on aged samples. Figure 3 shows the fluorescence curve of a waveguide (sample # S15) as performed 4 months after its production, compared with the one of a companion waveguide, i.e. produced in the same batch, (sample # S19) which had been measured just after its fabrication. No relevant differences in the spectrum exist, thus indicating a good time and environmental stability and demonstrating that both the material and the process are suitable for practical devices.

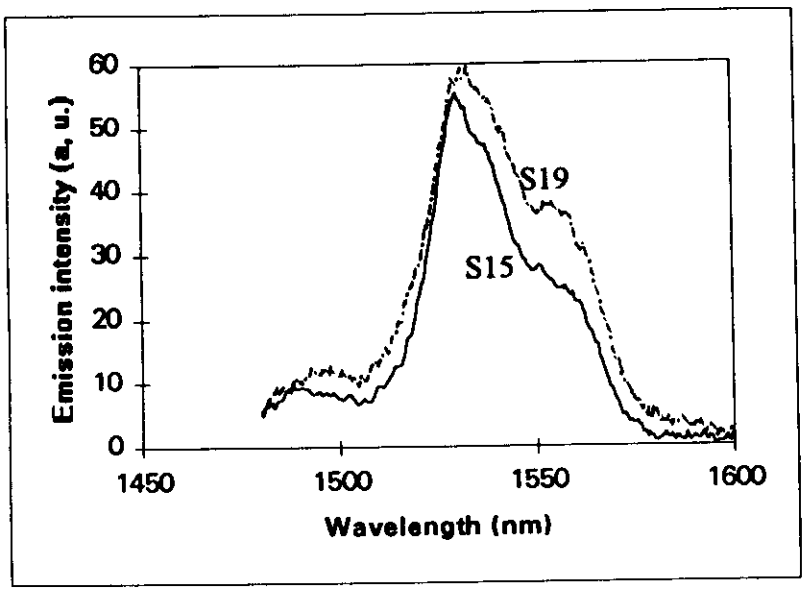

Figure 3. Fluorescence curves of two companion waveguides measured at 4-month distance from each other (sample # S15 was tested 4 months later than sample # S19).

A relevant problem still unsolved in waveguide fabrication is concerned with the realisation of channel waveguides in PG samples. As a matter of fact, these glasses did not prove able to withstand the whole photolithographic process; in particular, both the metal (aluminium) layer and the etching solution used to remove it caused unacceptable damage of the surface of the samples. Changing the metal and etching solutions did not improve the situation. We are therefore trying to use a different guiding structure, where lateral confinement of the light is achieved by realising strip-loaded waveguides. By choosing as loading material of an ion-exchanged planar waveguide a photoresist layer 0.2 μm thick, having 1.6 refractive index at 633 nm, where a strip of width of about 6 microns is defined, we got a multimode waveguide. Transversal confinement is thus achieved, but the quality of the waveguide is so far very poor, because it exhibits propagation losses higher than 15 dB/cm, too large for practical application. Tests are under way in order to improve the described process and therefore the quality of the waveguides.

PULSED LASER DEPOSITION (PLD) OF ACTIVE LAYERS

The impossibility of using ion-exchange to fabricate optical guiding layers in Kigre glasses led us to consider a different approach, based on the ablation of the material from this type of glass and its subsequent deposition as a thin film on any substrate.[12] A 12-ns pulsed ArF laser emitting at 193 nm with repetition rate of 6 Hz was focused onto the target, placed in a vacuum chamber at 45° with respect to the incident beam; energy density was varied in the range of 4 to 5 J/cm^2. After some preliminary tests in vacuum, it was decided to perform depositions in an oxygen atmosphere, at typical pressure of 0.06 mbar. Films of K-Q89 and K-SM glasses were deposited onto a number of substrates, namely silicon, silica on silicon, pure silica, and soda-lime glass.

The refractive index of the deposited material, measured by m-line technique in layers of thickness suitable to support at least two propagating modes, was in the range 1.562 to 1.570, slightly higher than the index of the bulk material (1.551). The high optical density of films prepared by PLD is usually due to the presence of energetic species bombardment during film growth.[12]

The spectroscopic properties of the deposited film are quite similar to those of the bulk glass, as demonstrated by Figure 4, where the fluorescence spectra of the bulk glass (K-Q89 type) and of a deposited film are shown. The difference in emission

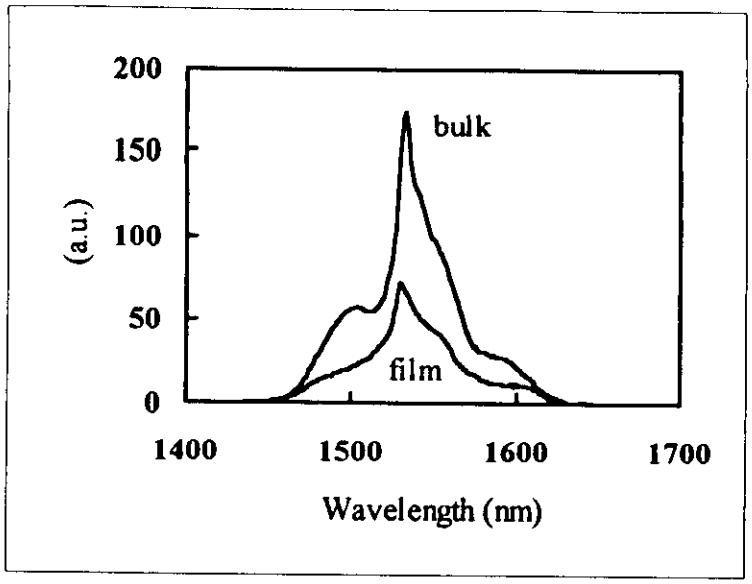

Figure 4. Fluorescence curves measured in bulk K-Q89 glass and in a pulsed-laser-deposited film from the same glass.

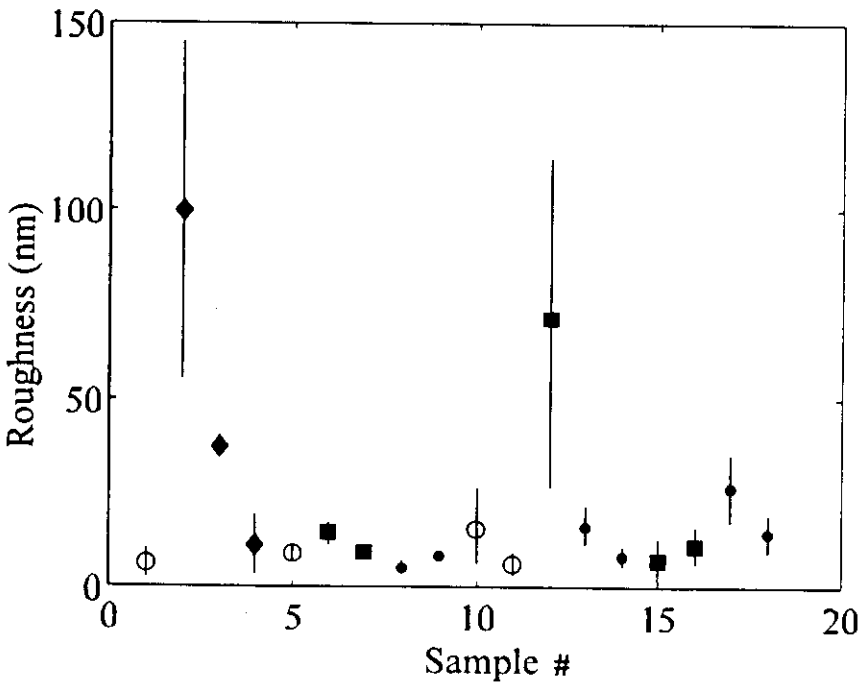

Figure 5 Surface roughness of films produced by laser ablation of Kigre Q89 glass targets. Measurements have been carried out by using an Alphastep stylus profilometer. Symbols indicate different substrates (see text).

intensity is obviously related to the different volumes of material contributing to fluorescence in the two cases, while a slight variation in the curve profile can be attributed to minor compositional and density changes in the host matrix during the film growth.

A major problem, however, is related to optical propagation losses in these planar waveguides: the values measured at 632.8 nm are in the range 11 to 20 dB/cm. This high loss is attributed to the scattering produced mainly by the surface roughness of the deposited films, which is confirmed by independent measurements carried out by using a scanning electron microscope (Zeiss-DSM960) and a stylus profilometer (Tencor Alphastep). Figure 5 shows the values of surface roughness measured by the profilometer in a number of samples. The various symbols indicate depositions made onto different substrates: ○ corresponds to silicon wafers, ◆ to soda-lime glass, ● to pure silica (fused quartz), and finally ■ refers to films deposited on top of a silica layer grown onto a silicon wafer. Since the measurements for each sample were carried out in a number of different surface zones, the vertical bars indicate the spreading of the measured values, their length corresponding to the standard deviation around the average value for that sample. It appears that soda-lime glasses constitute the worst type of substrate; however, even if we remove the two worst samples (likely obtained in deposition conditions not corresponding to the standard ones), the average surface roughness measured in all the samples is around 12 nm, a value which surely gives rise to a significant optical scattering of the light propagating in the films.

Further tests are now being carried out, with the deposition of new films produced from different glass targets; particular care is taken in the choice of substrates, in order to avoid detrimental effects due to the poor surface quality of the substrates themselves.

CONCLUSIONS

Planar waveguides have been produced in commercial and experimental erbium and erbium-ytterbium doped phosphate and alumino-phosphate glasses with the aim of developing processes suitable to the realisation of integrated optical lasers and amplifiers. Two technological routes have been tested, one using ion-exchange technique to locally modifying the refractive index of doped glasses containing Na_2O, and the other one using the deposition of active films through laser ablation of doped glass targets. Both techniques led to the production of optical waveguides with spectroscopic properties, in particular fluorescence lifetimes, fully compatible with the realisation of active devices. In both cases, however, processes have to be improved in order to produce low-loss channel waveguides. The use of alternative matrix glass compositions, namely silicate glasses, is now being investigated, and preliminary results seem to indicate that some of the above mentioned limitations are being overcome.

ACKNOWLEDGEMENTS

The assistance of B. Radicati with photometric measurements and R. Calzolai (both are with IROE CNR) for the cutting and polishing of the samples is gratefully acknowledged.
Part of this research has been carried out in the frame of CNR Special Project "Miniaturised laser sources in the visible-medium IR range".

REFERENCES

1. M.J. Weber, Laser glasses, in *From Galileo's "occhialino" to optoelectronics*, P. Mazzoldi, Ed. (World Sci., Singapore, 1993) 332-349.
2. G.C. Righini, Passive and active glasses for integrated optics, in *From Galileo's "occhialino" to optoelectronics*, P. Mazzoldi, Ed. (World Sci., Singapore, 1993) 272-294.
3. K. Hattori, T. Kitagawa, M. Oguma, Y. Ohmori, M. Horiguchi, Erbium-doped silica-based waveguide amplifier integrated with a 980/1530 nm WDM coupler, *Electron. Lett.* **30**, 11 (1994).
4. J.E. Roman, P. Camy, M. Hempstead, W.S. Brocklesby, S. Nouh, A. Beguin, C. Lerminiaux and J.S. Wilkinson, Ion-exchanged Er/Yb waveguide laser at 1.5 mm pumped by laser diode, *Electron. Lett.* **31**,1345 (1995).
5. T. Ohtsuki, N. Peyghambarian, S. Honkanen, S.I. Najafi, Gain charcteristics of a high concentration Er3+-doped phosphate glass waveguides, *J. Appl. Phys.* **78**, 3617 (1995).
6. S. Kawanishi, K. Hattori, H. Takara, M. Oguma, O. Kamatani, Y. Hibino, Actively modelocked ring laser using Er-doped silica-based planar waveguide amplifier, *Electron. Lett.* **31**, 363 (1995).
7. R.N. Ghosh, J. Shmulovich, C.F. Kane, M.R.X. de Barros, G. Nykolak, A.J. Bruce, P.C. Becker, 8-mW threshold Er3+-doped planar waveguide amplifier, *IEEE Ph.Tech. Lett.* **8**, 518 (1996).
8. P. Mazzoldi, G.C. Righini, Glasses for optoelectronic devices, in *Insulating Materials for Optoelectronics*, F. Agulló Lopez, Ed. (World Sci., Singapore, 1995) 367-392.
9. W.J. Miniscalco, Erbium-doped glasses for fiber amplifiers at 1500 nm, *J. Lightw. Techn.* **9**, 234 (1991).
10. Y. Yan, A.J. Faber, H. de Waal, Luminescence quenching by OH groups in highly Er-doped phosphate glasses, *J. Non-Cryst. Solids* **181**, 283 (1995).
11. S. Pelli and G.C. Righini, Introduction to Integrated Optics: Characterisation and Modelling of Optical Waveguides, in *Advances in Integrated Optics*, S. Martellucci et al. Eds. (Plenum Press, London, 1994) 1-20.
12. C.N. Afonso, J.M. Ballesteros, J. Gonzalo, G.C. Righini, S. Pelli, Rare-earth doped glass waveguides prepared by pulsed laser deposition, *Appl. Surface Sci.* **96-98**, 760 (1996).